Mathematical and Computational Applications

MDPI

Article

Towards Building the OP-Mapped WENO Schemes: A General Methodology

Ruo Li [1,†] **and Wei Zhong** [2,3,*,†]

[1] CAPT, LMAM and School of Mathematical Sciences, Peking University, Beijing 100871, China; rli@math.pku.edu.cn
[2] School of Mathematical Sciences, Peking University, Beijing 100871, China
[3] Northwest Institute of Nuclear Technology, Xi'an 710024, China
* Correspondence: zhongwei2016@pku.edu.cn or zhongwei@ac.nint.cn
† Both authors contributed equally to this work.

Abstract: A serious and ubiquitous issue in existing mapped WENO schemes is that most of them can hardly preserve high resolutions, but in the meantime prevent spurious oscillations in the solving of hyperbolic conservation laws with long output times. Our goal for this article was to address this widely known problem. In our previous work, the *order-preserving (OP)* criterion was originally introduced and carefully used to devise a new mapped WENO scheme that performs satisfactorily in long simulations, and hence it was indicated that the *OP* criterion plays a critical role in the maintenance of low-dissipation and robustness for mapped WENO schemes. Thus, in our present work, we firstly defined the family of mapped WENO schemes, whose mappings meet the *OP* criterion, as OP-Mapped WENO. Next, we attentively took a closer look at the mappings of various existing mapped WENO schemes and devised a general formula for them. That helped us to extend the *OP* criterion to the design of improved mappings. Then, we created a generalized implementation of obtaining a group of OP-Mapped WENO schemes, named MOP-WENO-X, as they are developed from the existing mapped WENO-X schemes, where the notation "X" is used to identify the version of the existing mapped WENO scheme. Finally, extensive numerical experiments and comparisons with competing schemes were conducted to demonstrate the enhanced performances of the MOP-WENO-X schemes.

Keywords: *order-preserving* mapping; OP-Mapped WENO; hyperbolic conservation laws

Citation: Li, R.; Zhong, W. Towards Building the OP-Mapped WENO Schemes: A General Methodology. *Math. Comput. Appl.* **2021**, *26*, 67. https://doi.org/10.3390/mca26040067

Academic Editor: Zhenli Xu

Received: 9 August 2021
Accepted: 13 September 2021
Published: 23 September 2021

1. Introduction

The essentially non-oscillatory (ENO) schemes [1–4] and the weighted ENO (WENO) schemes [5–8] have been developed quite successfully in recent decades to solve the hyperbolic conservation problems, especially those that may generate discontinuities and smooth small-scale structures as time evolves in their solutions, even if the initial condition is smooth. The main purpose of this study was to find a general method to introduce the *order-preserving (OP)* mapping proposed in our previous work [9] for improving the existing mapped WENO schemes for the approximation of the hyperbolic conservation laws in the form

$$\frac{\partial \mathbf{u}}{\partial t} + \nabla \cdot \mathbf{F}(\mathbf{u}) = 0, \tag{1}$$

where $\mathbf{u} = (u_1, \cdots, u_m) \in \mathbb{R}^m$ is the vector of the conserved variables and $\mathbf{F}(\mathbf{u})$ is the vector of the Cartesian components of flux. In recent years, there have been many works by Dumbser [10], Boscheri [11–13], Tsoutsanis [14,15], Titarev and Toro [16–19], Semplice [20,21], Puppo [22], Russo [23,24], and others on WENO approaches. These researches embraced a wide range of issues, e.g., the ADER-WENO finite volume schemes, the Cool WENO schemes, the unstructured WENO schemes, the Compact central WENO schemes, and so

on. However, because of space limitations, it is very difficult to provide detailed descriptions of them here, and we refer the reader to our references for more details. In the present study, our main concern was to improve the performances of the $(2r-1)$th-order mapped WENO schemes, so we briefly review recent developments in this field in the following.

Harten et al. [1] introduced the ENO schemes. They used the smoothest stencil from r possible candidate stencils based on the local smoothness to perform a polynomial reconstruction such that it yielded high-order accuracy in smooth regions but avoided spurious oscillations at or near discontinuities. Liu, Osher, and Chan [7] introduced the first WENO scheme, an improved version of the ENO methodology with a cell-averaged approach, by using a nonlinear convex combination of all the candidate stencils to achieve a higher order of accuracy than the ENO schemes, while retaining the essential non-oscillatory property at or near discontinuities. In other words, it achieves $(r+1)$th-order accuracy from the rth-order ENO schemes [1–3] in the smooth regions while behaving similarly to the rth-order ENO schemes in regions including discontinuities. In [8], Jiang and Shu proposed the classic WENO-JS scheme, along with a new measurement for the smoothness of the numerical solutions on substencils (hereafter, denoted by smoothness indicator), by using the sum of the normalized squares of the scaled L_2-norms of all the derivatives of r local interpolating polynomials, to obtain $(2r-1)$th-order accuracy from the rth-order ENO schemes.

The WENO-JS scheme has become a very popular and quite successful methodology for solving compressible flows modeled through hyperbolic conservation laws in the form of Equation (1). However, it was less than fifth-order for many cases, such as at or near critical points of order $n_{\mathrm{cp}} = 1$ in the smooth regions. Here, we refer to n_{cp} as the order of the critical point; e.g., $n_{\mathrm{cp}} = 1$ corresponds to $f' = 0, f'' \neq 0$ and $n_{\mathrm{cp}} = 2$ corresponds to $f' = 0, f'' = 0, f''' \neq 0$. In particular, Henrick et al. [25] identified that the fifth-order WENO-JS scheme fails to yield the optimal convergence order at or near critical points where the first derivative vanishes but the third derivative does not. Then, in the same article, they derived the necessary and sufficient conditions on the nonlinear weights for optimality of the convergence rate of the fifth-order WENO schemes and these conditions were reduced to a simpler sufficient condition [26] which could be easily extended to the $(2r-1)$th-order WENO schemes [27]. Moreover, also in [25], Henrick et al. devised the original mapped WENO scheme, named WENO-M hereafter, by constructing a mapping function that satisfies the sufficient condition to achieve the optimal order of accuracy.

Later, following the idea of incorporating a mapping procedure to keep the nonlinear weights of the convex combination of stencils as near as possible to the ideal weights of optimal order accuracy, various versions of mapped WENO schemes have been successfully proposed. In [27], Feng et al. rewrote the mapping function of the WENO-M scheme in a simple and more meaningful form and then extended it to a general class of improved mapping functions, leading to the family of the WENO-IM(k, A) schemes, where k is a positive even integer and A a positive real number. It was indicated that by taking $k = 2$ and $A = 0.1$ in the WENO-IM(k, A) scheme, far better numerical solutions with less dissipation and higher resolution could be obtained than that of the WENO-M scheme. Unfortunately, the numerical experiments in [28] showed that the seventh and ninth-order WENO-IM(2, 0.1) schemes generated evident spurious oscillations near discontinuities when the output time was large. In addition, our numerical experiments, as shown in Figures 10, 12 and 14, indicate that, even for the fifth-order WENO-IM(2, 0.1) scheme, the spurious oscillations are also produced when the grid number increases or a different initial condition is used. Recently, Feng et al. [29] pointed out that, when the WENO-M scheme is used for solving the problems with discontinuities for long output times, its mapping function may amplify the effect from the non-smooth stencils, leading to a potential loss of accuracy near discontinuities. To amend this drawback, a piecewise polynomial mapping function with two additional requirements, that is, $g'(0) = 0$ and $g'(1) = 0$ ($g(x)$ denotes the mapping function), to the original criteria in [25] was proposed. The recommended WENO-PM6 scheme [29] achieved significantly higher resolution than

the WENO-M scheme when computing the one-dimensional linear advection problem with long output times. However, it may generate spurious oscillations near the discontinuities, as shown in Figure 8 of [27] and Figures 3–8 of [28].

More mapped WENO schemes, such as the WENO-PPM*n* [30], WENO-RM(*mn*0) [28], WENO-MAIM*i* [31], WENO-ACM [32] schemes, and others, have been successfully developed to enhance the performances of the classic WENO-JS scheme in some ways, such as letting it achieve optimal convergence orders near critical points in smooth regions; having less numerical dissipation; letting it achieve higher resolutions near discontinuities; or reducing the computational costs. See the references for more details. However, as mentioned in previously published literature [27,28], most of the existing improved mapped WENO schemes could not prevent the spurious oscillations near discontinuities, especially for long-output-time simulations. Moreover, when simulating the two-dimensional problems with strong shock waves, the post-shock oscillations, which were systematically studied for WENO schemes by Zhang et al. [33], become very severe in the solutions of most of the existing improved mapped WENO schemes [32].

In our previous study [9], we studied the nonlinear weights of the existing mapped WENO schemes by taking the ones developed in [9,27,29,31] as examples. It was found that the order of the nonlinear weights for the substencils of the same global stencil has been changed at many points in the mapping processes of all these considered mapped WENO schemes. The order-change of nonlinear weights is caused by weight increasing of non-smooth substencils and weight decreasing of smooth substencils. It was revealed that this is the essential cause of the potential loss of accuracy of the WENO-M scheme and the spurious oscillation generation of the existing improved mapped WENO schemes, through theoretical analysis and extensive numerical tests. In the same article, the definition of the *order-preserving (OP)* mapping was given and suggested as an additional criterion in the design of the mapping function. Then a new mapped WENO scheme with its mapping function satisfying the additional criterion was proposed. Extensive numerical experiments showed that this scheme can achieve the optimal convergence order of accuracy, even at critical points. It also can decrease the numerical dissipation and obtain high resolution, but does not generate spurious oscillation near discontinuities, even if the output time is large. Moreover, it was observed clearly that it exhibits a significant advantage in reducing the post-shock oscillations when calculating the problems with strong shock waves in two dimensions.

In this article, the idea of introducing the *OP* criterion into the design of the mapping functions proposed in [9] is extended to various existing mapped WENO schemes. First of all, we give the common name of *OP-Mapped WENO* to the family of the mapped WENO schemes whose mappings are *OP*. A general formula for the mapping functions of various existing mapped WENO schemes is presented, which allows the extension of the *OP* criterion to all existing mapped WENO schemes. The notation MOP-WENO-X is used to denote the improved mapped WENO scheme considering the *OP* criterion based on the existing WENO-X scheme. A new function named **minDist** is defined (see Definition 4 in Section 3.3 below). A general algorithm to construct *OP* mappings through the existing mapping functions by using the **minDist** function is proposed.

Extensive numerical tests were conducted to demonstrate the performances of the MOP-WENO-X schemes: (1) A series of accuracy tests show the abilities of the MOP-WENO-X schemes to achieve optimal convergence order in smooth regions with first-order critical points and their advantages in long-output-time simulations of problems with very high-order critical points. (2) The one-dimensional linear advection equation with two kinds of initial conditions for long output times are presented to demonstrate that the MOP-WENO-X schemes can obtain high resolution, and meanwhile avoid spurious oscillation near discontinuities. (3) Some benchmark tests with strong shock waves modeled via the two-dimensional Euler equations were computed. It is clear that the MOP-WENO-X schemes also enjoy a significant advantage in reducing the post-shock oscillations.

The remainder of this paper is organized as follows. In Section 2, we briefly review the preliminaries to understand the finite volume method and the procedures of the WENO-JS [8], WENO-M [25], and other versions of mapped WENO schemes. Section 3 presents a general method to introduce the *OP* mapping for improving the existing mapped WENO schemes. Some numerical results are provided in Section 4 to illustrate the advantages of the proposed WENO schemes. Finally, concluding remarks are given in Section 5 to close this paper.

2. Brief Review of the WENO Schemes

For simplicity of presentation but without loss of generality, we denote our topic with the following one-dimensional linear hyperbolic conservation equation:

$$\frac{\partial u}{\partial t} + \frac{\partial f(u)}{\partial x} = 0, \quad x_l < x < x_r, t > 0, \tag{2}$$

with the initial condition $u(x,0) = u_0(x)$. We confine our attention to the uniform meshes in this paper, and for the WENO method with non-uniform meshes, one can refer to [34,35]. Throughout this paper, we assume that the given domain $[x_l, x_r]$ is discretized into the set of uniform cells $I_j := [x_{j-1/2}, x_{j+1/2}], j = 1, \cdots, N$ with the cell size $\Delta x = \frac{x_r - x_l}{N}$. The associated cell centers and cell boundaries are denoted by $x_j = x_l + (j - 1/2)\Delta x$ and $x_{j\pm1/2} = x_j \pm \Delta x/2$, respectively. The notation $\bar{u}(x_j, t) = \frac{1}{\Delta x}\int_{x_{j-1/2}}^{x_{j+1/2}} u(\xi, t)\mathrm{d}\xi$ indicates the cell average of I_j. The one-dimensional linear hyperbolic conservation equation in Equation (2) can be approximated by a system of ordinary differential equations, yielding the semi-discrete finite volume form:

$$\begin{aligned} &\frac{\mathrm{d}\bar{u}_j(t)}{\mathrm{d}t} \approx \mathcal{L}(u_j), \\ &\mathcal{L}(u_j) = -\frac{1}{\Delta x}\left(\hat{f}_{j+1/2} - \hat{f}_{j-1/2}\right), \end{aligned} \tag{3}$$

where $\bar{u}_j(t)$ is the numerical approximation of the cell average $\bar{u}(x_j, t)$, and the numerical flux $\hat{f}_{j\pm1/2}$ is a replacement of the physical flux function $f(u)$ at the cell boundaries $x_{j\pm1/2}$ and it is defined by $\hat{f}_{j\pm1/2} = \hat{f}(u^-_{j\pm1/2}, u^+_{j\pm1/2})$. $u^\pm_{j\pm1/2}$ refer to the limits of u, and their values of $u^\pm_{j\pm1/2}$ can be obtained by reconstruction, for instance, the WENO reconstruction procedures shown later. In this paper, we use the global Lax–Friedrichs flux:

$$\hat{f}(a,b) = \frac{1}{2}\left[f(a) + f(b) - \alpha(b-a)\right],$$

where $\alpha = \max_u |f'(u)|$ is a constant and the maximum is taken over the whole range of u.

2.1. The WENO-JS Reconstruction

Firstly, we review the process of the classic fifth-order WENO-JS reconstruction [8]. For brevity, we describe only the reconstruction procedure of the left-biased $u^-_{j+1/2}$, and the right-biased one $u^+_{j+1/2}$ can trivially be computed by mirror symmetry with respect to the location $x_{j+1/2}$ of $u^-_{j+1/2}$. We drop the subscript "-" below just for simplicity of notation.

To construct the values of $u_{j+1/2}$ from known cell average values $\overline{u}_j$, a 5-point global stencil $S^5 = \{I_{j-2}, I_{j-1}, I_j, I_{j+1}, I_{j+2}\}$ is used in the fifth-order WENO-JS scheme. It is subdivided into three 3-point substencils $S_s = \{I_{j+s-2}, I_{j+s-1}, I_{j+s}\}$ with $s = 0, 1, 2$. It is known that the third-order approximations of $u(x_{j+1/2}, t)$ associated with these substencils are explicitly given by

$$
\begin{aligned}
u_{j+1/2}^{0} &= \frac{1}{6}(2\bar{u}_{j-2} - 7\bar{u}_{j-1} + 11\bar{u}_{j}),\\
u_{j+1/2}^{1} &= \frac{1}{6}(-\bar{u}_{j-1} + 5\bar{u}_{j} + 2\bar{u}_{j+1}),\\
u_{j+1/2}^{2} &= \frac{1}{6}(2\bar{u}_{j} + 5\bar{u}_{j+1} - \bar{u}_{j+2}).
\end{aligned} \tag{4}
$$

Then the $u_{j+1/2}$ of global stencil S^5 is computed by a weighted average of those third-order approximations of substencils, taking the form

$$
u_{j+1/2} = \sum_{s=0}^{2} \omega_s u_{j+1/2}^{s}. \tag{5}
$$

The nonlinear weights ω_s in the classic WENO-JS scheme are defined as

$$
\omega_s^{\mathrm{JS}} = \frac{\alpha_s^{\mathrm{JS}}}{\sum_{l=0}^{2} \alpha_l^{\mathrm{JS}}}, \alpha_s^{\mathrm{JS}} = \frac{d_s}{(\epsilon + \beta_s)^2}, \quad s = 0, 1, 2, \tag{6}
$$

where d_0, d_1, d_2 are called the ideal weights of ω_s since they generate the central upstream fifth-order scheme for the global stencil S^5. It is known that $d_0 = 0.1, d_1 = 0.6, d_2 = 0.3$ and in smooth regions we can get $\sum_{s=0}^{2} d_s u_{j+1/2}^{s} = u(x_{j+1/2}, t) + O(\Delta x^5)$. ϵ is a small positive number introduced to prevent the denominator from becoming zero. The parameters β_s are the smoothness indicators for the third-order approximations $u_{j+1/2}^{s}$ and their explicit formulas can be obtained from [8], taking the form

$$
\begin{aligned}
\beta_0 &= \frac{13}{12}\left(\bar{u}_{j-2} - 2\bar{u}_{j-1} + \bar{u}_{j}\right)^2 + \frac{1}{4}\left(\bar{u}_{j-2} - 4\bar{u}_{j-1} + 3\bar{u}_{j}\right)^2,\\
\beta_1 &= \frac{13}{12}\left(\bar{u}_{j-1} - 2\bar{u}_{j} + \bar{u}_{j+1}\right)^2 + \frac{1}{4}\left(\bar{u}_{j-1} - \bar{u}_{j+1}\right)^2,\\
\beta_2 &= \frac{13}{12}\left(\bar{u}_{j} - 2\bar{u}_{j+1} + \bar{u}_{j+2}\right)^2 + \frac{1}{4}\left(3\bar{u}_{j} - 4\bar{u}_{j+1} + \bar{u}_{j+2}\right)^2.
\end{aligned}
$$

In general, the fifth-order WENO-JS scheme is able to recover the optimal convergence rate of accuracy in smooth regions. However, when at or near critical points where the first derivative vanishes but the third derivative does not simultaneously, it loses accuracy and its convergence rate of accuracy decreases to third-order or even less. We refer to [25] for more details.

2.2. The Mapped WENO Reconstructions

To address the issue of the WENO-JS scheme mentioned above, Henrick et al. [25] made a systematic truncation error analysis of Equation (3) in its corresponding finite difference version by using the Taylor series expansions of the Equation (4), and hence they derived the necessary and sufficient conditions on the weights for the fifth-order WENO scheme to achieve the formal fifth-order of convergence at smooth regions of the solution, taking the form

$$
\sum_{s=0}^{2}(\omega_s^{\pm} - d_s) = O(\Delta x^6), \quad \sum_{s=0}^{2} A_s(\omega_s^{+} - \omega_s^{-}) = O(\Delta x^3), \quad \omega_s^{\pm} - d_s = O(\Delta x^2), \tag{7}
$$

where the superscripts "+" and "−" on ω_s correspond to their use in either $u_{j+1/2}^{s}$ and $u_{j-1/2}^{s}$ stencils respectively, and the parameter A_s is independent of Δx and it is given explicitly in Equation (16) in [25] for the fifth-order version WENO-JS scheme. Since the first equation in Equation (7) always holds due to the normalization, a simpler sufficient condition for the fifth-order convergence is given as [26]

$$
\omega_s^{\pm} - d_s = O(\Delta x^3), \quad s = 0, 1, 2. \tag{8}
$$

The conditions Equation (7) or Equation (8) may not hold in the case of smooth extrema or at critical points when the fifth-order WENO-JS scheme is used. An innovative idea of fixing this deficiency, originally proposed by Henrick in [25], is to design a mapping function to make ω_s approximating the ideal weights d_s at critical points to the required third order $O(\Delta x^3)$. The first mapping function devised by Henrick et al. in [25] is given as

$$\left(g^{\mathrm{M}}\right)_s(\omega) = \frac{\omega\left(d_s + d_s^2 - 3d_s\omega + \omega^2\right)}{d_s^2 + (1-2d_s)\omega}, \qquad s = 0, 1, 2. \tag{9}$$

In Equation (9), $\omega = \omega^{\mathrm{JS}}$ is recommended according to the theoretical analysis of WENO-M by Henrick in [25] where the good properties of ω^{JS} to guarantee the success of the mapped function have been analyzed very carefully. Actually, $\omega = \omega^{\mathrm{JS}}$ is commonly used in almost all maping functions [9,27–32] although some other kind of nonlinear weights may also be available.

We can verify that $\left(g^{\mathrm{M}}\right)_s(\omega)$ meets the conditions in Equation (8) as it is a non-decreasing monotone function on $[0, 1]$ with finite slopes and satisfies the following properties.

Lemma 1. *The mapping function* $\left(g^{\mathrm{M}}\right)_s(\omega)$ *defined by Equation (9) satisfies:*

C1. $0 \le \left(g^{\mathrm{M}}\right)_s(\omega) \le 1, \left(g^{\mathrm{M}}\right)_s(0) = 0, \left(g^{\mathrm{M}}\right)_s(1) = 1;$
C2. $\left(g^{\mathrm{M}}\right)_s(d_s) = d_s;$
C3. $\left(g^{\mathrm{M}}\right)_s'(d_s) = \left(g^{\mathrm{M}}\right)_s''(d_s) = 0.$

Following Henrick's idea, a great many improved mapping functions were successfully proposed [9,27–32]. To clarify our major concern and provide convenience to readers but for brevity in the description, we only state some mapping functions in the following context, and we refer to references for properties similar to Lemma 1 and more details of these mapping functions.

■ WENO-IM(k, A) [27]

$$\left(g^{\mathrm{IM}}\right)_s(\omega; k, A) = d_s + \frac{\left(\omega - d_s\right)^{k+1} A}{\left(\omega - d_s\right)^k A + \omega(1-\omega)}, \quad A > 0, k = 2n, n \in \mathbb{N}^+. \tag{10}$$

■ WENO-PMk [29]

$$\left(g^{\mathrm{PM}}\right)_s(\omega) = c_1(\omega - d_s)^{k+1}(\omega + c_2) + d_s, \qquad k \ge 2, \tag{11}$$

where c_1, c_2 are constants with specified parameters k and d_s, taking the following forms

$$c_1 = \begin{cases} (-1)^k \dfrac{k+1}{d_s^{k+1}}, & 0 \le \omega \le d_s, \\ -\dfrac{k+1}{(1-d_s)^{k+1}}, & d_s < \omega \le 1, \end{cases} \qquad c_2 = \begin{cases} \dfrac{d_s}{k+1}, & 0 \le \omega \le d_s, \\ \dfrac{d_s - (k+2)}{k+1}, & d_s < \omega \le 1. \end{cases}$$

■ WENO-PPMn [30]

$$\left(g_s^{\mathrm{PPM}n}\right)_s(\omega) = \begin{cases} \left(g_{s,\mathrm{L}}^{\mathrm{PPM}n}\right)_s(\omega), & \omega \in [0, d_s] \\ \left(g_{s,\mathrm{R}}^{\mathrm{PPM}n}\right)_s(\omega), & \omega \in (d_s, 1], \end{cases} \tag{12}$$

and for $n = 5$,

$$\left(g_{s,\mathrm{L}}^{\mathrm{PPM5}}\right)_s(\omega) = d_s\left(1 + (a-1)^5\right), \quad \left(g_{s,\mathrm{R}}^{\mathrm{PPM5}}\right)_s(\omega) = d_s + b^4\left(\omega - d_s\right)^5. \tag{13}$$

where $a = \omega/d_s, b = 1/(d_s - 1)$.

■ WENO-RM$(mn0)$ [28]

$$\left(g^{\mathrm{RM}}\right)_s(\omega) = d_s + \frac{(\omega - d_s)^{n+1}}{a_0 + a_1\omega + \cdots + a_{m+1}\omega^{m+1}}, \quad m \le n \le 8, \tag{14}$$

where

$$\begin{cases} a_i = C_{n+1}^i(-d_s)^{n-i}, \quad i = 0, 1, \cdots, m, \\ a_{m+1} = (1-d_s)^n - \sum_{i=0}^{m} a_i. \end{cases} \tag{15}$$

Furthermore, $m = 2, n = 6$ is recommended in [28], then

$$\left(g^{\mathrm{RM}}\right)_s(\omega) = d_s + \frac{(\omega - d_s)^7}{a_0 + a_1\omega + a_2\omega^2 + a_3\omega^3}, \quad \omega \in [0,1] \tag{16}$$

where

$$a_0 = d_s^6, \quad a_1 = -7d_s^5, \quad a_2 = 21d_s^4, \quad a_3 = (1-d_s)^6 - \sum_{i=0}^{2} a_i. \tag{17}$$

■ WENO-MAIM1 [31]

$$\left(g^{\mathrm{MAIM1}}\right)_s(\omega) = d_s + \frac{f^{\mathrm{FIM}} \cdot (\omega - d_s)^{k+1}}{f^{\mathrm{FIM}} \cdot (\omega - d_s)^k + \omega^{\frac{d_s}{m_s\omega + \epsilon_{\mathrm{A}}}}(1-\omega)^{\frac{1-d_s}{m_s(1-\omega)+\epsilon_{\mathrm{A}}}}}, \tag{18}$$

with

$$f^{\mathrm{FIM}} = A\left(\frac{1+(-1)^k}{2} + \frac{1+(-1)^{k+1}}{2} \cdot \mathrm{sgm}(\omega - d_s, \delta, 1, k)\right), \tag{19}$$

and

$$\mathrm{sgm}(x, \delta, B, k) = \begin{cases} \dfrac{x}{|x|}, & |x| \ge \delta, \\ \dfrac{x}{\left(B\left(\delta^2 - x^2\right)\right)^{k+3} + |x|}, & |x| < \delta. \end{cases} \tag{20}$$

In Equations (18)–(20), $k \in \mathbb{N}^+, A > 0, \delta > 0$ with $\delta \to 0$, ϵ_{A} is a very small positive number to prevent the denominator from becoming zero, and $m_s \in \left[\frac{\alpha_s}{k+1}, M\right)$ with M being a finite positive constant real number and α_s a positive constant that only depends on s in the fifth-order WENO-MAIM1 scheme. In Equation (20), the positive parameter B is a scale transformation factor introduced to adjust the shape of the mapping function and it is set to be 1 in WENO-MAIM1 while to be other values in the following WENO-ACM schemes.

■ WENO-ACM [32]

$$\left(g^{\mathrm{ACM}}\right)_s(\omega) = \begin{cases} \dfrac{d_s}{2}\mathrm{sgm}(\omega - \mathrm{CFS}_s, \delta_s, B, k) + \dfrac{d_s}{2}, & \omega \le d_s, \\ \dfrac{1-d_s}{2}\mathrm{sgm}(\omega - \overline{\mathrm{CFS}}_s, \delta_s, B, k) + \dfrac{1+d_s}{2}, & \omega > d_s, \end{cases} \tag{21}$$

where $\mathrm{CFS}_s \in (0, d_s)$, $\overline{\mathrm{CFS}}_s = 1 - \frac{1-d_s}{d_s} \times \mathrm{CFS}_s$ with $\overline{\mathrm{CFS}}_s \in (d_s, 1)$, and $\delta_s < \min\left\{\mathrm{CFS}_s, d_s - \mathrm{CFS}_s, (1-d_s)\left(1 - \frac{\mathrm{CFS}_s}{d_s}\right), \frac{1-d_s}{d_s}\mathrm{CFS}_s\right\}$.

■ MIP-WENO-ACMk [9]

$$\left(g^{\mathrm{MIP-ACM}k}\right)_s(\omega) = \begin{cases} k_s\omega, & \omega \in [0, \mathrm{CFS}_s), \\ d_s, & \omega \in [\mathrm{CFS}_s, \overline{\mathrm{CFS}}_s], \\ 1 - k_s(1-\omega), & \omega \in (\overline{\mathrm{CFS}}_s, 1], \end{cases} \tag{22}$$

where $\mathrm{CFS}_s \in (0, d_s)$, $\overline{\mathrm{CFS}}_s = 1 - \frac{1-d_s}{d_s} \times \mathrm{CFS}_s$ with $\overline{\mathrm{CFS}}_s \in (d_s, 1)$, and $k_s \in \left[0, \frac{d_s}{\mathrm{CFS}_s}\right]$.

By using the mapping function $\left(g^{\mathrm{X}}\right)_s(\omega)$, where the superscript "X" corresponds to "M," "PM6," or "IM," etc., the nonlinear weights of the associated WENO-X scheme are defined as

$$\omega_s^{\mathrm{X}} = \frac{\alpha_s^{\mathrm{X}}}{\sum_{l=0}^{2} \alpha_l^{\mathrm{X}}}, \alpha_s^{\mathrm{X}} = \left(g^{\mathrm{X}}\right)_s(\omega_s^{\mathrm{JS}}), \quad s = 0, 1, 2,$$

where ω_s^{JS} are calculated by Equation (6).

In other studies, it has been analyzed and proved in detail that the WENO-X schemes can retain the optimal order of accuracy in smooth regions even at or near critical points.

3. A General Method to Introduce *Order-Preserving* Mapping for Mapped WENO Schemes

3.1. The OP-Mapped WENO

Before giving Definition 3 below, to maintain coherence and for the readers' convenience, we state the definition of *order-preserving/non-order-preserving* mapping and *OP/non-OP* point proposed in [9].

Definition 1 (*order-preserving/non-order-preserving* mapping)**.** *Suppose that* $\left(g^{\mathrm{X}}\right)_s(\omega), s = 0, \cdots, r-1$ *is a monotone increasing piecewise mapping function of the* $(2r-1)$*th-order mapped WENO-X scheme. If for* $\forall m, n \in \{0, \cdots, r-1\}$*, when* $\omega_m > \omega_n$*, we have*

$$\left(g^{\mathrm{X}}\right)_m(\omega_m) \geq \left(g^{\mathrm{X}}\right)_n(\omega_n). \tag{23}$$

and when $\omega_m = \omega_n$*, we have* $\left(g^{\mathrm{X}}\right)_m(\omega_m) = \left(g^{\mathrm{X}}\right)_n(\omega_n)$*, then we say the set of mapping functions* $\left\{\left(g^{\mathrm{X}}\right)_s(\omega), s = 0, \cdots, r-1\right\}$ *is* ***order-preserving (OP)****. Otherwise, we say the set of mapping functions* $\left\{\left(g^{\mathrm{X}}\right)_s(\omega), s = 0, \cdots, r-1\right\}$ *is* ***non-order-preserving (non-OP)****.*

Definition 2 (OP/non-OP point)**.** *Let* S^{2r-1} *denote the* $(2r-1)$*-point global stencil centered around* x_j*. Assume that* S^{2r-1} *is subdivided into r-point substencils* $\{S_0, \cdots, S_{r-1}\}$ *and* ω_s *are the nonlinear weights corresponding to the substencils* S_s *with* $s = 0, \cdots, r-1$*, which are used as the independent variables by the mapping function. Suppose that* $\left(g^{\mathrm{X}}\right)_s(\omega), s = 0, \cdots, r-1$ *is the mapping function of the mapped WENO-X scheme; then we say that a* ***non-OP*** *mapping process occurs at* x_j*, if* $\exists m, n \in \{0, \cdots, r-1\}$*, s.t.*

$$\begin{cases} (\omega_m - \omega_n)\left(\left(g^{\mathrm{X}}\right)_m(\omega_m) - \left(g^{\mathrm{X}}\right)_n(\omega_n)\right) < 0, & \text{if} \quad \omega_m \neq \omega_n, \\ \left(g^{\mathrm{X}}\right)_m(\omega_m) \neq \left(g^{\mathrm{X}}\right)_n(\omega_n), & \text{if} \quad \omega_m = \omega_n. \end{cases} \tag{24}$$

In addition, we say x_j *is a* ***non-OP point****. Otherwise, we say* x_j *is an* ***OP point****.*

Definition 3 (*OP*-Mapped WENO)**.** *The family of the mapped WENO schemes with OP mappings is collectively referred to as* ***OP-Mapped WENO*** *in our study.*

3.2. A General Formula for the Existing Mapping Functions

We rewrite the mapping function of the WENO-X scheme, that is, $\left(g^{\mathrm{X}}\right)_s(\omega), s = 0, 1, \cdots, r-1$, to be a general formula, given as

$$g^{\mathrm{X}}(\omega; m_{\mathrm{P}}, P_{s,1}, \cdots, P_{s,m_{\mathrm{P}}}) = \left(g^{\mathrm{X}}\right)_s(\omega), \tag{25}$$

where m_{P} is the number of the parameters related with s indicating the substencil, and $P_{s,1}, \cdots, P_{s,m_{\mathrm{P}}}$ are these parameters. Taking the WENO-IM(k, A) scheme as an example, besides the independent variable ω, there are the other three parameters in its mapping function (see Equation (10)), namely, d_s, k and A. It is easy to know that d_s is related to the substencil S_s, and k and A are not. Thus, for the WENO-IM(k, A) scheme, we have $m_{\mathrm{P}} = 1$ and $P_{s,1} = d_s$. We can also determine the value of m_{P} and the corresponding $P_{s,1}, \cdots, P_{s,m_{\mathrm{P}}}$

of other WENO schemes. Clearly, we have $m_{\mathrm{P}} = 0$ for the WENO-JS scheme and $m_{\mathrm{P}} \geq 1$ for other mapped WENO schemes. In Table 1, taking nine different WENO schemes as examples, we have presented their parameters of m_{P} and $P_{s,1}, \cdots, P_{s,m_{\mathrm{P}}}$. Let n_{X} denote the order of the specified critical point, namely, $\omega = d_s$, of the mapping function of the WENO-X scheme, that is, $\left(g^{\mathrm{X}}\right)_s'(d_s) = \cdots = \left(g^{\mathrm{X}}\right)_s^{(n_{\mathrm{X}})}(d_s) = 0, \left(g^{\mathrm{X}}\right)_s^{(n_{\mathrm{X}}+1)}(d_s) \neq 0$. To simplify the description of Theorem 2 below, we present n_{X} of the WENO-X scheme in the sixth column of Table 1.

Table 1. The parameters m_{P} and $P_{s,1}, \cdots, P_{s,m_{\mathrm{P}}}$ for the WENO-JS scheme and some existing mapped WENO schemes whose mapping functions are *non-OP*.

No.	Scheme, WENO-X	m_{P}	$P_{s,1}, \cdots, P_{s,m_{\mathrm{P}}}$	Parameters	n_{X}	Ref.
1	WENO-JS	0	None	None	None	See [8]
2	WENO-M	1	$P_{s,1} = d_s$	None	2	See [25]
3	WENO-IM(k, A)	1	$P_{s,1} = d_s$	$k = 2.0, A = 0.1$	k	See [27]
4	WENO-PMk	1	$P_{s,1} = d_s$	$k = 6$	k	See [29]
5	WENO-PPMn	1	$P_{s,1} = d_s$	$n = 5$	4	See [30]
6	WENO-RM(mn0)	1	$P_{s,1} = d_s$	$m = 2, n = 6$	3, 4	See [28]
7	WENO-MAIM1	2	$P_{s,1} = d_s, P_{s,2} = m_s$	$k = 10, A = 1.0\mathrm{e}{-6}, m_s = 0.06$	$k, k+1$	See [31]
8	WENO-ACM	2	$P_{s,1} = d_s, P_{s,2} = \mathrm{CFS}_s$	$A = 20, k = 2, \mu = 1\mathrm{e}{-6}, \mathrm{CFS}_s = d_s/10$	∞	See [32]
9	MIP-WENO-ACMk	3	$P_{s,1} = d_s, P_{s,2} = \mathrm{CFS}_s, P_{s,3} = k_s$	$k_s = 0.0, \mathrm{CFS}_s = d_s/10$	∞	See [9]

Lemma 2. *For the WENO-X scheme shown in Table 1, the mapping function* $\left(g^{\mathrm{X}}\right)_s(\omega), s = 0, 1, \cdots, r-1$ *is monotonically increasing over* $[0, 1]$.

Proof. See the corresponding references given in the last column of Table 1. □

3.3. The New Mapping Functions

Firstly, we give the **minDist** function by the following definition.

Definition 4 (**minDist** function)**.** *Define the* **minDist** *function as follows:*

$$\begin{cases} \textbf{minDist}\left(x_0, \cdots, x_{r-1}; d_0, \cdots, d_{r-1}; \omega\right) = x_{k^*}, \\ k^* = \min\left(\mathrm{IndexOf}\left(\min\left\{|\omega - d_0|, |\omega - d_1|, \cdots, |\omega - d_{r-1}|\right\}\right)\right), \end{cases} \tag{26}$$

where $d_s, s = 0, \cdots, r-1$ *is the optimal weight;* ω *is the nonlinear weight, being the independent variable of the mapping function; and the function* $\mathrm{IndexOf}(\cdot)$ *returns a set of the subscripts of "·"—that is, if* $\min\left\{|\omega - d_0|, |\omega - d_1|, \cdots, |\omega - d_{r-1}|\right\} = |\omega - d_{m_1}| = |\omega - d_{m_2}| = \cdots = |\omega - d_{m_M}|$, *then*

$$\mathrm{IndexOf}\left(\min\left\{|\omega - d_0|, |\omega - d_1|, \cdots, |\omega - d_{r-1}|\right\}\right) = \left\{m_1, m_2, \cdots, m_M\right\}. \tag{27}$$

Let $\mathcal{D} = \left\{d_0, d_1, \cdots, d_{r-1}\right\}$ be an array of all the ideal weights of the $(2r-1)$th-order WENO schemes. We build a new array by sorting the elements of $\mathcal{D}$ in ascending order—that is, $\widetilde{\mathcal{D}} = \left\{\widetilde{d}_0, \widetilde{d}_1, \cdots, \widetilde{d}_{r-1}\right\}$. In other words, the arrays $\mathcal{D}$ and $\widetilde{\mathcal{D}}$ have the same elements with different arrangements, and the elements of $\widetilde{\mathcal{D}}$ satisfy

$$0 < \widetilde{d}_0 < \widetilde{d}_1 < \cdots < \widetilde{d}_{r-1} < 1. \tag{28}$$

Definition 5. *Let* $\mathcal{G} = \left\{\left(g^{\mathrm{X}}\right)_0(\omega), \left(g^{\mathrm{X}}\right)_1(\omega), \cdots, \left(g^{\mathrm{X}}\right)_{r-1}(\omega)\right\}$ *be an array of all the mapping functions of the* $(2r-1)$*th-order mapped WENO-X scheme. We define a new array by sorting*

the elements of $\mathcal{G}$ *in a new order—that is,* $\widetilde{\mathcal{G}} = \left\{ \widetilde{(g^{\mathrm{X}})}_0(\omega), \widetilde{(g^{\mathrm{X}})}_1(\omega), \cdots, \widetilde{(g^{\mathrm{X}})}_{r-1}(\omega) \right\}$, *where* $\widetilde{(g^{\mathrm{X}})}_s(\omega)$ *is the mapping function associated with* $\widetilde{d}_s$.

Lemma 3. *Denote* $\widetilde{d}_{-1} = 0, \widetilde{d}_r = 1$. *Let* $\mathring{d}_{-1} = \widetilde{d}_{-1}, \mathring{d}_0 = \frac{\widetilde{d}_0+\widetilde{d}_1}{2}, \cdots, \mathring{d}_{r-2} = \frac{\widetilde{d}_{r-2}+\widetilde{d}_{r-1}}{2}, \mathring{d}_{r-1} = \widetilde{d}_r$. *For* $\forall i = 0, 1, \cdots, r-1$, *if* $\omega \in (\mathring{d}_{i-1}, \mathring{d}_i]$, *then*

$$\min\left(\text{IndexOf}\left(\min\left\{|\omega - \widetilde{d}_0|, |\omega - \widetilde{d}_1|, \cdots, |\omega - \widetilde{d}_{r-1}|\right\}\right)\right) = i.$$

Proof. (1) We first prove the cases of $i = 1, \cdots, r-2$. When $\widetilde{d}_i \le \omega \le \frac{\widetilde{d}_i+\widetilde{d}_{i+1}}{2}$, as Equation (28) holds, we get

$$\begin{cases} 0 \le \omega - \widetilde{d}_i \le \widetilde{d}_{i+1} - \omega < \cdots < \widetilde{d}_{r-1} - \omega, \\ 0 \le \omega - \widetilde{d}_i < \omega - \widetilde{d}_{i-1} < \cdots < \omega - \widetilde{d}_0. \end{cases} \tag{29}$$

Similarly, when $\frac{\widetilde{d}_{i-1}+\widetilde{d}_i}{2} < \omega < \widetilde{d}_i$, we get

$$\begin{cases} 0 < \widetilde{d}_i - \omega < \omega - \widetilde{d}_{i-1} < \cdots < \omega - \widetilde{d}_0, \\ 0 < \widetilde{d}_i - \omega < \widetilde{d}_{i+1} - \omega < \cdots < \widetilde{d}_{r-1} - \omega. \end{cases} \tag{30}$$

Then, according to Equations (29) and (30), we obtain

$$\begin{aligned} &\min\left\{|\omega - \widetilde{d}_0|, \cdots, |\omega - \widetilde{d}_{i-1}|, |\omega - \widetilde{d}_i|, |\omega - \widetilde{d}_{i+1}|, \cdots, |\omega - \widetilde{d}_{r-1}|\right\} \\ =&|\omega - \widetilde{d}_i| = |\omega - \widetilde{d}_{i+1}|, \end{aligned} \tag{31}$$

where $i = 1, \cdots, r-2$ and the last equality holds if and only if $\omega - \widetilde{d}_i = \widetilde{d}_{i+1} - \omega$.

(2) For the case of $i = 0$, we know that $\omega \in (\mathring{d}_{-1}, \mathring{d}_0] = \left(0, \frac{\widetilde{d}_0+\widetilde{d}_1}{2}\right]$. When $\widetilde{d}_0 \le \omega \le \frac{\widetilde{d}_0+\widetilde{d}_1}{2}$, we have

$$0 \le \omega - \widetilde{d}_0 \le \widetilde{d}_1 - \omega < \cdots < \widetilde{d}_{r-1} - \omega. \tag{32}$$

Additionally, when $0 < \omega < \widetilde{d}_0$, we have

$$0 < \widetilde{d}_0 - \omega < \widetilde{d}_1 - \omega < \cdots < \widetilde{d}_{r-1} - \omega. \tag{33}$$

Then, according to Equations (32) and (33), we obtain

$$\begin{aligned} &\min\left\{|\omega - \widetilde{d}_0|, \cdots, |\omega - \widetilde{d}_{i-1}|, |\omega - \widetilde{d}_i|, |\omega - \widetilde{d}_{i+1}|, \cdots, |\omega - \widetilde{d}_{r-1}|\right\} \\ =&|\omega - \widetilde{d}_0| = |\omega - \widetilde{d}_1|, \end{aligned} \tag{34}$$

where the last equality holds if and only if $\omega - \widetilde{d}_0 = \widetilde{d}_1 - \omega$.

(3) As the proof of the case of $i = r-1$ is very similar to that of the case $i = 0$, we do not state it here for simplicity. Additionally, we can get that, if $\omega \in (\mathring{d}_{r-2}, \mathring{d}_{r-1}]$, then

$$\min\left\{|\omega - \widetilde{d}_0|, \cdots, |\omega - \widetilde{d}_{i-1}|, |\omega - \widetilde{d}_i|, |\omega - \widetilde{d}_{i+1}|, \cdots, |\omega - \widetilde{d}_{r-1}|\right\} = |\omega - \widetilde{d}_{r-1}|. \tag{35}$$

(4) Thus, according to Equation (4) and Equations (31), (34), and (35), we obtain

$$\min\left(\text{IndexOf}\left(\min\left\{|\omega-\widetilde{d}_0|,\cdots,|\omega-\widetilde{d}_{i-1}|,|\omega-\widetilde{d}_i|,\right.\right.\right.$$
$$\left.\left.\left.|\omega-\widetilde{d}_{i+1}|,\cdots,|\omega-\widetilde{d}_{r-1}|\right\}\right)\right)=i.$$

Now, we have finished the proof of Lemma 3. □

For simplicity of description and according to Lemma 3, we introduce intervals Ω_i defined as follows.

$$\Omega_i=\left\{\omega|\textbf{minDist}(\widetilde{d}_0,\widetilde{d}_1,\cdots,\widetilde{d}_{r-1};\widetilde{d}_0,\widetilde{d}_1,\cdots,\widetilde{d}_{r-1};\omega)=\widetilde{d}_i\right\}=(\mathring{d}_{i-1},\mathring{d}_i], \tag{36}$$

where $i=0,1,\cdots,r-1$.

If $\omega\in\Omega=(0,1]$, it is trivial to verify that: (1) $\Omega=\Omega_0\bigcup\Omega_1\bigcup\cdots\bigcup\Omega_{r-1}$; (2) for $\forall i,j=0,1,\cdots,r-1$ and $i\neq j$, $\Omega_i\bigcap\Omega_j=\varnothing$.

Lemma 4. *Let $a,b\in\{0,1,\cdots,r-1\}$ and WENO-X be the scheme shown in Table 1. For $\forall a\geq b$ and $\omega_\alpha\in\Omega_a,\omega_\beta\in\Omega_b$, we have the following properties: C1. If $a=b$ and $\omega_\alpha>\omega_\beta$, then $\widetilde{\left(g^{\mathrm{X}}\right)}_a(\omega_\alpha)\geq\widetilde{\left(g^{\mathrm{X}}\right)}_b(\omega_\beta)$; C2. If $a=b$ and $\omega_\alpha=\omega_\beta$, then $\widetilde{\left(g^{\mathrm{X}}\right)}_a(\omega_\alpha)=\widetilde{\left(g^{\mathrm{X}}\right)}_b(\omega_\beta)$; C3. If $a>b$, then $\omega_\alpha>\omega_\beta$, $\widetilde{\left(g^{\mathrm{X}}\right)}_a(\omega_\alpha)>\widetilde{\left(g^{\mathrm{X}}\right)}_b(\omega_\beta)$.*

Proof. (1) We can directly get properties *C1* and *C2* from Lemma 2. (2) As $a>b$, according to Equations (28) and (36), we know that the interval Ω_a must be on the right side of the interval Ω_b, and $\omega_\alpha\in\Omega_a,\omega_\beta\in\Omega_b$ is given, then we get $\omega_\alpha>\omega_\beta$. Trivially, according to Definition 5, or by intuitively observing the curves of the mapping function $\widetilde{\left(g^{\mathrm{X}}\right)}_s(\omega)$ as shown in Figure 1, we can obtain $\widetilde{\left(g^{\mathrm{X}}\right)}_a(\omega_\alpha)>\widetilde{\left(g^{\mathrm{X}}\right)}_b(\omega_\beta)$. Thus, *C3* is proved. □

By employing the **minDist** function, we built a general method to introduce the *OP* criterion into the existing mappings which are *non-OP*. The general method is stated in Algorithm 1. It is worthy to note that Algorithm 1 actually does some sorting of the parameters of $P_{s,1},\cdots,P_{s,m_{\mathrm{P}}}$ in Equation (25), and this plays an important role in constructing the *OP* mappings from the existing *non-OP* mappings.

Theorem 1. *The set of mapping functions $\left\{\left(g^{\mathrm{MOP-X}}\right)_s(\omega_s^{\mathrm{JS}}),s=0,1,\cdots,r-1\right\}$ obtained through Algorithm 1 is OP.*

Proof. Let $\omega_m^{\mathrm{JS}},\omega_n^{\mathrm{JS}}\in[0,1]$ and $\forall m,n\in\{0,1,\cdots,r-1\}$. According to Algorithm 1 and without loss of generality, we can assume that $\omega_m^{\mathrm{JS}}\in\Omega_{k_m^*},\omega_n^{\mathrm{JS}}\in\Omega_{k_n^*}$, and then we get

$$\begin{cases}\left(g^{\mathrm{MOP-X}}\right)_m(\omega_m^{\mathrm{JS}})=g^{\mathrm{X}}\left(\omega_m^{\mathrm{JS}};m_{\mathrm{P}},P_{k_m^*,1},\cdots,P_{k_m^*,m_{\mathrm{P}}}\right),\\ \left(g^{\mathrm{MOP-X}}\right)_n(\omega_n^{\mathrm{JS}})=g^{\mathrm{X}}\left(\omega_n^{\mathrm{JS}};m_{\mathrm{P}},P_{k_n^*,1},\cdots,P_{k_n^*,m_{\mathrm{P}}}\right).\end{cases}$$

It is easy to verify that

$$\begin{cases}g^{\mathrm{X}}\left(\omega_m^{\mathrm{JS}};m_{\mathrm{P}},P_{k_m^*,1},\cdots,P_{k_m^*,m_{\mathrm{P}}}\right)=\widetilde{\left(g^{\mathrm{X}}\right)}_{k_m^*}(\omega_m^{\mathrm{JS}}),\\ g^{\mathrm{X}}\left(\omega_n^{\mathrm{JS}};m_{\mathrm{P}},P_{k_n^*,1},\cdots,P_{k_n^*,m_{\mathrm{P}}}\right)=\widetilde{\left(g^{\mathrm{X}}\right)}_{k_n^*}(\omega_n^{\mathrm{JS}}).\end{cases}$$

Therefore, according to Lemma 4, we can finish the proof trivially. □

We now define the modified weights which are *OP* as follows:

$$\omega_s^{\mathrm{MOP-X}} = \frac{\alpha_s^{\mathrm{MOP-X}}}{\sum_{l=0}^{r-1} \alpha_l^{\mathrm{MOP-X}}}, \quad \alpha_s^{\mathrm{MOP-X}} = \left(g^{\mathrm{MOP-X}}\right)_s(\omega_s^{\mathrm{JS}}), \quad s = 0, \cdots, r-1, \tag{37}$$

where $\left(g^{\mathrm{MOP-X}}\right)_s(\omega_s^{\mathrm{JS}})$ is obtained from Algorithm 1. The associated scheme will be referred to as MOP-WENO-X.

The mapping functions of the WENO-X schemes presented in Table 1 and those of the associated MOP-WENO-X schemes are shown in Figure 1. We can find that, for the mapping functions of the MOP-WENO-X schemes: (1) the monotonicity over the whole domain $(0, 1)$ is maintained; (2) the differentiability is reduced and limited to the neighborhood of the optimal weights d_s; (3) the *OP* property is obtained. We summarize these properties as follows.

Algorithm 1: A general method to construct *OP* mappings.

input : s, index indicating the substencil S_s and $s = 0, 1, \cdots, r-1$
d_s, optimal weights
ω_s^{JS}, nonlinear weights computed by the WENO-JS scheme
m_{P}, the number of the parameters related with s
$P_{s,j}$, parameters related with s and $j = 1, \cdots, m_{\mathrm{P}}$

output: $\left\{\left(g^{\mathrm{MOP-X}}\right)_s(\omega_s^{\mathrm{JS}}), s = 0, 1, \cdots, r-1\right\}$, the new set of mapping functions that is *OP*

$\left(g^{\mathrm{X}}\right)_s(\omega), s = 0, 1, \cdots, r-1$ *is a monotonically increasing mapping function over* $[0, 1]$, *and the set of mapping functions* $\left\{\left(g^{\mathrm{X}}\right)_s(\omega), s = 0, 1, \cdots, r-1\right\}$ *is non-OP*;

```
// implementation of the ''minDist'' function in Definition 4
for s = 0; s ≤ r − 1; s++ do
    // get k* in Equation (26)
    set d^min = |ω_s^JS − d_0|, k_s^* = 0;
    for i = 1; i ≤ r − 1; i++ do
        if |ω_s^JS − d_i| < d^min then
            d^min = |ω_s^JS − d_i|,
            k_s^* = i;
        end
    end
    // remark: the for loop above indicates that ω_s^JS ∈ Ω_{k_s^*}
    // get x_{k^*} in Equation (26)
    for j = 1; j ≤ m_P; j++ do
        P̄_{s,j} = P_{k_s^*, j};
    end
end
// get (g^{MOP-X})_s(ω_s^JS)
for s = 0; s ≤ r − 1; s++ do
    (g^{MOP-X})_s(ω_s^JS) = g^X(ω_s^JS; m_P, P̄_{s,1}, ..., P̄_{s,m_P}).
end
```

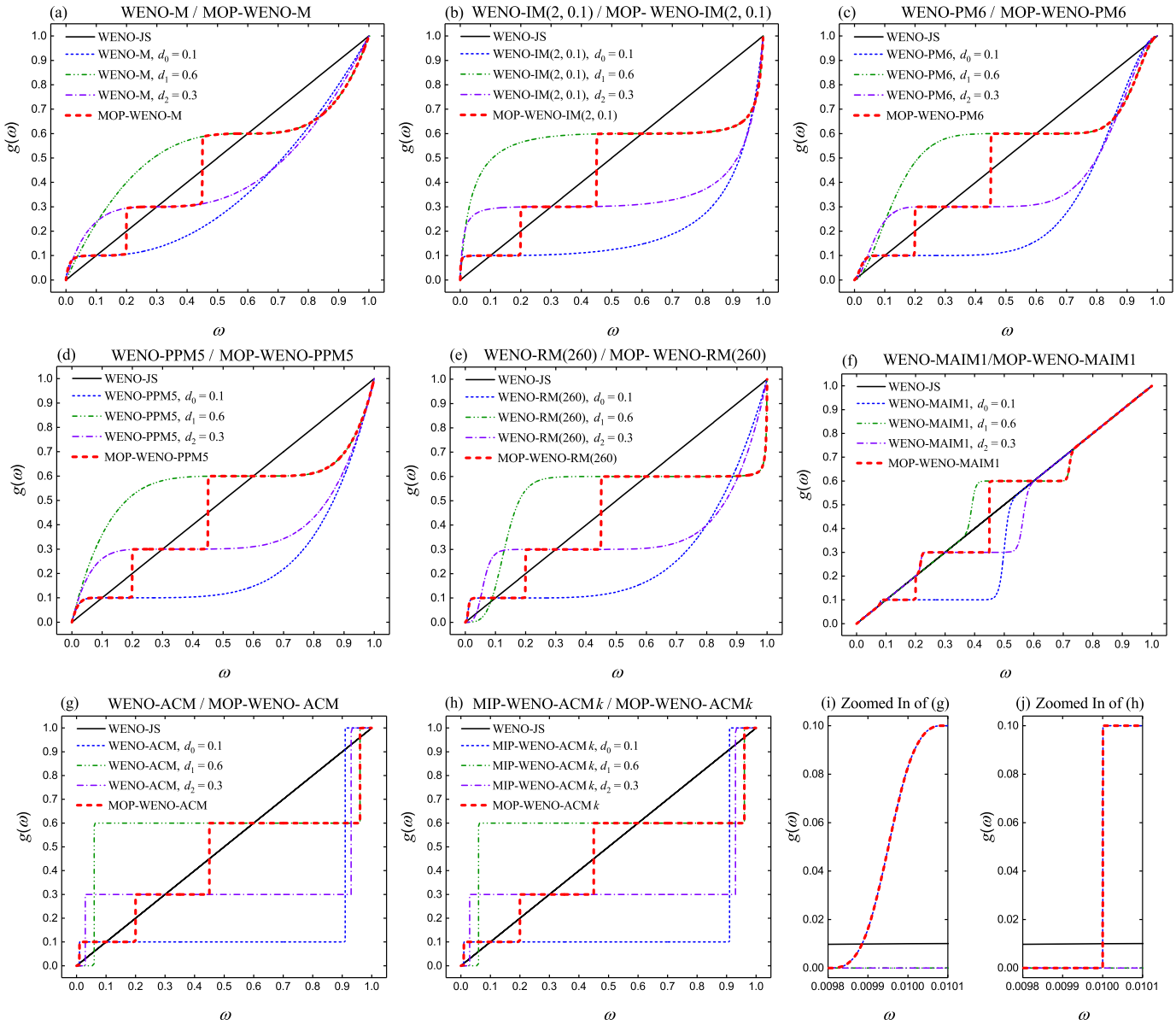

Figure 1. A comparison of the mapping functions for WENO-X (shown in Table 1) and MOP-WENO-X.

Theorem 2. *Let* $\overline{\Omega}_i = \left\{\omega \in \Omega_i \cap \omega \neq \partial\Omega_i\right\}, i = 0, 1, \cdots, r-1$. *The mapping function* $\left(g^{\mathrm{MOP-X}}\right)_s(\omega)$ *obtained from Althorithm 1 satisfies the following properties:*

C1. For $\forall\omega \in \overline{\Omega}_i, i = 0, 1, \cdots, r-1$, $\left(g^{\mathrm{MOP-X}}\right)_s'(\omega) \geq 0$;

C2. For $\forall\omega \in \Omega$, $0 \leq \left(g^{\mathrm{MOP-X}}\right)_s(\omega) \leq 1$, *and* $\left(g^{\mathrm{MOP-X}}\right)_s(0) = 0, \left(g^{\mathrm{MOP-X}}\right)_s(1) = 1$;

C3. For $\forall s \in \left\{0, 1, \cdots, r-1\right\}$, $\widetilde{d}_s \in \Omega_s$, *and* $\left(g^{\mathrm{MOP-X}}\right)_s(\widetilde{d}_s) = \widetilde{d}_s, \left(g^{\mathrm{MOP-X}}\right)_s'(\widetilde{d}_s) = \cdots = \left(g^{\mathrm{MOP-X}}\right)_s^{(n_X)}(\widetilde{d}_s) = 0$ *where* n_X *is given in Table 1;*

C4. $\left(g^{\mathrm{MOP-X}}\right)_s'(0) = \left(g^{\mathrm{X}}\right)_s'(0), \left(g^{\mathrm{MOP-X}}\right)_s'(1) = \left(g^{\mathrm{X}}\right)_s'(1)$;

C5. For $\forall m, n \in \left\{0, \cdots, r-1\right\}$, *if* $\omega_m > \omega_n$, *then* $\left(g^{\mathrm{MOP-X}}\right)_m(\omega_m) \geq \left(g^{\mathrm{MOP-X}}\right)_n(\omega_n)$, *and if* $\omega_m = \omega_n$, *then* $\left(g^{\mathrm{MOP-X}}\right)_m(\omega_m) = \left(g^{\mathrm{MOP-X}}\right)_n(\omega_n)$.

Remark 1. *(1) The properties C1–C3 are designed to recover the optimal convergence rate of accuracy in a smooth region even in the presence of critical points, and the detailed theoretical analysis has been proposed in Section 5 of [25], Section 3.2 of [27], Section 3.1 of [29], etc. (2) The property C4 is designed to decrease the effect from non-smooth stencils, and we refer to Sections 3.1*

and 3.2 of [29], Remark 1 of [28], Section 2.2 of [30], and Section 3.3 of [31] for more details. (3) The property C5 is designed to enhance the performance for long-output-time simulations and to remove or reduce post-shock numerical oscillations, and we have analyzed this in [9] systematically and carefully.

3.4. Convergence Properties

According to Theorem 2, we get the convergence properties for the $(2r-1)$th-order MOP-WENO-X schemes as given in Theorem 3. The proof is almost identical to that of the associated WENO-X schemes in the references presented in Table 1.

Theorem 3. *The requirements for the $(2r-1)$th-order MOP-WENO-X schemes to achieve the optimal order of accuracy are identical to that of the associated $(2r-1)$th-order WENO-X schemes.*

For the integrity of this paper and the benefit of the reader, we concisely express the following Corollaries of Theorem 3.

Corollary 1. *If n mapping is used in the $(2r-1)$th-order MOP-WENO-M scheme, then for different values of n_{cp}, the weights $\omega_s^{\mathrm{MOP-M}}$ in the $(2r-1)$th-order MOP-WENO-M scheme satisfy*

$$\omega_s^{\mathrm{MOP-M}} - d_s = O\Big((\Delta x)^{3^n\times(r-1-n_{\mathrm{cp}})}\Big), \quad r = 2,3,\cdots,9, \quad n_{\mathrm{cp}} = 0,1,\cdots,r-1,$$

and the rate of convergence is

$$r_{\mathrm{c}} = \begin{cases} 2r-1, & \text{if} \quad n_{\mathrm{cp}} = 0,\cdots,\left\lfloor \dfrac{3^n-1}{3^n}r-1 \right\rfloor, \\ (3^n+1)(r-1)-3^n\times n_{\mathrm{cp}}, & \text{if} \quad n_{\mathrm{cp}} = \left\lfloor \dfrac{3^n-1}{3^n}r-1 \right\rfloor+1,\cdots,r-1, \end{cases}$$

where $\lfloor x \rfloor$ is a floor function of x.

Proof. The proof is almost identical to that of Lemma 6 in [31]. □

Corollary 2. *When $n_{\mathrm{cp}} = 1$, the $(2r-1)$th-order MOP-WENO-IM(k, A) schemes can achieve the optimal order of accuracy if the mapping function $\left(g^{\mathrm{MOP-IM}}\right)_s(\omega)$ is applied to the original weights in the $(2r-1)$th-order WENO-JS schemes with the requirement of $k \geq 2$ (except for the case of $r = 2$).*

Proof. The proof is almost identical to that of Theorem 2 in [27]. □

Corollary 3. *The $(2r-1)$th-order MOP-WENO-PMk schemes can achieve the optimal order of accuracy if the mapping function $\left(g^{\mathrm{MOP-PM}}\right)_s(\omega)$ is applied to the original weights in the $(2r-1)$th-order WENO-JS schemes with specific requirements for k in following different cases: (I) require $k \geq 1$ for $n_{\mathrm{cp}} = 0$; (II) require $k \geq 1$ for $n_{\mathrm{cp}} = 1$; (III) require $k \geq 3$ for $n_{\mathrm{cp}} = 2$.*

Proof. The proof is almost identical to that of Proposition 1 in [29]. □

Corollary 4. *The $(2r-1)$th-order MOP-WENO-RM(mn0) schemes can recover the optimal order of accuracy if the mapping function $\left(g^{\mathrm{MOP-RM}}\right)_s(\omega)$ is applied to the original weights in the $(2r-1)$th-order WENO-JS schemes with requirement of $n \geq \frac{1+n_{\mathrm{cp}}}{r-1-n_{\mathrm{cp}}}$ for different values of n_{cp} with $1 \leq n_{\mathrm{cp}} < r-1$.*

Proof. The proof is almost identical to that of Theorem 3 in [28]. □

Corollary 5. *Let $\lceil x \rceil$ be a ceiling function of x. For $n_{cp} < r-1$, the $(2r-1)$th-order MOP-WENO-MAIM1 schemes can achieve the optimal order of accuracy if the mapping function $(g^{\mathrm{MOP-MAIM1}})_s(\omega)$ is applied to the original weights in the $(2r-1)$th-order WENO-JS schemes with requirement of $k \geq k^{\mathrm{MAIM}}$, where*

$$k^{\mathrm{MAIM}} = \left\lceil \frac{r}{r-1-n_{cp}} - 2 \right\rceil + \frac{1 + \left(-1\right)^{\left\lceil \frac{r}{r-1-n_{cp}} - 2 \right\rceil}}{2}.$$

Proof. The proof is almost identical to that of Theorem 2 in [31]. □

Corollary 6. *For $n_{cp} < r-1$, the $(2r-1)$th-order MOP-WENO-ACM schemes can achieve the optimal order of accuracy if the mapping function $(g^{\mathrm{MOP-ACM}})_s(\omega)$ is applied to the original weights in the $(2r-1)$th-order WENO-JS schemes.*

Proof. The proof is almost identical to that of Theorem 2 in [32]. □

Corollary 7. *When $\mathrm{CFS}_s \ll \widetilde{d}_0$, for $n_{cp} < r-1$, the $(2r-1)$th-order MOP-WENO-ACMk schemes can achieve the optimal order of accuracy if the mapping function $(g^{\mathrm{MOP-ACM}k})_s(\omega)$ is applied to the original weights in the $(2r-1)$th-order WENO-JS schemes.*

Proof. The proof is almost identical to that of Theorem 2 in [9]. □

4. Numerical Results

In this section, we compare the numerical performances of the MOP-WENO-X schemes with the associated existing mapped WENO-X schemes shown in Table 1, and the classic WENO-JS scheme. To further demonstrate the superiority of the MOP-WENO-X schemes, some comparisons with other WENO type reconstructions, e.g., WENO-Z [26] (in Sections 4.1 and 4.2) and the central WENO schemes of WENO-NW6 [36], WENO-CU6 [37], and WENO-θ6 [38] (in Section 4.3), have also been performed. As the performances of the WENO-ACM scheme and the MOP-WENO-ACM scheme are almost identical to those of the MIP-WENO-ACM*k* scheme and the MOP-WENO-ACM*k* scheme, respectively, we do not present the solutions of the WENO-ACM scheme and the MOP-WENO-ACM scheme below for simplicity. It should be noted that although we mainly provide the solutions of the fifth-order WENO methods (WENO5) in present study, the methodology proposed in this paper can be successfully extended to higher order WENO methods, such as WENO-7 or WENO-9, and because of the space limitations, we do not show their solutions here.

Typical one-dimensional linear advection equation and two-dimensional Euler equations, with different initial conditions, are used to test the considered schemes. The presentation of these numerical tests in this section starts with the accuracy test of one-dimensional linear advection equation with four different initial conditions, followed by the long-output-time simulations of it with two different initial conditions, including discontinuities, and finishes with two-dimensional simulations on the shock-vortex interaction and the 2D Riemann problem. In all calculations below, ϵ is taken to be 10^{-40} for all schemes following the recommendations in [25,27].

In the following numerical tests, the ODEs resulting from the semi-discretized PDEs are marched in time using the following explicit, third-order, strong stability preserving (SSP) Runge–Kutta method [5,39,40]:

$$\begin{aligned}
\overrightarrow{U}^{*} &= \overrightarrow{U}^{n} + \Delta t \mathcal{L}(\overrightarrow{U}^{n}),\\
\overrightarrow{U}^{**} &= \frac{3}{4}\overrightarrow{U}^{n} + \frac{1}{4}\overrightarrow{U}^{*} + \frac{1}{4}\Delta t \mathcal{L}(\overrightarrow{U}^{*}),\\
\overrightarrow{U}^{n+1} &= \frac{1}{3}\overrightarrow{U}^{n} + \frac{2}{3}\overrightarrow{U}^{**} + \frac{2}{3}\Delta t \mathcal{L}(\overrightarrow{U}^{**}),
\end{aligned}$$

where $\vec{U}^*$, $\vec{U}^{**}$ are the intermediate stages, $\vec{U}^n$ is the value of $\vec{U}$ at time level $t^n = n\Delta t$, and Δt is the time step satisfying some proper CFL condition. The spatial operator $\mathcal{L}$ is defined as in Equation (3), and the WENO reconstructions will be applied to obtain it.

4.1. Accuracy Test

In this subsection, we solve the following one-dimensional linear advection equation:

$$\frac{\partial u}{\partial t} + \frac{\partial u}{\partial x} = 0, \quad -1 \le x \le 1, \tag{38}$$

with different initial conditions to test the accuracy of the considered WENO schemes. In all accuracy tests, the L_1, L_2, L_∞ norms of the error are given as

$$\begin{aligned} L_1 &= h \cdot \sum_j \left| u_j^{\text{exact}} - (u_h)_j \right|, \\ L_2 &= \sqrt{h \cdot \sum_j (u_j^{\text{exact}} - (u_h)_j)^2}, \\ L_\infty &= \max_j \left| u_j^{\text{exact}} - (u_h)_j \right|, \end{aligned}$$

where $h = \Delta x$ is the uniform spatial step size, $(u_h)_j$ is the numerical solution, and u_j^{exact} is the exact solution.

Example 1. *We calculate Equation (38) with the periodic boundary condition using the following initial condition [27]:*

$$u(x, 0) = \sin(\pi x). \tag{39}$$

It is trivial to verify that although the initial condition in Equation (39) has two first-order critical points, their first and third derivatives vanish simultaneously. It is known that the rate of the temporal convergence is $O(\Delta t^3)$ for the third-order Runge–Kutta method [5,39,40] and the CFL number is defined by $\text{CFL} = \frac{|\alpha|\Delta t}{\Delta x}$ leading to $\Delta t = \text{CFL} \cdot \frac{\Delta x}{|\alpha|}$ where $|\alpha| = 1$ here. Therefore, note that we consider only the fifth-order methods here, and to ensure that the error for the overall scheme is a measure of the spatial convergence only, we set the CFL number to be $(\Delta x)^{2/3}$. The calculation was run until a time of $t = 2.0$.

In Table 2, we show the L_1, L_2, L_∞ errors and corresponding convergence orders of various considered WENO schemes. Unsurprisingly, the MOP-WENO-X schemes and the associated WENO-X schemes, along with the WENO-Z scheme, provide more accurate results than the WENO-JS scheme do in general. Naturally and as expected, all the considered schemes have gained the fifth-order convergence rate of accuracy. It can be found that the results of the MOP-WENO-X schemes are identical to those of the associated WENO-X schemes for all grid numbers except $N = 10$. As discussed in [9], the cause of the accuracy loss for the computing cases of all MOP-WENO-X schemes with $N = 10$ is that the mapping functions of the MOP-WENO-X schemes have narrower optimal weight intervals (standing for the intervals about $\omega = d_s$ over which the mapping process attempts to use the corresponding optimal weights; see [31,32]) than the associated WENO-X schemes.

Figure 2 shows the overall L_∞ convergence behavior of various considered schemes. We can observe that: (1) the solutions of all schemes converge at fifth-order, as evidenced by the slope of the lines; (2) the MOP-WENO-X schemes and their associated WENO-X schemes, along with the WENO-Z scheme, are significantly more accurate than the classic WENO-JS scheme; (3) the errors and convergence orders of the MOP-WENO-X schemes are almost identical to those of their associated WENO-X schemes.

We use this example to discuss the computational cost of the MOP-WENO-X scheme compared with its associated WENO-X scheme and the classic WENO-JS scheme. In Figure 3, we drew the graphs for the CPU time versus the computing errors (we only present the results of the L_∞-norm error here just for the sake of brevity in the presentation,

hereinafter the same). From Figure 3, we can easily see that: (1) generally speaking, the MOP-WENO-X schemes have better efficiency than the WENO-JS scheme; (2) for all MOP-WENO-X schemes except the case of "X = M," they perform almost identically to their associated WENO-X schemes; (3) for the MOP-WENO-M scheme, it has a slightly lower efficiency than its associated WENO-M scheme and it has significantly higher efficiency than the WENO-JS scheme.

Table 2. Convergence properties of considered schemes on solving $u_t + u_x = 0$ with initial condition $u(x,0) = \sin(\pi x)$. To be continued.

Scheme	N	L_1 Error	L_1 Order	L_2 Error	L_2 Order	L_∞ Error	L_∞ Order
WENO-JS	10	6.18328×10^{-2}	-	4.72306×10^{-2}	-	4.87580×10^{-2}	-
	20	2.96529×10^{-3}	4.3821	2.42673×10^{-3}	4.2826	2.57899×10^{-3}	4.2408
	40	9.27609×10^{-5}	4.9985	7.64332×10^{-5}	4.9887	9.05453×10^{-5}	4.8320
	80	2.89265×10^{-6}	5.0031	2.33581×10^{-6}	5.0322	2.90709×10^{-6}	4.9610
	160	9.03392×10^{-8}	5.0009	7.19259×10^{-8}	5.0213	8.85753×10^{-8}	5.0365
	320	2.82330×10^{-9}	4.9999	2.23105×10^{-9}	5.0107	2.72458×10^{-9}	5.0228
WENO-Z	10	1.64485×10^{-2}	-	1.27535×10^{-2}	-	1.18974×10^{-2}	-
	20	5.04450×10^{-4}	5.0271	3.98253×10^{-4}	5.0011	3.94040×10^{-4}	4.9162
	40	1.59132×10^{-5}	4.9864	1.25050×10^{-5}	4.9931	1.24948×10^{-5}	4.9789
	80	4.98858×10^{-7}	4.9955	3.91834×10^{-7}	4.9961	3.91804×10^{-7}	4.9951
	160	1.56020×10^{-8}	4.9988	1.22541×10^{-8}	4.9989	1.22538×10^{-8}	4.9988
	320	4.88356×10^{-10}	4.9977	3.83568×10^{-10}	4.9976	3.83541×10^{-10}	4.9977
WENO-M	10	2.01781×10^{-2}	-	1.55809×10^{-2}	-	1.47767×10^{-2}	-
	20	5.18291×10^{-4}	5.2829	4.06148×10^{-4}	5.2616	3.94913×10^{-4}	5.2256
	40	1.59422×10^{-5}	5.0228	1.25236×10^{-5}	5.0193	1.24993×10^{-5}	4.9816
	80	4.98914×10^{-7}	4.9979	3.91875×10^{-7}	4.9981	3.91808×10^{-7}	4.9956
	160	1.56021×10^{-8}	4.9990	1.22541×10^{-8}	4.9991	1.22538×10^{-8}	4.9988
	320	4.88356×10^{-10}	4.9977	3.83568×10^{-10}	4.9976	3.83541×10^{-10}	4.9977
MOP-WENO-M	10	3.64427×10^{-2}	-	2.95270×10^{-2}	-	2.81876×10^{-2}	-
	20	5.18291×10^{-4}	6.1357	4.06148×10^{-4}	6.1839	3.94913×10^{-4}	6.1574
	40	1.59422×10^{-5}	5.0228	1.25236×10^{-5}	5.0193	1.24993×10^{-5}	4.9816
	80	4.98914×10^{-7}	4.9979	3.91875×10^{-7}	4.9981	3.91808×10^{-7}	4.9956
	160	1.56021×10^{-8}	4.9990	1.22541×10^{-8}	4.9991	1.22538×10^{-8}	4.9988
	320	4.88356×10^{-10}	4.9977	3.83568×10^{-10}	4.9976	3.83541×10^{-10}	4.9977
WENO-IM(2, 0.1)	10	1.58051×10^{-2}	-	1.23553×10^{-2}	-	1.19178×10^{-2}	-
	20	5.04401×10^{-4}	4.9697	3.96236×10^{-4}	4.9626	3.94458×10^{-4}	4.9171
	40	1.59160×10^{-5}	4.9860	1.25033×10^{-5}	4.9860	1.24963×10^{-5}	4.9803
	80	4.98863×10^{-7}	4.9957	3.91836×10^{-7}	4.9959	3.91797×10^{-7}	4.9953
	160	1.56020×10^{-8}	4.9988	1.22541×10^{-8}	4.9989	1.22538×10^{-8}	4.9988
	320	4.88355×10^{-10}	4.9977	3.83568×10^{-10}	4.9976	3.83547×10^{-10}	4.9977
MOP-WENO-IM(2, 0.1)	10	3.35513×10^{-2}	-	2.75968×10^{-2}	-	2.71898×10^{-2}	-
	20	5.04401×10^{-4}	6.0557	3.96236×10^{-4}	6.1220	3.94458×10^{-4}	6.1071

Table 2. *Cont.*

Scheme	N	L_1 Error	L_1 Order	L_2 Error	L_2 Order	L_∞ Error	L_∞ Order
	40	1.59160×10^{-5}	4.9860	1.25033×10^{-5}	4.9860	1.24963×10^{-5}	4.9803
	80	4.98863×10^{-7}	4.9957	3.91836×10^{-7}	4.9959	3.91797×10^{-7}	4.9953
	160	1.56020×10^{-8}	4.9988	1.22541×10^{-8}	4.9989	1.22538×10^{-8}	4.9988
	320	4.88355×10^{-10}	4.9977	3.83568×10^{-10}	4.9976	3.83547×10^{-10}	4.9977
WENO-PM6	10	1.74869×10^{-2}	-	1.35606×10^{-2}	-	1.27577×10^{-2}	-
	20	5.02923×10^{-4}	5.1198	3.95215×10^{-4}	5.1006	3.94515×10^{-4}	5.0151
	40	1.59130×10^{-5}	4.9821	1.25010×10^{-5}	4.9825	1.24960×10^{-5}	4.9805
	80	4.98858×10^{-7}	4.9954	3.91831×10^{-7}	4.9957	3.91795×10^{-7}	4.9952
	160	1.56020×10^{-8}	4.9988	1.22541×10^{-8}	4.9989	1.22538×10^{-8}	4.9988
	320	4.88355×10^{-10}	4.9977	3.83568×10^{-10}	4.9976	3.83543×10^{-10}	4.9977
MOP-WENO-PM6	10	3.54584×10^{-2}	-	2.88246×10^{-2}	-	2.76902×10^{-2}	-
	20	5.02923×10^{-4}	6.1396	3.95215×10^{-4}	6.1885	3.94515×10^{-4}	6.1332
	40	1.59130×10^{-5}	4.9821	1.25010×10^{-5}	4.9825	1.24960×10^{-5}	4.9805
	80	4.98858×10^{-7}	4.9954	3.91831×10^{-7}	4.9957	3.91795×10^{-7}	4.9952
	160	1.56020×10^{-8}	4.9988	1.22541×10^{-8}	4.9989	1.22538×10^{-8}	4.9988
	320	4.88355×10^{-10}	4.9977	3.83568×10^{-10}	4.9976	3.83543×10^{-10}	4.9977
WENO-PPM5	10	1.73978×10^{-2}	-	1.34998×10^{-2}	-	1.27018×10^{-2}	-
	20	5.03464×10^{-4}	5.1109	3.95644×10^{-4}	5.0926	3.94865×10^{-4}	5.0075
	40	1.59131×10^{-5}	4.9836	1.25011×10^{-5}	4.9841	1.24961×10^{-5}	4.9818
	80	4.98858×10^{-7}	4.9954	3.91831×10^{-7}	4.9957	3.91795×10^{-7}	4.9952
	160	1.56020×10^{-8}	4.9988	1.22541×10^{-8}	4.9989	1.22538×10^{-8}	4.9988
	320	4.88356×10^{-10}	4.9977	3.83568×10^{-10}	4.9976	3.83528×10^{-10}	4.9978
MOP-WENO-PPM5	10	3.49872×10^{-2}	-	2.85173×10^{-2}	-	2.75955×10^{-2}	-
	20	5.03464×10^{-4}	6.1188	3.95644×10^{-4}	6.1715	3.94865×10^{-4}	6.1269
	40	1.59131×10^{-5}	4.9836	1.25011×10^{-5}	4.9841	1.24961×10^{-5}	4.9818
	80	4.98858×10^{-7}	4.9954	3.91831×10^{-7}	4.9957	3.91795×10^{-7}	4.9952
	160	1.56020×10^{-8}	4.9988	1.22541×10^{-8}	4.9989	1.22538×10^{-8}	4.9988
	320	4.88356×10^{-10}	4.9977	3.83568×10^{-10}	4.9976	3.83528×10^{-10}	4.9978
WENO-RM(260)	10	1.52661×10^{-2}	-	1.19792×10^{-2}	-	1.17698×10^{-2}	-
	20	5.02845×10^{-4}	4.9241	3.95138×10^{-4}	4.9220	3.94406×10^{-4}	4.8993
	40	1.59130×10^{-5}	4.9818	1.25010×10^{-5}	4.9822	1.24960×10^{-5}	4.9801
	80	4.98858×10^{-7}	4.9954	3.91831×10^{-7}	4.9957	3.91795×10^{-7}	4.9952
	160	1.56020×10^{-8}	4.9988	1.22541×10^{-8}	4.9989	1.22538×10^{-8}	4.9988
	320	4.88355×10^{-10}	4.9977	3.83568×10^{-10}	4.9976	3.83543×10^{-10}	4.9977
MOP-WENO-RM(260)	10	3.29243×10^{-2}	-	2.73131×10^{-2}	-	2.73015×10^{-2}	-
	20	5.02845×10^{-4}	6.0329	3.95138×10^{-4}	6.1111	3.94406×10^{-4}	6.1132
	40	1.59130×10^{-5}	4.9818	1.25010×10^{-5}	4.9822	1.24960×10^{-5}	4.9801
	80	4.98858×10^{-7}	4.9954	3.91831×10^{-7}	4.9957	3.91795×10^{-7}	4.9952
	160	1.56020×10^{-8}	4.9988	1.22541×10^{-8}	4.9989	1.22538×10^{-8}	4.9988
	320	4.88355×10^{-10}	4.9977	3.83568×10^{-10}	4.9976	3.83543×10^{-10}	4.9977
WENO-MAIM1	10	6.13264×10^{-2}	-	4.81375×10^{-2}	-	4.86913×10^{-2}	-
	20	5.08205×10^{-4}	6.9150	4.26155×10^{-4}	6.8196	5.03701×10^{-4}	6.5950
	40	1.59130×10^{-5}	4.9971	1.25010×10^{-5}	5.0913	1.24960×10^{-5}	5.3330
	80	4.98858×10^{-7}	4.9954	3.91831×10^{-7}	4.9957	3.91795×10^{-7}	4.9952
	160	1.56020×10^{-8}	4.9988	1.22541×10^{-8}	4.9989	1.22538×10^{-8}	4.9988
	320	4.88355×10^{-10}	4.9977	3.83568×10^{-10}	4.9976	3.83543×10^{-10}	4.9977
MOP-WENO-MAIM1	10	6.63923×10^{-2}	-	5.17462×10^{-2}	-	5.19799×10^{-2}	-
	20	5.08205×10^{-4}	7.0295	4.26155×10^{-4}	6.9239	5.03701×10^{-4}	6.6892
	40	1.59130×10^{-5}	4.9971	1.25010×10^{-5}	5.0913	1.24960×10^{-5}	5.3330
	80	4.98858×10^{-7}	4.9954	3.91831×10^{-7}	4.9957	3.91795×10^{-7}	4.9952
	160	1.56020×10^{-8}	4.9988	1.22541×10^{-8}	4.9989	1.22538×10^{-8}	4.9988
	320	4.88355×10^{-10}	4.9977	3.83568×10^{-10}	4.9976	3.83543×10^{-10}	4.9977

Table 2. *Cont.*

Scheme	N	L_1 Error	L_1 Order	L_2 Error	L_2 Order	L_∞ Error	L_∞ Order
MIP-WENO-ACMk	10	1.52184×10^{-2}	-	1.19442×10^{-2}	-	1.17569×10^{-2}	-
	20	5.02844×10^{-4}	4.9196	3.95138×10^{-4}	4.9178	3.94406×10^{-4}	4.8977
	40	1.59130×10^{-5}	4.9818	1.25010×10^{-5}	4.9822	1.24960×10^{-5}	4.9801
	80	4.98858×10^{-7}	4.9954	3.91831×10^{-7}	4.9957	3.91795×10^{-7}	4.9952
	160	1.56020×10^{-8}	4.9988	1.22541×10^{-8}	4.9989	1.22538×10^{-8}	4.9988
	320	4.88355×10^{-10}	4.9977	3.83568×10^{-10}	4.9976	3.83543×10^{-10}	4.9977
MOP-WENO-ACMk	10	3.29609×10^{-2}	-	2.72363×10^{-2}	-	2.70295×10^{-2}	-
	20	5.02844×10^{-4}	6.0345	3.95138×10^{-4}	6.1070	3.94406×10^{-4}	6.0987
	40	1.59130×10^{-5}	4.9818	1.25010×10^{-5}	4.9822	1.24960×10^{-5}	4.9801
	80	4.98858×10^{-7}	4.9954	3.91831×10^{-7}	4.9957	3.91795×10^{-7}	4.9952
	160	1.56020×10^{-8}	4.9988	1.22541×10^{-8}	4.9989	1.22538×10^{-8}	4.9988
	320	4.88355×10^{-10}	4.9977	3.83568×10^{-10}	4.9976	3.83543×10^{-10}	4.9977

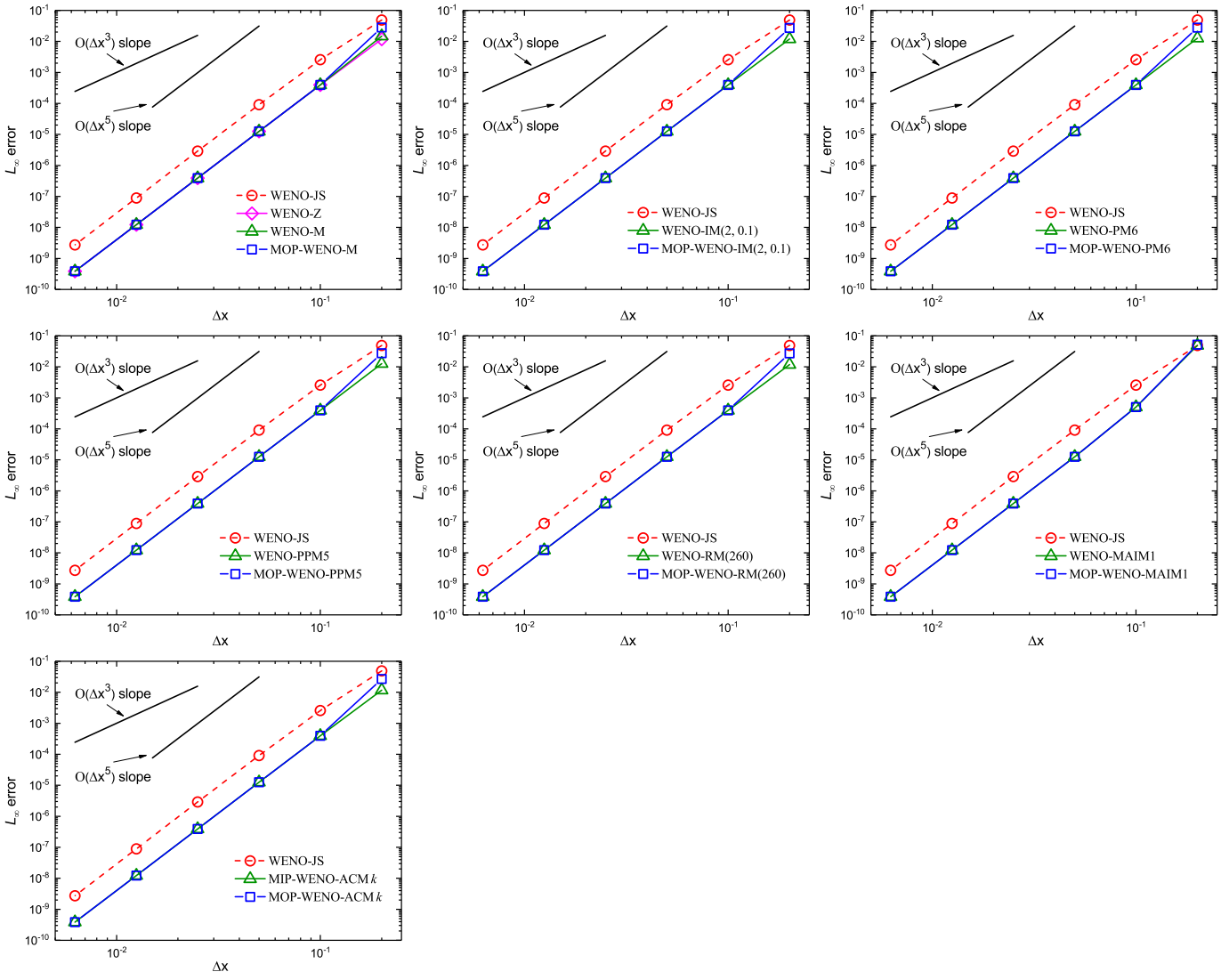

Figure 2. L_∞-norm error plots for various WENO schemes for Example 1.

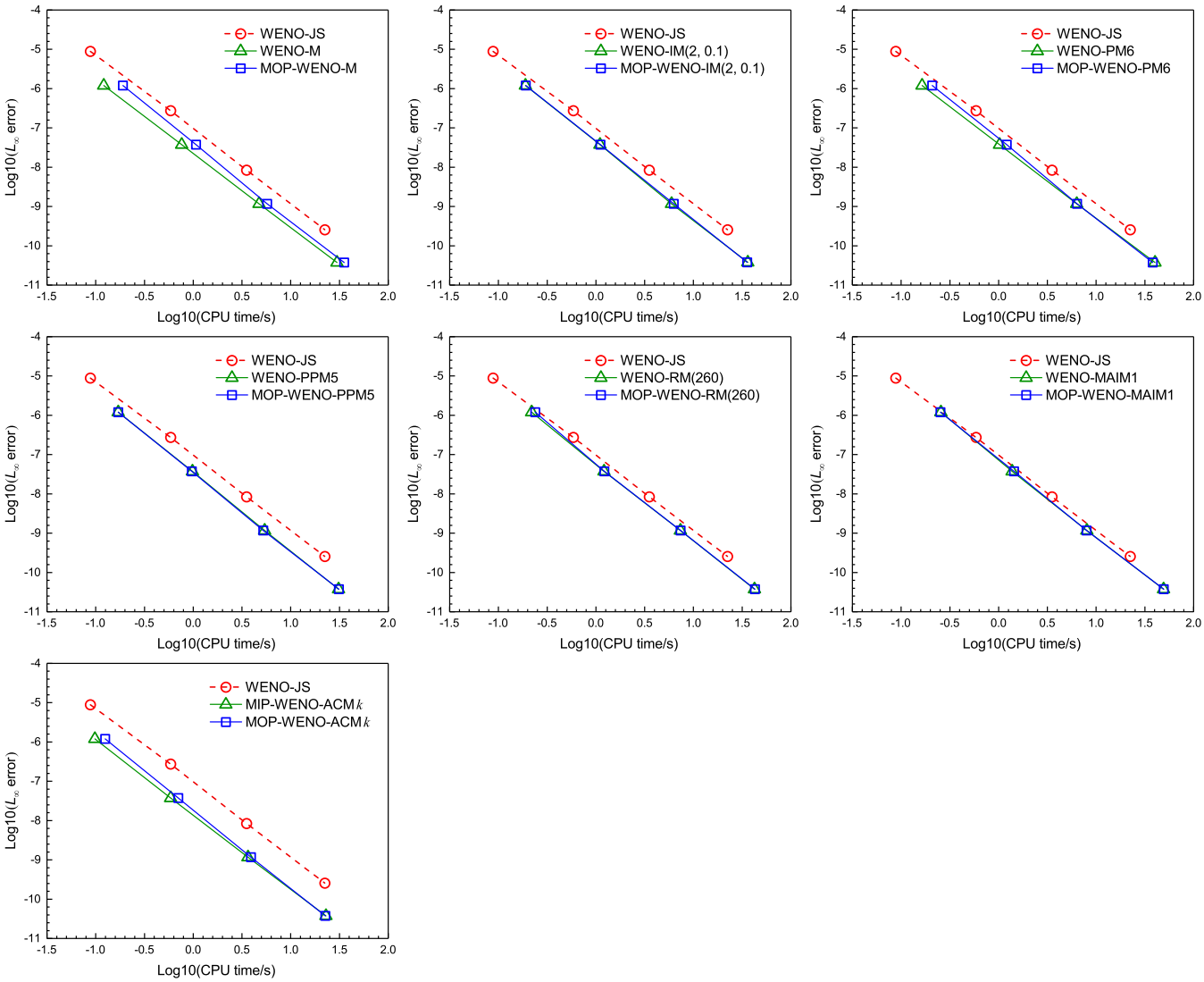

Figure 3. Comparison of various WENO schemes for Example 1 in CPU time and L_∞-norm computing errors.

Example 2. *We calculate Equation (38) with the periodic boundary condition using the following initial condition [25]:*

$$u(x,0) = \sin\left(\pi x - \frac{\sin(\pi x)}{\pi}\right). \tag{40}$$

This particular initial condition has two first-order critical points, which both have a non-vanishing third derivative. Again, the CFL number was set to be $(\Delta x)^{2/3}$ and the calculation was run until a time of $t = 2.0$.

Table 3 compares the L_1, L_2, L_∞ errors and corresponding convergence orders obtained from the considered schemes. It is evident that the WENO-X schemes and the associated MOP-WENO-X schemes can achieve the optimal convergence orders, and this verifies the properties $C1 \sim C3$ of Theorem 2. Unsurprisingly, the WENO-JS scheme gives less accurate results than the other schemes, and its L_∞ convergence order decreases by almost 2 orders leading to the noticeable drops of the L_1 and L_2 convergence orders. It is noteworthy that when the grid number is too small, such as $N \leq 40$, in terms of accuracy, the MOP-WENO-X schemes provide less accurate results than those of the associated WENO-X schemes. As mentioned in Example 1, the cause of this kind of accuracy loss is that the mapping functions of the MOP-WENO-X schemes have narrower optimal weight intervals than the

associated WENO-X schemes, and this issue can surely be addressed by increasing the grid number. Therefore, as expected, the MOP-WENO-X schemes show equally accurate numerical solutions like those of the associated WENO-X schemes when the grid number $N \geq 80$.

Figure 4 shows the overall L_∞ convergence behavior of various considered schemes. We can observe that: (1) the solutions of all MOP-WENO-X schemes and their associated WENO-X schemes, and of the WENO-Z scheme, converge at fifth-order, as evidenced by the slope of the lines, especially for larger (slightly) grid numbers; (2) for the classic WENO-JS scheme, its solution converges at third-order, as evidenced by its slope of the line; (3) naturally, the MOP-WENO-X schemes and their associated WENO-X schemes, and the WENO-Z scheme, are significantly more accurate than the classic WENO-JS scheme; (4) the errors and convergence orders of the MOP-WENO-X schemes are very close to those of their associated WENO-X schemes.

We also use this example to discuss the computational cost of the MOP-WENO-X scheme compared with its associated WENO-X scheme and the classic WENO-JS scheme. In Figure 5, we drew the graphs for the CPU time versus the L_∞-norm computing errors. From Figure 5, we can easily see that: (1) as expected, the WENO-JS scheme has the lowest efficiency; (2) again, for all MOP-WENO-X schemes except the case of "X = M," they perform almost identically to their associated WENO-X schemes; (3) for the MOP-WENO-M scheme, despite the fact that it has slightly less efficiency than its associated WENO-M scheme, it has significantly superior efficiency to the WENO-JS scheme.

Table 3. Convergence properties of considered schemes on solving $u_t + u_x = 0$ with initial condition $u(x,0) = \sin(\pi x - \sin(\pi x)/\pi)$. To be continued.

Scheme	N	L_1 Error	L_1 Order	L_2 Error	L_2 Order	L_∞ Error	L_∞ Order
WENO-JS	10	1.24488×10^{-1}	-	1.09463×10^{-1}	-	1.24471×10^{-1}	-
	20	1.01260×10^{-2}	3.6199	8.72198×10^{-3}	3.6496	1.43499×10^{-2}	3.1167
	40	7.22169×10^{-4}	3.8096	6.76133×10^{-4}	3.6893	1.09663×10^{-3}	3.7099
	80	3.42286×10^{-5}	4.3991	3.63761×10^{-5}	4.2162	9.02485×10^{-5}	3.6030
	160	1.58510×10^{-6}	4.4326	2.29598×10^{-6}	3.9858	8.24022×10^{-6}	3.4531
	320	7.95517×10^{-8}	4.3165	1.68304×10^{-7}	3.7700	8.31702×10^{-7}	3.3085
WENO-Z	10	5.85966×10^{-2}	-	4.83441×10^{-2}	-	5.14928×10^{-2}	-
	20	3.21455×10^{-3}	4.1881	2.72340×10^{-3}	4.1499	3.67979×10^{-3}	3.8067
	40	1.35382×10^{-4}	4.5695	1.35344×10^{-4}	4.3307	2.31013×10^{-4}	3.9936
	80	4.67008×10^{-6}	4.8574	4.50404×10^{-6}	4.9093	6.79475×10^{-6}	5.0874
	160	1.50985×10^{-7}	4.9510	1.42363×10^{-7}	4.9836	2.14556×10^{-7}	4.9850
	320	4.76201×10^{-9}	4.9867	4.45798×10^{-9}	4.9970	6.71078×10^{-9}	4.9987
WENO-M	10	7.53259×10^{-2}	-	6.39017×10^{-2}	-	7.49250×10^{-2}	-
	20	3.70838×10^{-3}	4.3443	3.36224×10^{-3}	4.2484	5.43666×10^{-3}	3.7847
	40	1.45082×10^{-4}	4.6758	1.39007×10^{-4}	4.5962	2.18799×10^{-4}	4.6350
	80	4.80253×10^{-6}	4.9169	4.52646×10^{-6}	4.9406	6.81451×10^{-6}	5.0049
	160	1.52120×10^{-7}	4.9805	1.42463×10^{-7}	4.9897	2.14545×10^{-7}	4.9893
	320	4.77083×10^{-9}	4.9948	4.45822×10^{-9}	4.9980	6.71080×10^{-9}	4.9987
MOP-WENO-M	10	9.41832×10^{-2}	-	8.03446×10^{-2}	-	9.78919×10^{-2}	-
	20	6.59540×10^{-3}	3.8359	6.37937×10^{-3}	3.6547	8.97094×10^{-3}	3.4479
	40	2.60456×10^{-4}	4.6623	2.50868×10^{-4}	4.6684	4.10480×10^{-4}	4.4499
	80	4.80253×10^{-6}	5.7611	4.52646×10^{-6}	5.7924	6.81451×10^{-6}	5.9126
	160	1.52120×10^{-7}	4.9805	1.42463×10^{-7}	4.9897	2.14545×10^{-7}	4.9893
	320	4.77083×10^{-9}	4.9948	4.45822×10^{-9}	4.9980	6.71080×10^{-9}	4.9987

Table 3. *Cont.*

Scheme	N	L_1 Error	L_1 Order	L_2 Error	L_2 Order	L_∞ Error	L_∞ Order
WENO-IM(2, 0.1)	10	8.38131×10^{-2}	-	6.71285×10^{-2}	-	7.62798×10^{-2}	-
	20	4.30725×10^{-3}	4.2823	3.93700×10^{-3}	4.0918	5.84039×10^{-3}	3.7072
	40	1.51327×10^{-4}	4.8310	1.41737×10^{-4}	4.7958	2.10531×10^{-4}	4.7940
	80	4.85592×10^{-6}	4.9618	4.53602×10^{-6}	4.9656	6.82606×10^{-6}	4.9468
	160	1.52659×10^{-7}	4.9914	1.42479×10^{-7}	4.9926	2.14534×10^{-7}	4.9918
	320	4.77654×10^{-9}	4.9982	4.45805×10^{-9}	4.9982	6.71079×10^{-9}	4.9986
MOP-WENO-IM(2, 0.1)	10	8.49795×10^{-2}	-	7.29388×10^{-2}	-	9.47429×10^{-2}	-
	20	7.01287×10^{-3}	3.5990	6.80019×10^{-3}	3.4230	9.96943×10^{-3}	3.2484
	40	2.59767×10^{-4}	4.7547	2.51121×10^{-4}	4.7591	4.01785×10^{-4}	4.6330
	80	4.85592×10^{-6}	5.7413	4.53602×10^{-6}	5.7908	6.82606×10^{-6}	5.8792
	160	1.52659×10^{-7}	4.9914	1.42479×10^{-7}	4.9926	2.14534×10^{-7}	4.9918
	320	4.77654×10^{-9}	4.9982	4.45805×10^{-9}	4.9982	6.71079×10^{-9}	4.9986
WENO-PM6	10	9.51313×10^{-2}	-	7.83600×10^{-2}	-	9.32356×10^{-2}	-
	20	4.82173×10^{-3}	4.3023	4.29510×10^{-3}	4.1894	5.91037×10^{-3}	3.9796
	40	1.55428×10^{-4}	4.9552	1.43841×10^{-4}	4.9001	2.09540×10^{-4}	4.8180
	80	4.87327×10^{-6}	4.9952	4.54036×10^{-6}	4.9855	6.83270×10^{-6}	4.9386
	160	1.52750×10^{-7}	4.9956	1.42488×10^{-7}	4.9939	2.14532×10^{-7}	4.9932
	320	4.77729×10^{-9}	4.9988	4.45807×10^{-9}	4.9983	6.71079×10^{-9}	4.9986
MOP-WENO-PM6	10	1.00298×10^{-1}	-	8.49034×10^{-2}	-	9.88357×10^{-2}	-
	20	5.84504×10^{-3}	4.1009	5.80703×10^{-3}	3.8699	9.01779×10^{-3}	3.4542
	40	2.51725×10^{-4}	4.5373	2.40678×10^{-4}	4.5926	3.66822×10^{-4}	4.6196
	80	4.87327×10^{-6}	5.6908	4.54036×10^{-6}	5.7282	6.83270×10^{-6}	5.7465
	160	1.52750×10^{-7}	4.9956	1.42488×10^{-7}	4.9939	2.14532×10^{-7}	4.9932
	320	4.77729×10^{-9}	4.9988	4.45807×10^{-9}	4.9983	6.71079×10^{-9}	4.9986
WENO-PPM5	10	9.22982×10^{-2}	-	7.46925×10^{-2}	-	8.46229×10^{-2}	-
	20	4.68376×10^{-3}	4.3006	4.18882×10^{-3}	4.1563	5.92748×10^{-3}	3.8356
	40	1.55745×10^{-4}	4.9104	1.44018×10^{-4}	4.8622	2.09420×10^{-4}	4.8229
	80	4.88795×10^{-6}	4.9938	4.54528×10^{-6}	4.9857	6.83617×10^{-6}	4.9371
	160	1.52852×10^{-7}	4.9990	1.42506×10^{-7}	4.9953	2.14527×10^{-7}	4.9940
	320	4.77759×10^{-9}	4.9997	4.45812×10^{-9}	4.9984	6.71080×10^{-9}	4.9985
MOP-WENO-PPM5	10	9.50369×10^{-2}	-	8.08190×10^{-2}	-	9.65522×10^{-2}	-
	20	6.27179×10^{-3}	3.9215	6.11267×10^{-3}	3.7248	8.98120×10^{-3}	3.4263
	40	2.52600×10^{-4}	4.6340	2.41656×10^{-4}	4.6608	3.69338×10^{-4}	4.6039
	80	4.88795×10^{-6}	5.6915	4.54528×10^{-6}	5.7324	6.83617×10^{-6}	5.7556
	160	1.52852×10^{-7}	4.9990	1.42506×10^{-7}	4.9953	2.14527×10^{-7}	4.9940
	320	4.77759×10^{-9}	4.9997	4.45812×10^{-9}	4.9984	6.71080×10^{-9}	4.9985
WENO-RM(260)	10	8.24328×10^{-2}	-	6.64590×10^{-2}	-	7.64206×10^{-2}	-
	20	4.37642×10^{-3}	4.2354	4.00547×10^{-3}	4.0524	5.88375×10^{-3}	3.6992
	40	1.52200×10^{-4}	4.8457	1.42162×10^{-4}	4.8164	2.09889×10^{-4}	4.8090
	80	4.86434×10^{-6}	4.9676	4.53769×10^{-6}	4.9694	6.83016×10^{-6}	4.9416
	160	1.52735×10^{-7}	4.9931	1.42486×10^{-7}	4.9931	2.14533×10^{-7}	4.9926
	320	4.77728×10^{-9}	4.9987	4.45807×10^{-9}	4.9983	6.71079×10^{-9}	4.9986
MOP-WENO-RM(260)	10	8.96509×10^{-2}	-	7.51169×10^{-2}	-	9.20962×10^{-2}	-
	20	6.87612×10^{-3}	3.7047	6.65488×10^{-3}	3.4967	9.75043×10^{-3}	3.2396
	40	2.59418×10^{-4}	4.7282	2.51194×10^{-4}	4.7275	4.03065×10^{-4}	4.5964
	80	4.86434×10^{-6}	5.7369	4.53769×10^{-6}	5.7907	6.83016×10^{-6}	5.8829
	160	1.52735×10^{-7}	4.9931	1.42486×10^{-7}	4.9931	2.14533×10^{-7}	4.9926
	320	4.77728×10^{-9}	4.9987	4.45807×10^{-9}	4.9983	6.71079×10^{-9}	4.9986

Table 3. *Cont.*

Scheme	N	L_1 Error	L_1 Order	L_2 Error	L_2 Order	L_∞ Error	L_∞ Order
WENO-MAIM1	10	1.24659×10^{-1}	-	1.14152×10^{-1}	-	1.40438×10^{-1}	-
	20	8.07923×10^{-3}	3.9476	7.08117×10^{-3}	4.0108	1.03772×10^{-2}	3.7584
	40	3.32483×10^{-4}	4.6029	3.36264×10^{-4}	4.3963	6.62891×10^{-4}	3.9685
	80	1.01162×10^{-5}	5.0385	1.49724×10^{-5}	4.4892	4.48554×10^{-5}	3.8854
	160	1.52910×10^{-7}	6.0478	1.42515×10^{-7}	6.7150	2.14522×10^{-7}	7.7080
	320	4.77728×10^{-9}	5.0003	4.45807×10^{-9}	4.9986	6.71079×10^{-9}	4.9985
MOP-WENO-MAIM1	10	1.27999×10^{-1}	-	1.12692×10^{-1}	-	1.31113×10^{-1}	-
	20	7.62753×10^{-3}	4.0688	6.93240×10^{-3}	4.0229	1.27480×10^{-2}	3.3625
	40	3.37132×10^{-4}	4.4998	3.36497×10^{-4}	4.3647	6.40953×10^{-4}	4.3139
	80	1.01162×10^{-5}	5.0586	1.49724×10^{-5}	4.4902	4.48554×10^{-5}	3.8369
	160	1.52910×10^{-7}	6.0478	1.42515×10^{-7}	6.7150	2.14522×10^{-7}	7.7080
	320	4.77728×10^{-9}	5.0003	4.45807×10^{-9}	4.9986	6.71079×10^{-9}	4.9985
MIP-WENO-ACMk	10	8.75629×10^{-2}	-	6.98131×10^{-2}	-	7.91292×10^{-2}	-
	20	4.39527×10^{-3}	4.3163	4.02909×10^{-3}	4.1150	5.89045×10^{-3}	3.7478
	40	1.52219×10^{-4}	4.8517	1.42172×10^{-4}	4.8247	2.09893×10^{-4}	4.8107
	80	4.86436×10^{-6}	4.9678	4.53770×10^{-6}	4.9695	6.83017×10^{-6}	4.9416
	160	1.52735×10^{-7}	4.9931	1.42486×10^{-7}	4.9931	2.14533×10^{-7}	4.9926
	320	4.77728×10^{-9}	4.9987	4.45807×10^{-9}	4.9983	6.71079×10^{-9}	4.9986
MOP-WENO-ACMk	10	9.08634×10^{-2}	-	7.58160×10^{-2}	-	9.29135×10^{-2}	-
	20	7.09246×10^{-3}	3.6793	6.88532×10^{-3}	3.4609	1.01479×10^{-2}	3.1947
	40	2.59429×10^{-4}	4.7729	2.51208×10^{-4}	4.7766	4.03069×10^{-4}	4.6540
	80	4.86436×10^{-6}	5.7369	4.53770×10^{-6}	5.7908	6.83017×10^{-6}	5.8830
	160	1.52735×10^{-7}	4.9931	1.42486×10^{-7}	4.9931	2.14533×10^{-7}	4.9926
	320	4.77728×10^{-9}	4.9987	4.45807×10^{-9}	4.9983	6.71079×10^{-9}	4.9986

Example 3. *We calculate Equation (38) using the following initial condition [29]:*

$$u(x,0) = \sin^9(\pi x), \tag{41}$$

with the periodic boundary condition. It is trivial to verify that this initial condition has high-order critical points. We also set the CFL number to be $(\Delta x)^{2/3}$.

We use the L_1- and L_∞-norm of numerical errors to measure the dissipations of the schemes. It is easy to check that the exact solution is $u(x,t) = \sin^9\left(\pi(x-t)\right)$. Moreover, we consider the increased errors (in percentage) compared to the MIP-WENO-ACMk scheme that gives solutions with highly low dissipations. For the L_1- and L_∞-norms of numerical errors of the scheme "Y," their associated increased errors at output time t are defined by

$$\chi_1 = \frac{L_1^{\mathrm{Y}}(t) - L_1^{\mathrm{MIP-WENO-ACM}k}(t)}{L_1^{\mathrm{MIP-WENO-ACM}k}(t)} \times 100\%,$$
$$\chi_\infty = \frac{L_\infty^{\mathrm{Y}}(t) - L_\infty^{\mathrm{MIP-WENO-ACM}k}(t)}{L_\infty^{\mathrm{MIP-WENO-ACM}k}(t)} \times 100\%,$$

where $L_1^{\mathrm{MIP-WENO-ACM}k}(t)$ and $L_\infty^{\mathrm{MIP-WENO-ACM}k}(t)$ are the L_1- and L_∞-norms of numerical errors of the MIP-WENO-ACMk scheme.

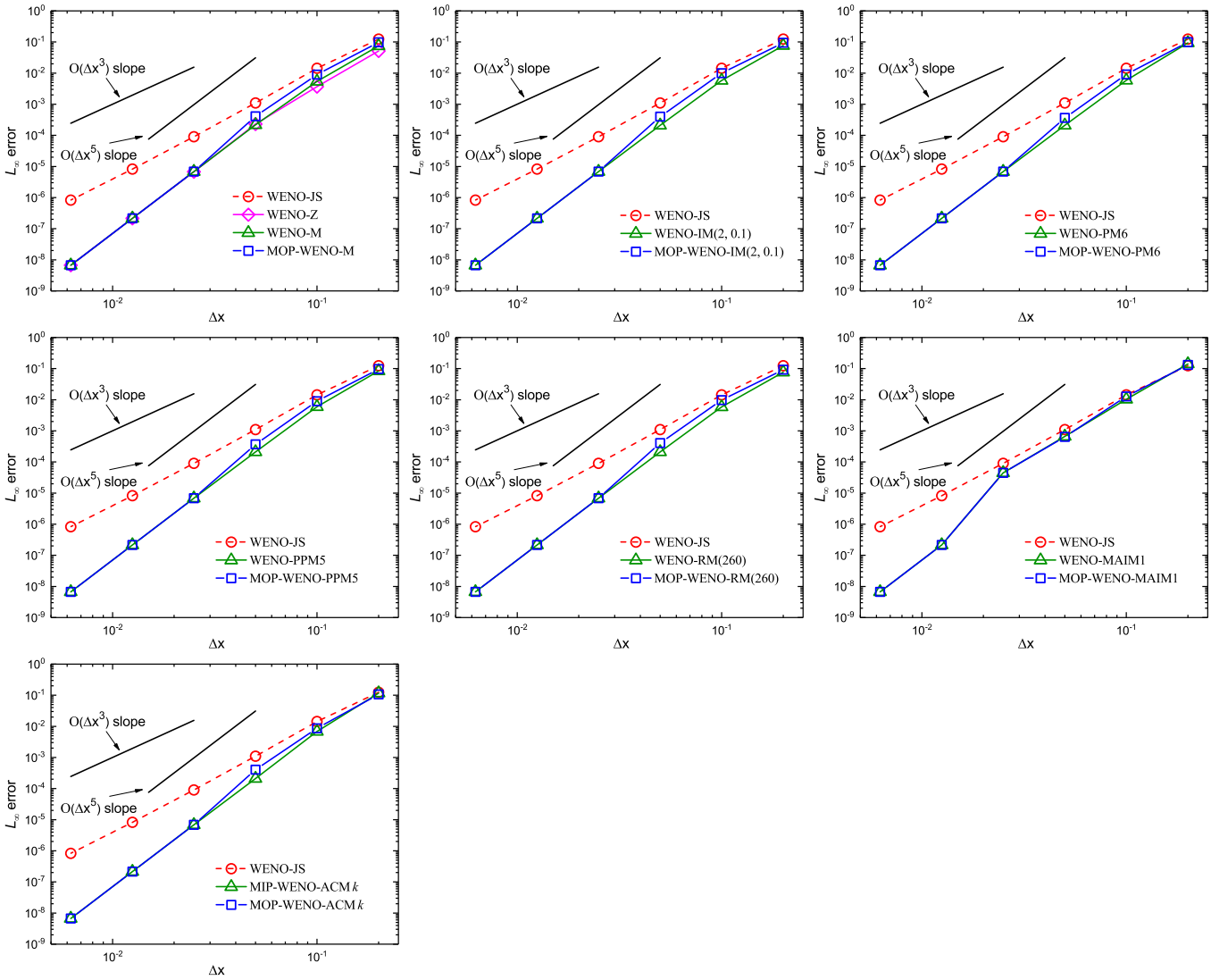

Figure 4. L_∞-norm error plots for various WENO schemes for Example 2.

Table 4 shows the L_1- and L_∞-norm numerical errors and their increased errors by using a uniform grid cell of $N = 200$ at different output times of $t = 10, 100, 200, 500, 1000$. From Table 4, we can observe that: (1) the WENO-JS scheme has the largest increased errors for no matter short or long output times; (2) for short output times, such as $t \leq 100$, the solutions computed by the WENO-M scheme are closer to those of the MIP-WENO-ACM*k* scheme, leading to smaller increased errors than the associated MOP-WENO-M scheme; (3) however, when the output time is larger, such as $t \geq 200$, the solutions computed by the MOP-WENO-M scheme, whose increased errors do not get larger but evidently decreased, are closer to those of the MIP-WENO-ACM*k* scheme than the associated WENO-M scheme, whose errors increases dramatically, leading to significantly larger increased errors; (4) the performance of the WENO-Z scheme is very similar to that of the WENO-M scheme; (5) although the errors of the MOP-WENO-X schemes except the MOP-WENO-M scheme are not as small as those of the associated WENO-X schemes, these errors can be maintained considerable levels leading to acceptable increases in errors that are much lower than those of the WENO-JS and WENO-M schemes.

Actually, as mentioned in Examples 1 and 2, the cause of the slight accuracy loss discussed above is that the mapping function of the MOP-WENO-X scheme has narrower optimal weight intervals than the associated WENO-X schemes, and one can easily overcome this drawback by increasing the grid number. To demonstrate this, we calculate this problem using the same schemes at the same output times with a larger grid number

of $N = 800$. The results are shown in Table 5, and we can see that: (1) the errors of the MOP-WENO-X schemes get closer to those of the MIP-WENO-ACMk scheme when the grid number increases from $N = 200$ to $N = 800$, resulting in the significant decrease of the increased errors, and in different words, the errors of the MOP-WENO-X schemes and the MIP-WENO-ACMk scheme are so close that one can ignore their differences; (2) although the errors of the WENO-JS, WENO-M and WENO-Z schemes get smaller when the grid number increases from $N = 200$ to $N = 800$, their increased errors become very large; (3) naturally, the increased errors of the MOP-WENO-X schemes are far smaller than those of the WENO-JS, WENO-M and WENO-Z schemes. Actually, it is an important advantage of the MOP-WENO-X schemes that can maintain comparably high resolution for long output times. In the next subsection we have further discussion of this.

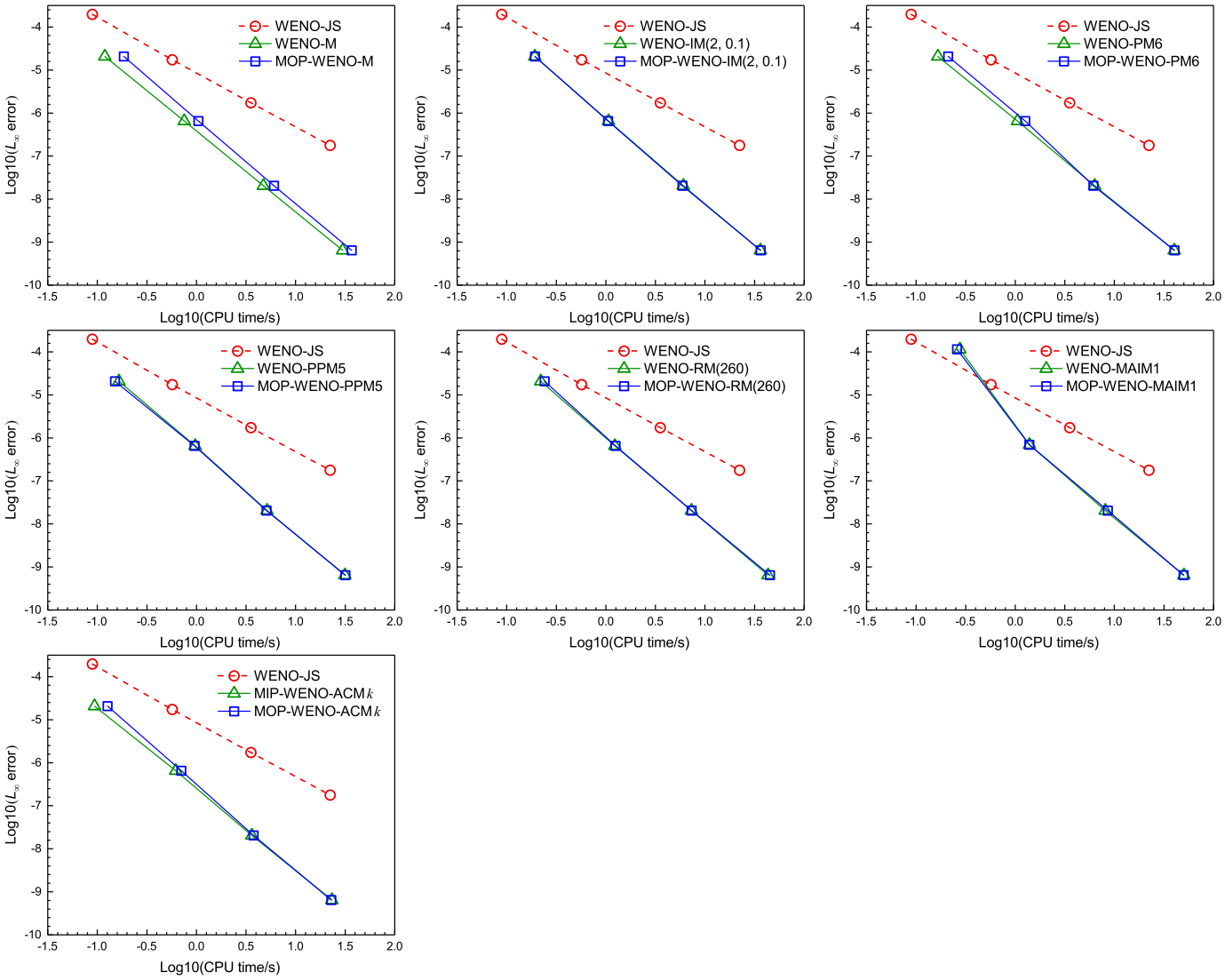

Figure 5. Comparison of various WENO schemes for Example 2 in CPU time and L_∞-norm computing errors.

Table 4. Performances of various considered schemes on solving $u_t + u_x = 0$ with $u(x,0) = \sin^9(\pi x), N = 200$.

	MIP-WENO-ACMk				MOP-WENO-ACMk			
Time, t	L_1 error	χ_1	L_∞ error	χ_∞	L_1 error	χ_1	L_∞ error	χ_∞
10	8.42873×10^{-5}	–	1.38205×10^{-4}	–	1.55900×10^{-4}	85%	5.22964×10^{-4}	278%
100	8.35747×10^{-4}	–	1.36404×10^{-3}	–	2.72470×10^{-3}	226%	9.83147×10^{-3}	621%
200	1.65557×10^{-3}	–	2.68955×10^{-3}	–	4.11740×10^{-3}	149%	6.66166×10^{-3}	148%
500	3.95849×10^{-3}	–	6.45564×10^{-3}	–	8.34435×10^{-3}	111%	1.83215×10^{-2}	184%
1000	7.24723×10^{-3}	–	1.21593×10^{-2}	–	1.54830×10^{-2}	114%	3.16523×10^{-2}	160%
	WENO−JS				WENO−Z			
Time, t	L_1 error	χ_1	L_∞ error	χ_∞	L_1 error	χ_1	L_∞ error	χ_∞
10	3.86931×10^{-4}	359%	5.36940×10^{-4}	289%	9.25912×10^{-5}	10%	1.38334×10^{-4}	0%
100	5.42288×10^{-3}	549%	1.20056×10^{-2}	780%	1.45856×10^{-3}	75%	3.76895×10^{-3}	176%
200	2.35657×10^{-2}	1323%	6.47820×10^{-2}	2309%	8.32696×10^{-3}	403%	3.37176×10^{-2}	1154%
500	1.55650×10^{-1}	3832%	2.57663×10^{-1}	3891%	8.95980×10^{-2}	2163%	1.94577×10^{-1}	2914%
1000	2.91359×10^{-1}	3920%	4.44664×10^{-1}	3557%	1.42377×10^{-1}	1865%	2.80558×10^{-1}	2207%
	WENO−M				MOP−WENO−M			
Time, t	L_1 error	χ_1	L_∞ error	χ_∞	L_1 error	χ_1	L_∞ error	χ_∞
10	8.90890×10^{-5}	6%	1.38348×10^{-4}	0%	1.56466×10^{-4}	86%	5.08956×10^{-4}	268%
100	1.29154×10^{-3}	55%	3.32665×10^{-3}	144%	2.88442×10^{-3}	245%	1.01393×10^{-2}	643%
200	5.74021×10^{-3}	247%	2.37125×10^{-2}	782%	5.11795×10^{-3}	209%	1.02172×10^{-2}	280%
500	4.89290×10^{-2}	1136%	1.78294×10^{-1}	2662%	9.09352×10^{-3}	130%	1.98022×10^{-2}	207%
1000	1.34933×10^{-1}	1762%	3.17199×10^{-1}	2509%	1.75990×10^{-2}	143%	4.01776×10^{-2}	230%
	WENO-IM(2, 0.1)				MOP-WENO-IM(2, 0.1)			
Time, t	L_1 error	χ_1	L_∞ error	χ_∞	L_1 error	χ_1	L_∞ error	χ_∞
10	8.46989×10^{-5}	0%	1.38220×10^{-4}	0%	1.55777×10^{-4}	85%	5.08361×10^{-4}	268%
100	8.39425×10^{-4}	0%	1.36420×10^{-3}	0%	2.74109×10^{-3}	228%	9.88287×10^{-3}	625%
200	1.67834×10^{-3}	1%	2.68977×10^{-3}	0%	4.16210×10^{-3}	151%	6.81406×10^{-3}	153%
500	4.17514×10^{-3}	5%	8.13666×10^{-3}	12%	8.37898×10^{-3}	112%	1.84998×10^{-2}	187%
1000	6.45231×10^{-3}	0%	1.21388×10^{-2}	0%	1.25166×10^{-2}	73%	2.02754×10^{-2}	67%
	WENO−PM6				MOP−WENO−PM6			
Time, t	L_1 error	χ_1	L_∞ error	χ_∞	L_1 error	χ_1	L_∞ error	χ_∞
10	8.40259×10^{-5}	0%	1.38205×10^{-4}	0%	1.53937×10^{-4}	83%	4.92116×10^{-4}	256%
100	8.30374×10^{-4}	−1%	1.36410×10^{-3}	0%	2.70283×10^{-3}	223%	9.52154×10^{-3}	598%
200	1.63963×10^{-3}	−1%	2.68938×10^{-3}	0%	4.07454×10^{-3}	146%	6.49923×10^{-3}	142%
500	3.88864×10^{-3}	−2%	6.45650×10^{-3}	0%	8.46326×10^{-3}	114%	1.83171×10^{-2}	184%
1000	7.17606×10^{-3}	−1%	1.21637×10^{-2}	0%	1.54196×10^{-2}	113%	3.15065×10^{-2}	159%
	WENO−PPM5				MOP−WENO−PPM5			
Time, t	L_1 error	χ_1	L_∞ error	χ_∞	L_1 error	χ_1	L_∞ error	χ_∞
10	8.40198×10^{-5}	0%	1.38206×10^{-4}	0%	1.53322×10^{-4}	82%	4.97691×10^{-4}	260%
100	8.30119×10^{-4}	−1%	1.36411×10^{-3}	0%	2.70476×10^{-3}	224%	9.71919×10^{-3}	613%
200	1.63931×10^{-3}	−1%	2.68939×10^{-3}	0%	4.17894×10^{-3}	152%	6.89990×10^{-3}	157%
500	3.89396×10^{-3}	−2%	6.45658×10^{-3}	0%	8.34997×10^{-3}	111%	1.83470×10^{-2}	184%
1000	7.20573×10^{-3}	−1%	1.21629×10^{-2}	0%	1.21149×10^{-2}	67%	1.87607×10^{-2}	54%
	WENO−RM(260)				MOP−WENO−RM(260)			
Time, t	L_1 error	χ_1	L_∞ error	χ_∞	L_1 error	χ_1	L_∞ error	χ_∞
10	8.43348×10^{-5}	0%	1.38206×10^{-4}	0%	1.55787×10^{-4}	85%	5.05390×10^{-4}	266%
100	8.35534×10^{-4}	0%	1.36404×10^{-3}	0%	2.72147×10^{-3}	226%	9.74612×10^{-3}	615%
200	1.65314×10^{-3}	0%	2.68956×10^{-3}	0%	4.13179×10^{-3}	150%	6.71615×10^{-3}	150%
500	3.94006×10^{-3}	0%	6.45544×10^{-3}	0%	8.32505×10^{-3}	110%	1.83262×10^{-2}	184%
1000	7.25689×10^{-3}	0%	1.21576×10^{-2}	0%	1.57577×10^{-2}	117%	3.30552×10^{-2}	172%
	WENO−MAIM1				MOP−WENO−MAIM1			
Time, t	L_1 error	χ_1	L_∞ error	χ_∞	L_1 error	χ_1	L_∞ error	χ_∞
10	8.24623×10^{-5}	−2%	1.38215×10^{-4}	0%	9.97376×10^{-5}	18%	1.38172×10^{-4}	0%
100	8.03920×10^{-4}	−4%	1.36392×10^{-3}	0%	8.16839×10^{-4}	−2%	1.36470×10^{-3}	0%
200	1.58626×10^{-3}	−4%	2.68849×10^{-3}	0%	1.60912×10^{-3}	−3%	2.68832×10^{-3}	0%
500	3.77900×10^{-3}	−5%	6.46356×10^{-3}	0%	6.83393×10^{-3}	73%	1.63188×10^{-2}	153%
1000	7.04287×10^{-3}	−3%	1.21473×10^{-2}	0%	1.24817×10^{-2}	72%	2.22178×10^{-2}	83%

Table 5. Performance of various considered schemes on solving $u_t + u_x = 0$ with $u(x,0) = \sin^9(\pi x), N = 800$.

	MIP-WENO-ACMk				MOP-WENO-ACMk			
Time, t	L_1 error	χ_1	L_∞ error	χ_∞	L_1 error	χ_1	L_∞ error	χ_∞
10	8.28794×10^{-8}	-	1.36172×10^{-7}	-	8.47930×10^{-8}	2%	1.36172×10^{-7}	0%
100	8.28891×10^{-7}	-	1.36206×10^{-6}	-	9.73202×10^{-7}	17%	1.79160×10^{-6}	32%
200	1.65782×10^{-6}	-	2.72415×10^{-6}	-	1.78369×10^{-6}	8%	2.72415×10^{-6}	0%
500	4.14451×10^{-6}	-	6.81018×10^{-6}	-	4.84739×10^{-6}	17%	8.79296×10^{-6}	29%
1000	8.28868×10^{-6}	-	1.36194×10^{-5}	-	8.61232×10^{-6}	4%	1.36194×10^{-5}	0%
	WENO-JS				WENO-Z			
Time, t	L_1 error	χ_1	L_∞ error	χ_∞	L_1 error	χ_1	L_∞ error	χ_∞
10	4.23531×10^{-7}	411%	6.95290×10^{-7}	411%	8.28830×10^{-8}	0%	1.36173×10^{-7}	0%
100	4.74028×10^{-6}	472%	1.09481×10^{-5}	704%	8.28938×10^{-7}	0%	1.36207×10^{-6}	0%
200	7.29285×10^{-5}	4299%	9.51604×10^{-4}	34832%	2.10734×10^{-6}	27%	9.02795×10^{-6}	231%
500	3.11698×10^{-2}	751974%	8.63989×10^{-2}	1268573%	9.91182×10^{-4}	23816%	1.65219×10^{-2}	242506%
1000	1.01278×10^{-1}	1221783%	2.13485×10^{-1}	1567407%	2.82670×10^{-3}	34003%	1.85472×10^{-2}	136082%
	WENO-M				MOP-WENO-M			
Time, t	L_1 error	χ_1	L_∞ error	χ_∞	L_1 error	χ_1	L_∞ error	χ_∞
10	8.28912×10^{-8}	0%	1.36173×10^{-7}	0%	8.48762×10^{-8}	2%	1.36173×10^{-7}	0%
100	8.29015×10^{-7}	0%	1.36207×10^{-6}	0%	9.93577×10^{-7}	20%	2.03738×10^{-6}	50%
200	2.27991×10^{-6}	38%	1.22731×10^{-5}	351%	1.81123×10^{-6}	9%	2.72417×10^{-6}	0%
500	1.41413×10^{-3}	34021%	1.90785×10^{-2}	280047%	4.68314×10^{-6}	13%	6.81022×10^{-6}	0%
1000	1.83325×10^{-2}	221075%	1.38215×10^{-1}	1014739%	8.53126×10^{-6}	3%	1.36195×10^{-5}	0%
	WENO-IM(2, 0.1)				MOP-WENO-IM(2, 0.1)			
Time, t	L_1 error	χ_1	L_∞ error	χ_∞	L_1 error	χ_1	L_∞ error	χ_∞
10	8.28803×10^{-8}	0%	1.36172×10^{-7}	0%	8.48292×10^{-8}	2%	1.36172×10^{-7}	0%
100	8.28891×10^{-7}	0%	1.36206×10^{-6}	0%	9.80868×10^{-7}	18%	1.87953×10^{-6}	38%
200	1.65781×10^{-6}	0%	2.72415×10^{-6}	0%	1.79137×10^{-6}	8%	2.72415×10^{-6}	0%
500	4.14443×10^{-6}	0%	6.81019×10^{-6}	0%	4.88306×10^{-6}	18%	9.14624×10^{-6}	34%
1000	8.28840×10^{-6}	0%	1.36194×10^{-5}	0%	8.63424×10^{-6}	4%	1.36194×10^{-5}	0%
	WENO-PM6				MOP-WENO-PM6			
Time, t	L_1 error	χ_1	L_∞ error	χ_∞	L_1 error	χ_1	L_∞ error	χ_∞
10	8.28795×10^{-8}	0%	1.36172×10^{-7}	0%	8.47719×10^{-8}	2%	1.36172×10^{-7}	0%
100	8.28892×10^{-7}	0%	1.36206×10^{-6}	0%	9.71688×10^{-7}	17%	1.78452×10^{-6}	31%
200	1.65782×10^{-6}	0%	2.72415×10^{-6}	0%	1.78163×10^{-6}	7%	2.72415×10^{-6}	0%
500	4.14452×10^{-6}	0%	6.81018×10^{-6}	0%	4.93547×10^{-6}	19%	1.08735×10^{-5}	60%
1000	8.84565×10^{-6}	7%	1.38461×10^{-5}	2%	8.65269×10^{-6}	4%	1.36194×10^{-5}	0%
	WENO-PPM5				MOP-WENO-PPM5			
Time, t	L_1 error	χ_1	L_∞ error	χ_∞	L_1 error	χ_1	L_∞ error	χ_∞
10	8.28794×10^{-8}	0%	1.36172×10^{-7}	0%	8.47367×10^{-8}	2%	1.36172×10^{-7}	0%
100	8.28890×10^{-7}	0%	1.36206×10^{-6}	0%	1.04103×10^{-6}	26%	1.78285×10^{-6}	31%
200	1.65781×10^{-6}	0%	2.72415×10^{-6}	0%	1.83725×10^{-6}	11%	2.72415×10^{-6}	0%
500	4.14448×10^{-6}	0%	6.81018×10^{-6}	0%	4.30721×10^{-6}	4%	6.81018×10^{-6}	0%
1000	8.28862×10^{-6}	0%	1.36194×10^{-5}	0%	8.27506×10^{-6}	0%	1.36194×10^{-5}	0%
	WENO-RM(260)				MOP-WENO-RM(260)			
Time, t	L_1 error	χ_1	L_∞ error	χ_∞	L_1 error	χ_1	L_∞ error	χ_∞
10	8.28794×10^{-8}	0%	1.36172×10^{-7}	0%	8.48225×10^{-8}	2%	1.36172×10^{-7}	0%
100	8.28889×10^{-7}	0%	1.36206×10^{-6}	0%	9.56819×10^{-7}	15%	1.58577×10^{-6}	16%
200	1.65781×10^{-6}	0%	2.72415×10^{-6}	0%	1.77008×10^{-6}	7%	2.72415×10^{-6}	0%
500	4.14448×10^{-6}	0%	6.81018×10^{-6}	0%	4.72311×10^{-6}	14%	6.81018×10^{-6}	0%
1000	8.28860×10^{-6}	0%	1.36194×10^{-5}	0%	8.55573×10^{-6}	3%	1.36194×10^{-5}	0%
	WENO-MAIM1				MOP-WENO-MAIM1			
Time, t	L_1 error	χ_1	L_∞ error	χ_∞	L_1 error	χ_1	L_∞ error	χ_∞
10	8.28796×10^{-8}	0%	1.36172×10^{-7}	0%	8.28791×10^{-8}	0%	1.36172×10^{-7}	0%
100	8.28893×10^{-7}	0%	1.36206×10^{-6}	0%	8.28894×10^{-7}	0%	1.36206×10^{-6}	0%
200	1.65782×10^{-6}	0%	2.72415×10^{-6}	0%	1.65783×10^{-6}	0%	2.72415×10^{-6}	0%
500	4.14450×10^{-6}	0%	6.81018×10^{-6}	0%	4.14454×10^{-6}	0%	6.81018×10^{-6}	0%
1000	8.28865×10^{-6}	0%	1.36194×10^{-5}	0%	8.28830×10^{-6}	0%	1.36194×10^{-5}	0%

In Figures 6 and 7, we plot the solutions computed by various schemes at output time $t = 1000$ with the grid numbers of $N = 200$ and $N = 800$, respectively. For $N = 200$, Figure 6 shows that: (1) the MOP-WENO-M scheme provides results with far higher resolution than the associated WENO-M scheme and the WENO-Z scheme, which give results with slightly better resolution than the worst one computed by the WENO-JS scheme; (2) the results of the MOP-WENO-MAIM1 scheme are very close to those of its associated WENO-MAIM1 scheme; (3) the results of the other MOP-WENO-X schemes show far better resolutions than the WENO-M , WENO-Z, and WENO-JS schemes, although they give

results with very slightly lower resolutions than their associated WENO-X schemes because of the narrower optimal weight intervals. Actually, we can amend this minor issue by using a larger grid number. Consequently, for $N = 800$, it can be seen from Figure 7 that: (1) all the MOP-WENO-X schemes produce results very close to those of their associated mapped WENO-X schemes with extremely high resolutions except the case of X = M; (2) the MOP-WENO-M scheme also produces results with very high resolution, whereas the resolutions of the results from the WENO-M , WENO-Z, and WENO-JS schemes have far lower resolutions.

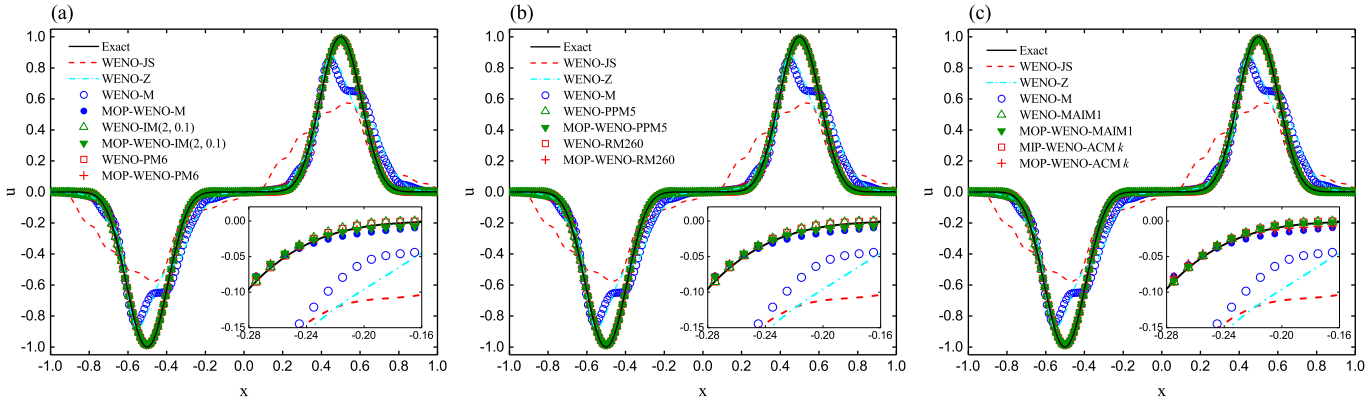

Figure 6. Performances of various WENO schemes for Example 3 at output time $t = 1000$ with a uniform mesh size of $N = 200$.

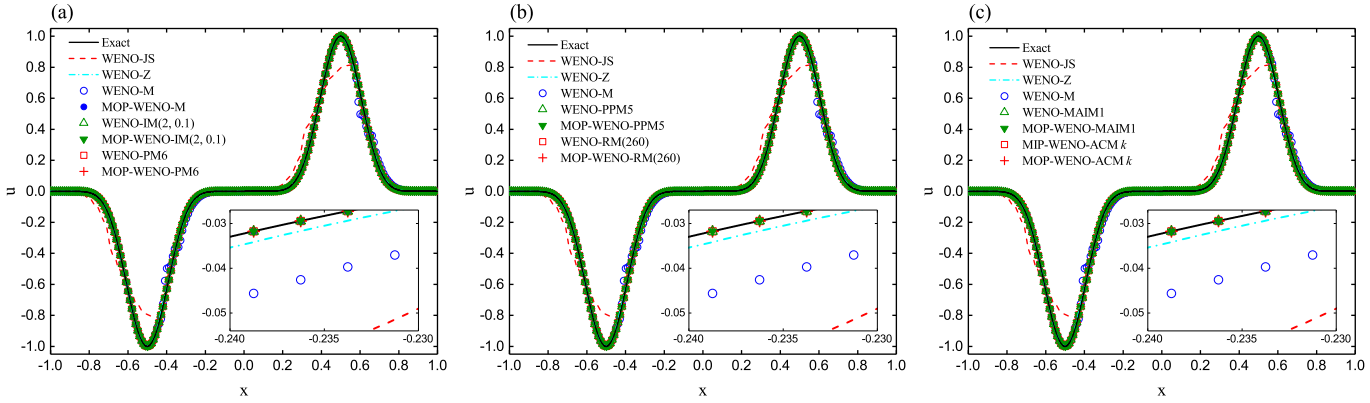

Figure 7. Performances of various WENO schemes for Example 3 at output time $t = 1000$ with a uniform mesh size of $N = 800$.

Example 4. *We calculate Equation (38) using the following initial condition [8]:*

$$u(x,0) = \begin{cases} \frac{1}{6}\left[G(x,\beta,z-\hat{\delta}) + 4G(x,\beta,z) + G(x,\beta,z+\hat{\delta})\right], & x \in [-0.8,-0.6], \\ 1, & x \in [-0.4,-0.2], \\ 1 - \left|10(x-0.1)\right|, & x \in [0.0,0.2], \\ \frac{1}{6}\left[F(x,\alpha,a-\hat{\delta}) + 4F(x,\alpha,a) + F(x,\alpha,a+\hat{\delta})\right], & x \in [0.4,0.6], \\ 0, & \text{otherwise}, \end{cases} \tag{42}$$

where $G(x,\beta,z) = \mathrm{e}^{-\beta(x-z)^2}$, $F(x,\alpha,a) = \sqrt{\max\left(1-\alpha^2(x-a)^2, 0\right)}$, and the constants are $z = -0.7, \hat{\delta} = 0.005, \beta = \frac{\log 2}{36\hat{\delta}^2}, a = 0.5$, and $\alpha = 10$. The periodic boundary condition is used. Although the CFL number can be chosen from a wide range of values—for example, CFL $= 0.6$ usually works well—we set CFL $= 0.1$ here to keep the consistent with the literatures [27,29,31,32] having strong relevance to the present study and to make thorough comparisons with the results of these literature. For brevity in the presentation, we call

this ***l****inear* ***p****roblem* SLP as it is presented by Shu et al. in [8]. It is known that this problem consists of a Gaussian, a square wave, a sharp triangle, and a semi-ellipse.

In Tables 6 and 7, we present the L_1, L_2, L_∞ errors and the corresponding convergence rates of accuracy with $t = 2$ and $t = 2000$, respectively. For the case of $t = 2$, it can be seen that: (1) the L_1 and L_2 orders of all considered schemes are approximately 1.0 and about 0.35 to 0.5, respectively; (2) negative values of the L_∞ orders of all considered schemes are generated; (3) in terms of accuracy, the MOP-WENO-X schemes produce less accurate results than the associated WENO-X schemes. For the case of $t = 2000$, it can be seen that: (1) the L_1, L_2 orders of the WENO-JS, WENO-M, and WENO-Z schemes decrease to very small values and even become negative; (2) however, the L_1 and L_2 orders of all the MOP-WENO-X schemes, and the associated mapped WENO-X schemes without WENO-M, are clearly larger than 1.0 and around 0.5 to 0.9, respectively; (3) the L_∞ orders of all WENO-X schemes are very small, and some of them are even negative (e.g., the WENO-JS, WENO-PPM5 and MIP-WENO-ACM*k* schemes), and those of the MOP-WENO-X schemes are all positive, although they are also very small; (4) in terms of accuracy, on the whole, the MOP-WENO-X schemes produce accurate and comparable results to the associated WENO-X schemes, except the WENO-M scheme. However, if we take a closer look, we can find that the resolution of the results computed by the WENO-M scheme is significantly lower than that of the MOP-WENO-M scheme, and the other mapped WENO-X schemes generate spurious oscillations, but the associated MOP-WENO-X schemes do not. Detailed tests are conducted and the solutions are presented carefully to demonstrate this in the following subsection.

Table 6. Convergence properties of various considered schemes on solving $u_t + u_x = 0$ with initial condition Equation (42), $t = 2$. To be continued.

Scheme	N	L_1 Error	L_1 Order	L_2 Error	L_2 Order	L_∞ Error	L_∞ Order
WENO-JS	200	6.30497×10^{-2}	-	1.08621×10^{-1}	-	4.09733×10^{-1}	-
	400	2.81654×10^{-2}	1.2103	7.71111×10^{-2}	0.4943	4.19594×10^{-1}	−0.0343
	800	1.41364×10^{-2}	0.9945	5.69922×10^{-2}	0.4362	4.28463×10^{-1}	−0.0302
WENO-Z	200	4.98422×10^{-2}	-	9.59452×10^{-2}	-	3.92478×10^{-1}	-
	400	2.37836×10^{-2}	1.0674	6.98647×10^{-2}	0.4576	4.03601×10^{-1}	−0.0403
	800	1.19851×10^{-2}	0.9887	5.14607×10^{-2}	0.4411	4.13262×10^{-1}	−0.0341
WENO-M	200	4.77201×10^{-2}	-	9.53073×10^{-2}	-	3.94243×10^{-1}	-
	400	2.23407×10^{-2}	1.0949	6.91333×10^{-2}	0.4632	4.05856×10^{-1}	−0.0419
	800	1.11758×10^{-2}	0.9993	5.09232×10^{-2}	0.4411	4.16937×10^{-1}	−0.0389
MOP-WENO-M	200	5.72690×10^{-2}	-	1.00827×10^{-1}	-	4.14785×10^{-1}	-
	400	2.72999×10^{-2}	1.0689	7.33765×10^{-2}	0.4585	4.45144×10^{-1}	-0.1019
	800	1.42908×10^{-2}	0.9338	5.57886×10^{-2}	0.3953	4.64024×10^{-1}	−0.0599
WENO-IM(2, 0.1)	200	4.40293×10^{-2}	-	9.19118×10^{-2}	-	3.86789×10^{-1}	-
	400	2.02331×10^{-2}	1.1217	6.68479×10^{-2}	0.4594	3.98769×10^{-1}	−0.0441
	800	1.01805×10^{-2}	0.9909	4.95333×10^{-2}	0.4325	4.09515×10^{-1}	−0.0383
MOP-WENO-IM(2, 0.1)	200	6.09985×10^{-2}	-	1.03438×10^{-1}	-	4.35238×10^{-1}	-
	400	2.86731×10^{-2}	1.0891	7.56598×10^{-2}	0.4512	4.62098×10^{-1}	−0.0864
	800	1.45601×10^{-2}	0.9777	5.61842×10^{-2}	0.4294	4.64674×10^{-1}	−0.0080
WENO-PM6	200	4.66681×10^{-2}	-	9.45566×10^{-2}	-	3.96866×10^{-1}	-
	400	2.13883×10^{-2}	1.1256	6.82948×10^{-2}	0.4694	4.06118×10^{-1}	−0.0332
	800	1.06477×10^{-2}	1.0063	5.03724×10^{-2}	0.4391	4.15277×10^{-1}	−0.0322
MOP-WENO-PM6	200	5.45129×10^{-2}	-	9.95654×10^{-2}	-	4.02785×10^{-1}	-
	400	2.61755×10^{-2}	1.0584	7.16656×10^{-2}	0.4744	4.26334×10^{-1}	−0.0820
	800	1.38981×10^{-2}	0.9133	5.44733×10^{-2}	0.3957	4.63134×10^{-1}	−0.1194

Table 6. *Cont.*

Scheme	N	L_1 Error	L_1 Order	L_2 Error	L_2 Order	L_∞ Error	L_∞ Order
WENO-PPM5	200	4.54081×10^{-2}	-	9.33165×10^{-2}	-	3.91076×10^{-1}	-
	400	2.07948×10^{-2}	1.1267	6.76172×10^{-2}	0.4647	4.02214×10^{-1}	−0.0405
	800	1.04018×10^{-2}	0.9994	4.99580×10^{-2}	0.4367	4.12113×10^{-1}	−0.0351
MOP-WENO-PPM5	200	5.51553×10^{-2}	-	9.94592×10^{-2}	-	4.04763×10^{-1}	-
	400	2.65464×10^{-2}	1.0550	7.19973×10^{-2}	0.4662	4.32887×10^{-1}	−0.0969
	800	1.41381×10^{-2}	0.9089	5.52704×10^{-2}	0.3814	4.68577×10^{-1}	−0.1143
WENO-RM(260)	200	4.63072×10^{-2}	-	9.40674×10^{-2}	-	3.96762×10^{-1}	-
	400	2.13545×10^{-2}	1.1167	6.81954×10^{-2}	0.4640	4.08044×10^{-1}	−0.0405
	800	1.06392×10^{-2}	1.0052	5.03289×10^{-2}	0.4383	4.16722×10^{-1}	−0.0304
MOP-WENO-RM(260)	200	5.54343×10^{-2}	-	9.93009×10^{-2}	-	4.04041×10^{-1}	-
	400	2.71415×10^{-2}	1.0303	7.22823×10^{-2}	0.4582	4.38358×10^{-1}	−0.1176
	800	1.45563×10^{-2}	0.8989	5.66845×10^{-2}	0.3507	4.70380×10^{-1}	−0.1017
WENO-MAIM1	200	5.71142×10^{-2}	-	1.03257×10^{-1}	-	4.15051×10^{-1}	-
	400	2.48065×10^{-2}	1.2031	7.29236×10^{-2}	0.5018	4.23185×10^{-1}	−0.0280
	800	1.21078×10^{-2}	1.0348	5.32803×10^{-2}	0.4528	4.28710×10^{-1}	−0.0187
MOP-WENO-MAIM1	200	5.98640×10^{-2}	-	1.05066×10^{-1}	-	4.12365×10^{-1}	-
	400	2.64819×10^{-2}	1.1767	7.38102×10^{-2}	0.5094	4.26841×10^{-1}	−0.0498
	800	1.33647×10^{-2}	0.9866	5.44089×10^{-2}	0.4400	4.38310×10^{-1}	−0.0383
MIP-WENO-ACMk	200	4.45059×10^{-2}	-	9.24356×10^{-2}	-	3.92505×10^{-1}	-
	400	2.03633×10^{-2}	1.1280	6.69718×10^{-2}	0.4649	4.03456×10^{-1}	−0.0397
	800	1.02139×10^{-2}	0.9954	4.95672×10^{-2}	0.4342	4.13217×10^{-1}	−0.0345
MOP-WENO-ACMk	200	5.56533×10^{-2}	-	9.94223×10^{-2}	-	4.03765×10^{-1}	-
	400	2.79028×10^{-2}	0.9961	7.33101×10^{-2}	0.4396	4.48412×10^{-1}	−0.1513
	800	1.43891×10^{-2}	0.9554	5.51602×10^{-2}	0.4104	4.67036×10^{-1}	−0.0587

Table 7. Convergence properties of various considered schemes on solving $u_t + u_x = 0$ with initial condition Equation (42), $t = 2000$.

Scheme	N	L_1 Error	L_1 Order	L_2 Error	L_2 Order	L_∞ Error	L_∞ Order
WENO-JS	200	6.12899×10^{-1}	-	5.08726×10^{-1}	-	7.99265×10^{-1}	-
	400	5.99215×10^{-1}	0.0326	5.01160×10^{-1}	0.0216	8.20493×10^{-1}	−0.0378
	800	5.50158×10^{-1}	0.1232	4.67585×10^{-1}	0.1000	8.14650×10^{-1}	0.0103
WENO-Z	200	3.86995×10^{-1}	-	3.42335×10^{-1}	-	6.85835×10^{-1}	-
	400	2.02287×10^{-1}	0.9359	2.18125×10^{-1}	0.6503	5.18993×10^{-1}	0.4021
	800	1.66703×10^{-1}	0.2791	1.94240×10^{-1}	0.1673	5.04564×10^{-1}	0.0407
WENO-M	200	3.81597×10^{-1}	-	3.59205×10^{-1}	-	6.89414×10^{-1}	-
	400	3.25323×10^{-1}	0.2302	3.12970×10^{-1}	0.1988	6.75473×10^{-1}	0.0295
	800	3.48528×10^{-1}	−0.0994	3.24373×10^{-1}	−0.0516	6.25645×10^{-1}	0.1106
MOP-WENO-M	200	3.85134×10^{-1}	-	3.48164×10^{-1}	-	7.41230×10^{-1}	-
	400	1.74987×10^{-1}	1.1381	1.86418×10^{-1}	0.9012	5.04987×10^{-1}	0.5537
	800	6.40251×10^{-2}	1.4505	1.07629×10^{-1}	0.7925	4.81305×10^{-1}	0.0693
WENO-IM(2, 0.1)	200	2.17411×10^{-1}	-	2.30000×10^{-1}	-	5.69864×10^{-1}	-
	400	1.12590×10^{-1}	0.9493	1.64458×10^{-1}	0.4839	4.82180×10^{-1}	0.2410
	800	5.18367×10^{-2}	1.1190	9.98968×10^{-2}	0.7192	4.73102×10^{-1}	0.02784
MOP-WENO-IM(2, 0.1)	200	3.83289×10^{-1}	-	3.47817×10^{-1}	-	7.25185×10^{-1}	-
	400	1.67452×10^{-1}	1.1947	1.76550×10^{-1}	0.9783	5.24538×10^{-1}	0.4673
	800	6.44253×10^{-2}	1.3780	1.05858×10^{-1}	0.7379	5.19333×10^{-1}	0.0144
WENO-PM6	200	2.17323×10^{-1}	-	2.28655×10^{-1}	-	5.63042×10^{-1}	-
	400	1.05197×10^{-1}	1.0467	1.47518×10^{-1}	0.6323	5.04977×10^{-1}	0.1570
	80	4.47030×10^{-2}	1.2347	9.34250×10^{-2}	0.6590	4.71368×10^{-1}	0.0994

Table 7. *Cont.*

Scheme	N	L_1 Error	L_1 Order	L_2 Error	L_2 Order	L_∞ Error	L_∞ Order
MOP-WENO-PM6	200	4.51487×10^{-1}	-	4.01683×10^{-1}	-	7.71539×10^{-1}	-
	400	1.75875×10^{-1}	1.3601	1.83478×10^{-1}	1.1305	5.06314×10^{-1}	0.6077
	800	6.32990×10^{-2}	1.4743	1.04688×10^{-1}	0.8095	4.76091×10^{-1}	0.0888
WENO-PPM5	200	2.17174×10^{-1}	-	2.29008×10^{-1}	-	5.65575×10^{-1}	-
	400	1.03201×10^{-1}	1.0734	1.46610×10^{-1}	0.6434	5.06463×10^{-1}	0.1593
	800	4.81637×10^{-2}	1.0994	9.47748×10^{-2}	0.6294	5.14402×10^{-1}	-0.0224
MOP-WENO-PPM5	200	3.86292×10^{-1}	-	3.49072×10^{-1}	-	7.36405×10^{-1}	-
	400	1.75232×10^{-1}	1.1404	1.88491×10^{-1}	0.8890	5.14732×10^{-1}	0.5167
	800	6.36336×10^{-2}	1.4614	1.06801×10^{-1}	0.8196	4.98424×10^{-1}	0.0464
WENO-RM(260)	200	2.17363×10^{-1}	-	2.28662×10^{-1}	-	5.62933×10^{-1}	-
	400	1.04347×10^{-1}	1.0587	1.47093×10^{-1}	0.6365	4.98644×10^{-1}	0.1750
	800	4.45176×10^{-2}	1.2289	9.33066×10^{-2}	0.6567	4.71450×10^{-1}	0.0809
MOP-WENO-RM(260)	200	4.56942×10^{-1}	-	4.06524×10^{-1}	-	7.71747×10^{-1}	-
	400	2.25420×10^{-1}	1.0194	2.25814×10^{-1}	0.8482	5.12018×10^{-1}	0.5919
	800	8.02414×10^{-2}	1.4902	1.18512×10^{-1}	0.9301	4.90610×10^{-1}	0.0616
WENO-MAIM1	200	2.18238×10^{-1}	-	2.29151×10^{-1}	-	5.63682×10^{-1}	-
	400	1.09902×10^{-1}	0.9897	1.51024×10^{-1}	0.6015	4.94657×10^{-1}	0.1885
	800	4.41601×10^{-2}	1.3154	9.35506×10^{-2}	0.6910	4.72393×10^{-1}	0.0664
MOP-WENO-MAIM1	200	2.39900×10^{-1}	-	2.47191×10^{-1}	-	6.06985×10^{-1}	-
	400	1.41890×10^{-1}	0.7577	1.71855×10^{-1}	0.5244	5.61908×10^{-1}	0.1113
	800	5.43475×10^{-2}	1.3845	1.02170×10^{-1}	0.7502	5.10242×10^{-1}	0.1392
MIP-WENO-ACMk	200	2.21312×10^{-1}	-	2.28433×10^{-1}	-	5.36234×10^{-1}	-
	400	1.06583×10^{-1}	1.0541	1.46401×10^{-1}	0.6418	5.03925×10^{-1}	0.0897
	800	4.76305×10^{-2}	1.1620	9.40930×10^{-2}	0.6378	5.15924×10^{-1}	-0.0339
MOP-WENO-ACMk	200	3.83033×10^{-1}	-	3.46814×10^{-1}	-	7.18464×10^{-1}	-
	400	1.77114×10^{-1}	1.1128	1.87369×10^{-1}	0.8883	5.05980×10^{-1}	0.5058
	800	6.70535×10^{-2}	1.4013	1.09368×10^{-1}	0.7767	4.80890×10^{-1}	0.0734

4.2. 1D Linear Advection Problems with Long Output Times

The objective of this subsection is to demonstrate the advantage of the MOP-WENO-X schemes on long-output-time simulations that can obtain high resolution and meanwhile do not generate spurious oscillations.

The one-dimensional linear advection problem Equation (38) is solved with the periodic boundary condition by taking the following two initial conditions.

Case 1. (SLP) The initial condition is given by Equation (42).

Case 2. (BiCWP) The initial condition is given by

$$u(x,0) = \begin{cases} 0, & x \in [-1.0,-0.8] \bigcup (-0.2,0.2] \bigcup (0.8,1.0], \\ 0.5, & x \in (-0.6,-0.4] \bigcup (0.2,0.4] \bigcup (0.6,0.8], \\ 1, & x \in (-0.8,-0.6] \bigcup (-0.4,-0.2] \bigcup (0.4,0.6]. \end{cases} \tag{43}$$

Case 1 and Case 2 were carefully simulated in [9]. Case 1 is called SLP as mentioned earlier in this paper. Case 2 consists of several constant states separated by sharp discontinuities at $x = \pm 0.8, \pm 0.6, \pm 0.4, \pm 0.2$ and it was called BiCWP for brevity in the presentation as the profile of the exact solution for this ***P**roblem* looks like the ***B**reach **i**n **C**ity **W**all*.

In Figures 8–11, we show the comparison of considered schemes for SLP and BiCWP, respectively, by taking $t = 2000$ and $N = 800$. It can be seen that: (1) all the MOP-WENO-X schemes produce results with considerable resolutions which are significantly higher than those of the WENO-JS, WENO-M and WENO-Z schemes, and what is more, they all do not generate spurious oscillations, while most of their associated WENO-X schemes do, when solving both SLP and BiCWP; (2) it should be reminded that the WENO-IM(2, 0.1) scheme appears not to generate spurious oscillations and it gives better resolution than

the MOP-WENO-IM(2, 0.1) scheme in most of the region when solving SLP on present computing condition, however, from Figure 8b, one can observe that the MOP-WENO-IM(2, 0.1) scheme gives a better resolution of the Gaussian than the WENO-IM(2, 0.1) scheme, and if taking a closer look, one can see that the WENO-IM(2, 0.1) scheme generates a very slight spurious oscillation near $x = -0.435$ as shown in Figure 8c; (3) it is very evident as shown in Figure 10 that, when solving BiCWP, the WENO-IM(2, 0.1) scheme generates the spurious oscillations.

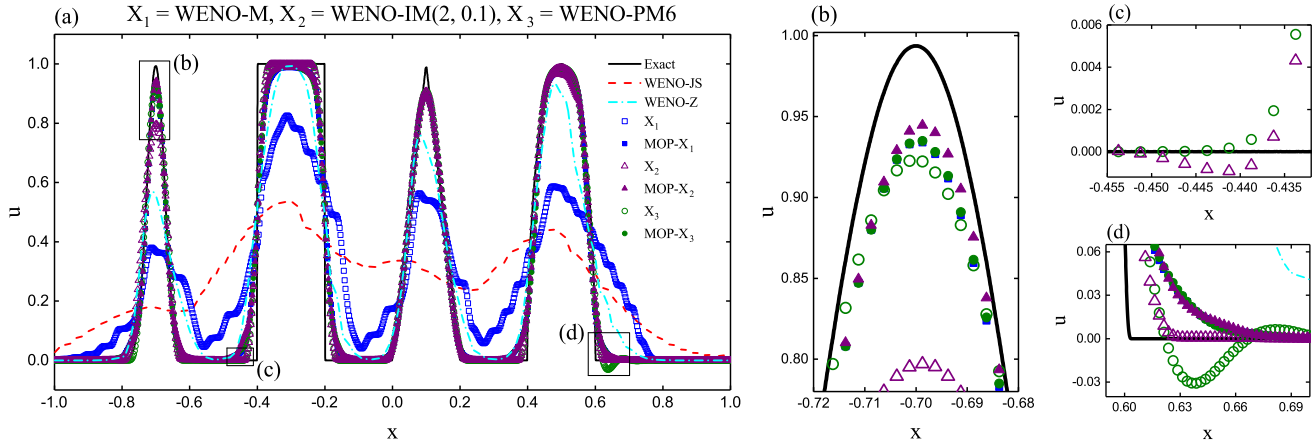

Figure 8. Performance of the WENO-JS, WENO-M, MOP-WENO-M, WENO-IM(2, 0.1), MOP-WENO-IM(2, 0.1), WENO-PM6 and MOP-WENO-PM6 schemes for the SLP at output time $t = 2000$ with a uniform mesh size of $N = 800$.

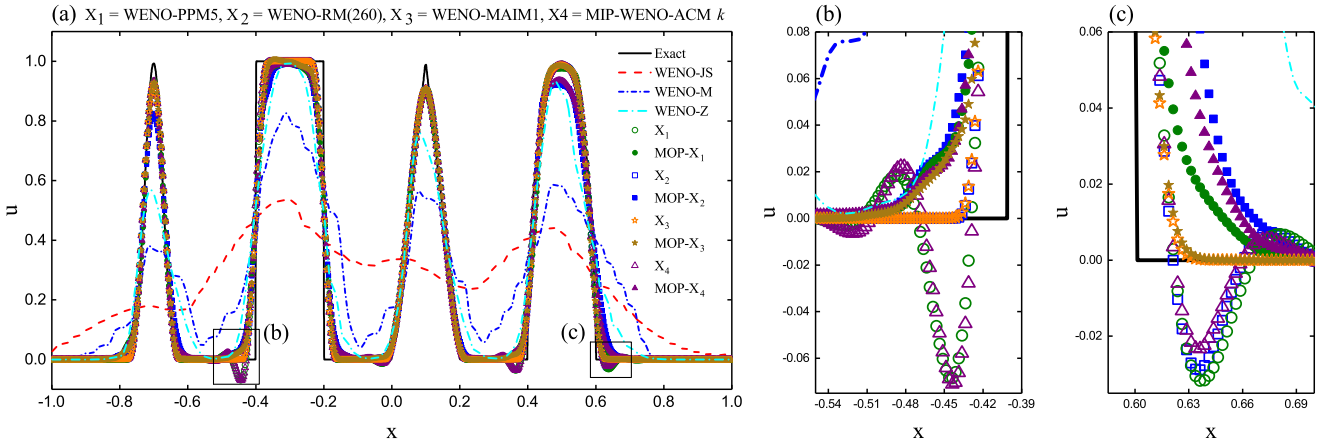

Figure 9. Performance of the WENO-JS, WENO-M, WENO-PPM5, MOP-WENO-PPM5, WENO-RM260, MOP-WENO-RM260, WENO-MAIM1, MOP-WNEO-MAIM1, MIP-WENO-ACM*k* and MOP-WENO-ACM*k* schemes for the SLP at output time $t = 2000$ with a uniform mesh size of $N = 800$.

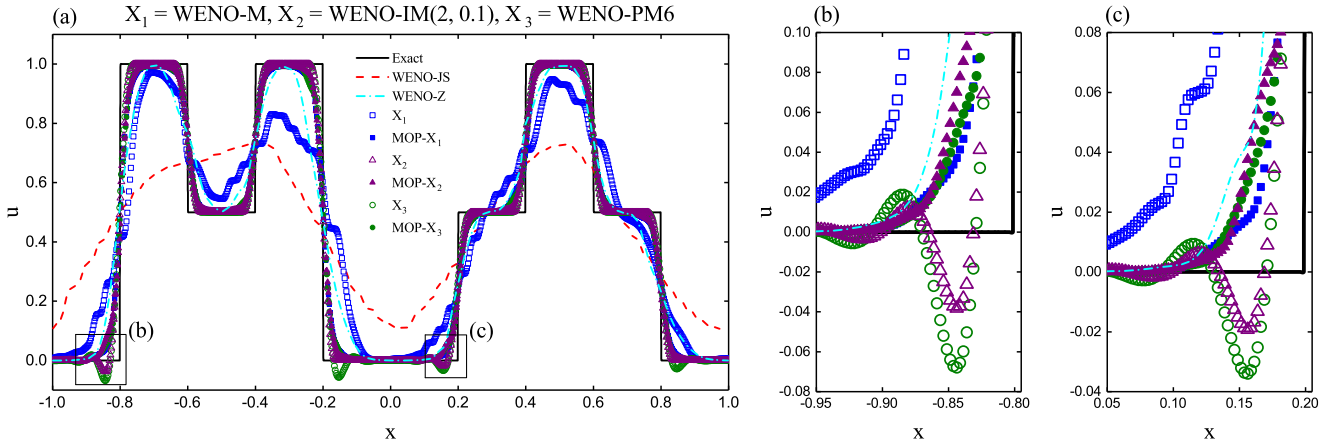

Figure 10. Performance of the WENO-JS, WENO-M, MOP-WENO-M, WENO-IM(2, 0.1), MOP-WENO-IM(2, 0.1), WENO-PM6 and MOP-WENO-PM6 schemes for the BiCWP at output time $t = 2000$ with a uniform mesh size of $N = 800$.

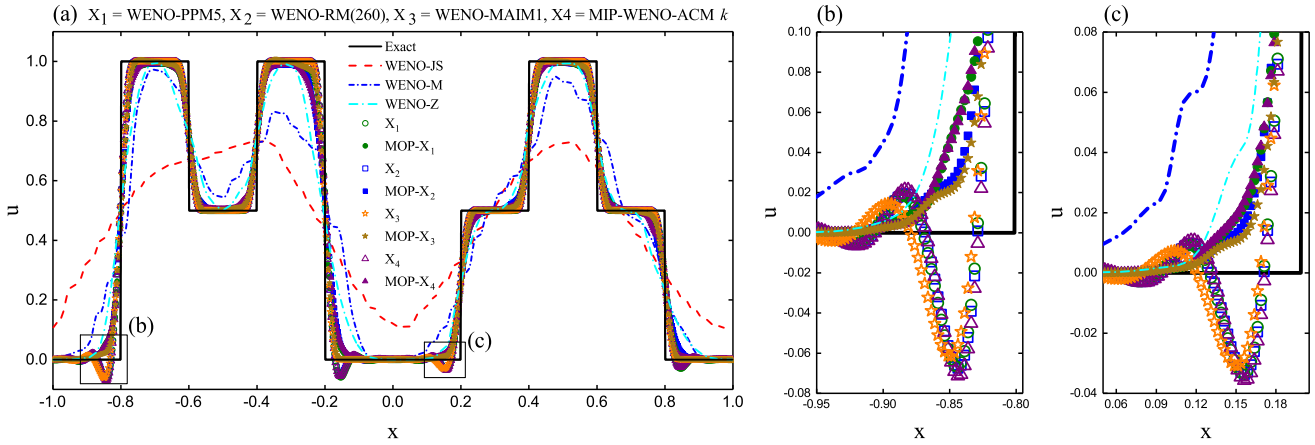

Figure 11. Performance of the WENO-JS, WENO-M, WENO-PPM5, MOP-WENO-PPM5, WENO-RM260, MOP-WENO-RM260, WENO-MAIM1, MOP-WNEO-MAIM1, MIP-WENO-ACM*k* and MOP-WENO-ACM*k* schemes for the BiCWP at output time $t = 2000$ with a uniform mesh size of $N = 800$.

In Figures 12–15, we show the comparison of considered schemes for SLP and BiCWP respectively, by taking $t = 200$ and $N = 3200$. From these solutions computed with larger grid numbers and a reduced but still long output time, it can be seen that: (1) firstly, the WENO-IM(2, 0.1) scheme generates spurious oscillations but the MOP-WENO-IM(2, 0.1) scheme does not while provides an improved resolution when solving SLP; (2) although the resolutions of the results computed by the WENO-JS, WENO-M and WENO-Z schemes are significantly improved for both SLP and BiCWP, the MOP-WENO-X schemes still evidently provide much better resolutions; (3) the spurious oscillations generated by the WENO-X schemes appear to be more evident and more intense as the grid number increases, while the associated MOP-WENO-X schemes can still avoid spurious oscillations but obtain higher resolutions, when solving both SLP and BiCWP.

For the further interpretation, without loss of generality, in Figure 16, we present the *non-OP points* of the numerical solutions of SLP computed by the WENO-M and MOP-WENO-M schemes with $N = 800, t = 2000$, and the *non-OP points* of the numerical solutions of BiCWP computed by the WENO-PM6 and MOP-WENO-PM6 schemes with $N = 3200, t = 200$. We can find that there are a great many *non-OP points* in the solutions of the WENO-M and WENO-PM6 schemes while the numbers of the *non-OP points* in the solutions of the MOP-WENO-M and MOP-WENO-PM6 schemes are zero. Actually, there are many *non-OP points* for all considered mapped WENO-X schemes. Furthermore, as expected, there are no *non-OP points* for the associated MOP-WENO-X schemes and the

WENO-JS scheme for all computing cases here. We do not show the results of the *non-OP points* for all computing cases here just for the simplicity of illustration.

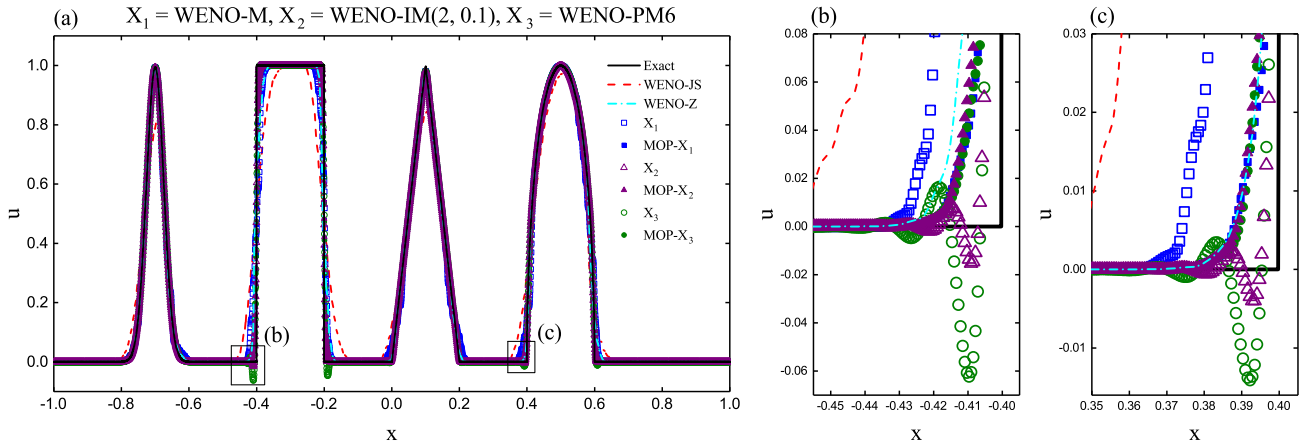

Figure 12. Performance of the WENO-JS, WENO-M, MOP-WENO-M, WENO-IM(2, 0.1), MOP-WENO-IM(2, 0.1), WENO-PM6 and MOP-WENO-PM6 schemes for the SLP at output time $t = 200$ with a uniform mesh size of $N = 3200$.

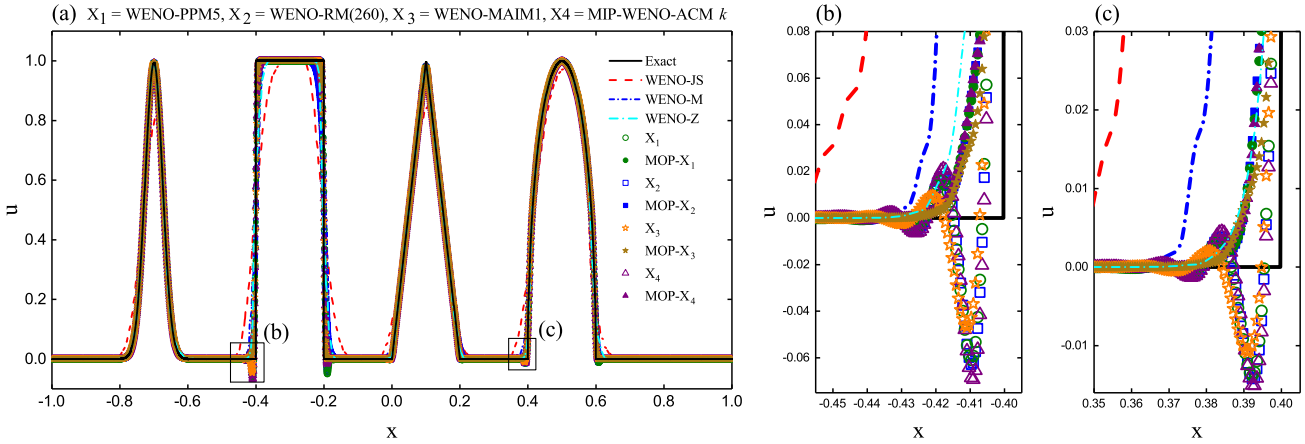

Figure 13. Performance of the WENO-JS, WENO-M, WENO-PPM5, MOP-WENO-PPM5, WENO-RM260, MOP-WENO-RM260, WENO-MAIM1, MOP-WNEO-MAIM1, MIP-WENO-ACM*k* and MOP-WENO-ACM*k* schemes for the SLP at output time $t = 200$ with a uniform mesh size of $N = 3200$.

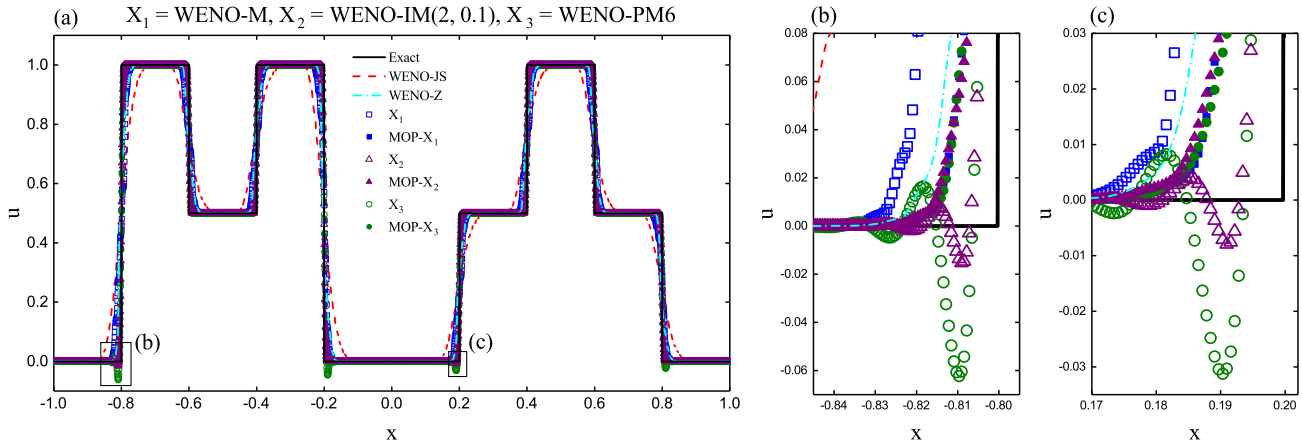

Figure 14. Performance of the WENO-JS, WENO-M, MOP-WENO-M, WENO-IM(2, 0.1), MOP-WENO-IM(2, 0.1), WENO-PM6 and MOP-WENO-PM6 schemes for the BiCWP at output time $t = 200$ with a uniform mesh size of $N = 3200$.

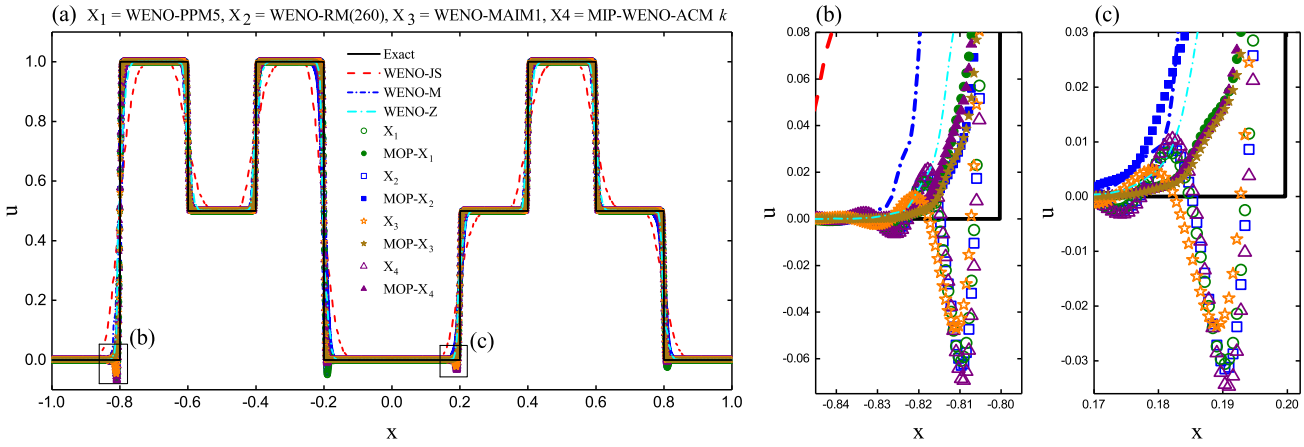

Figure 15. Performance of the WENO-JS, WENO-M, WENO-PPM5, MOP-WENO-PPM5, WENO-RM260, MOP-WENO-RM260, WENO-MAIM1, MOP-WNEO-MAIM1, MIP-WENO-ACM*k* and MOP-WENO-ACM*k* schemes for the BiCWP at output time $t = 200$ with a uniform mesh size of $N = 3200$.

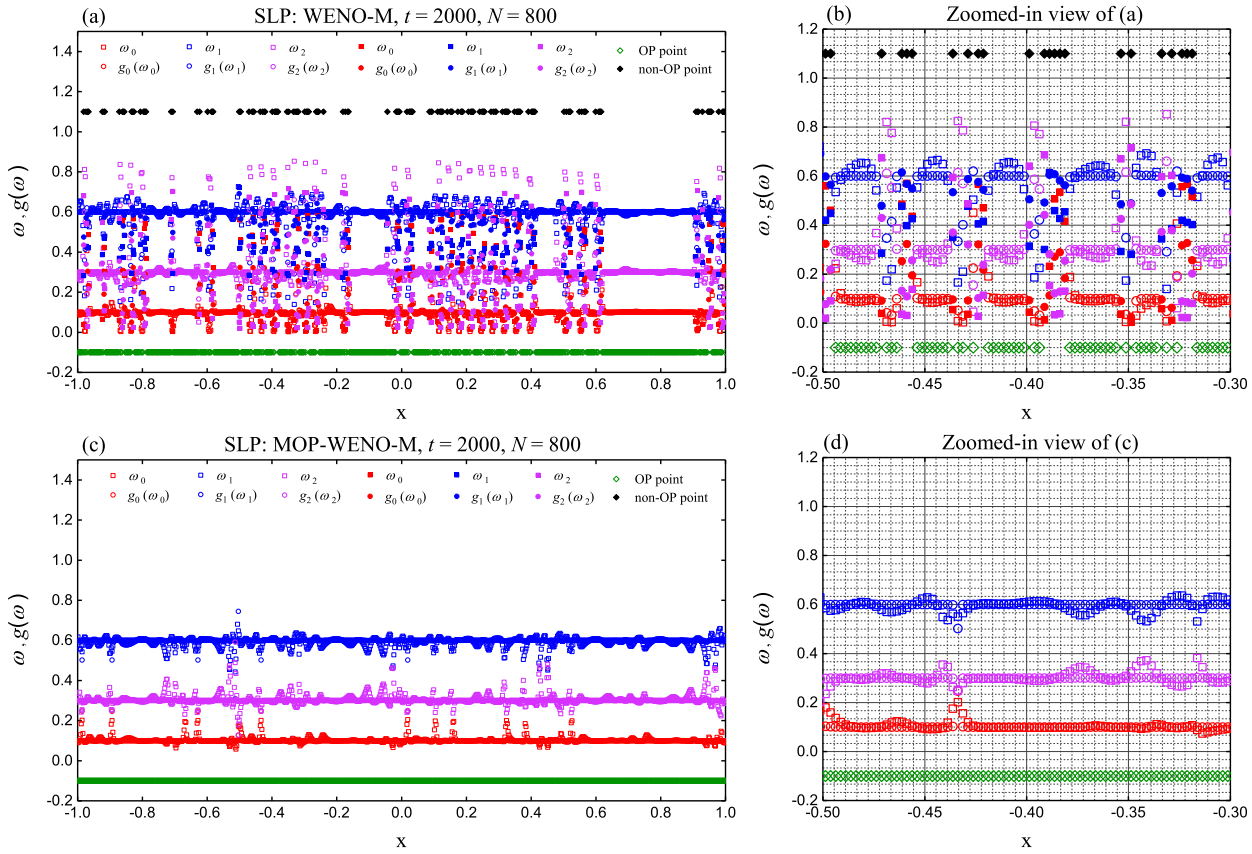

Figure 16. *Cont.*

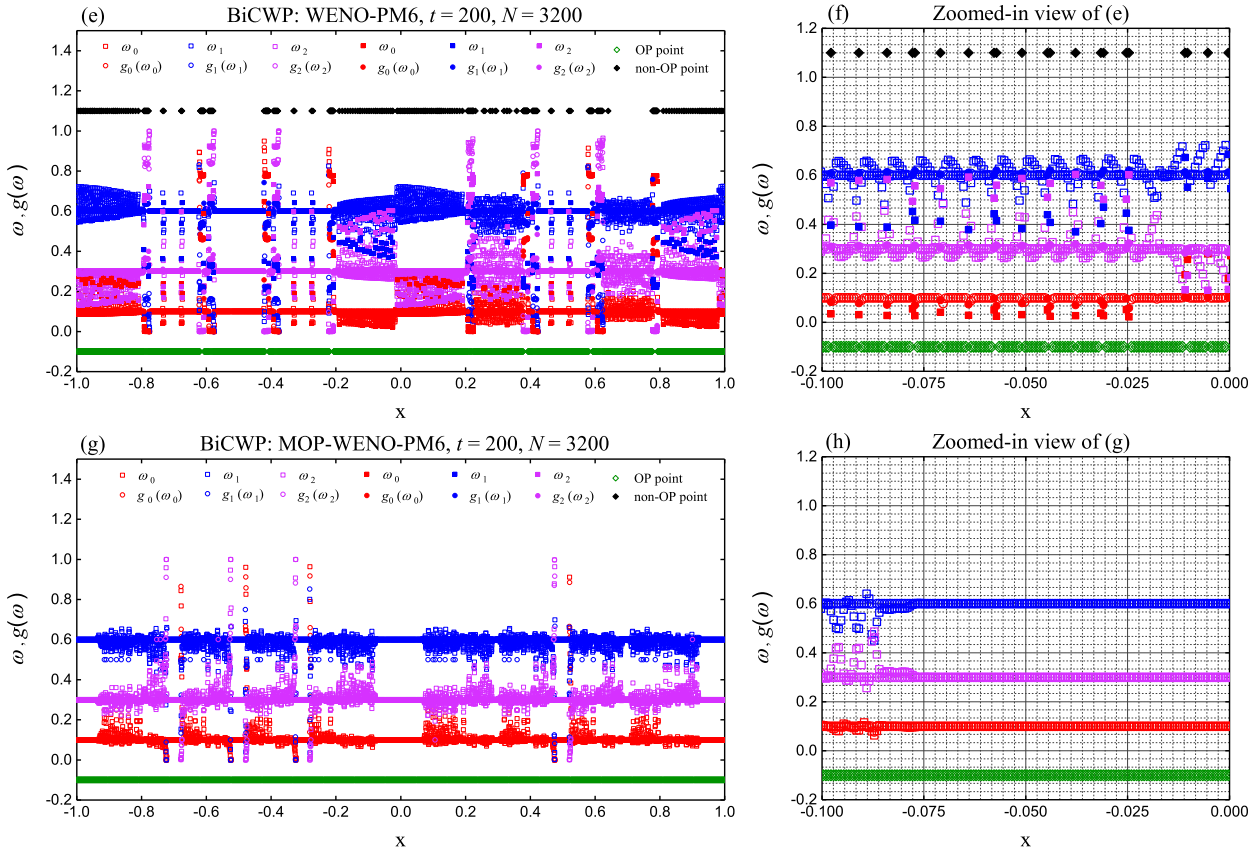

Figure 16. The *non-OP points* in the numerical solutions of SLP computed by the WENO-M and MOP-WENO-M schemes with $N = 800, t = 2000$, and the *non-OP points* in the numerical solutions of BiCWP computed by the WENO-PM6 and MOP-WENO-PM6 schemes with $N = 3200, t = 200$.

In summary, the solutions in this subsection could be regarded as numerical verifications of properties *C*4, *C*5 of Theorem 2. In other words, it could be indicated that the general method to introduce the *OP* mapping can help to gain the advantage of achieving high resolutions and in the meantime preventing spurious oscillations when solving problems with discontinuities for long output times. Additionally, this is the most important point we want to report in this paper.

4.3. Comparison with Central WENO Schemes

In this subsection, we compare the performances of the MOP-WENO-X schemes with the quite recent approach, called central WENO (CWENO) schemes. For simplicity, only the cases of the WENO-NW6 [36], WENO-CU6 [37] and WENO-θ6 [38] schemes are taken into account in the following discussion.

We firstly consider the following example.

Example 5. *We compute*

$$\begin{cases} u_t + u_x = 0, \quad x \in (-1, 1), \\ u(x, 0) = \max(-\sin(\pi x), 0), \end{cases} \tag{44}$$

with periodic boundary conditions.

We calculate this problem by the fifth-order MOP-WENO-X schemes proposed in the present work and the sixth-order central schemes of WENO-NW6, WENO-CU6 and WENO-θ6 schemes. The output time is taken to be $t = 2.4$ and the cell number is $N = 200$. The solutions are plotted in Figure 17. It clearly shows that the sixth-order central WENO schemes of WENO-NW6 and WENO-CU6 perform worse than the fifth-order MOP-WENO-

X schemes. It was reported by Jung et al. [38] that this loss of resolution is an important issue since there are many problems whose solution often exhibits the same behavior as this example. Therefore, we claim that the MOP-WENO-X schemes are more favorable than the central WENO schemes of WENO-NW6 and WENO-CU6 for this kind of problems. In addition, the the central WENO scheme of WENO-θ6 performs as well as the MOP-WENO-X schemes in this test. Unfortunately, it performs worse and gives significantly lower resolution than the MOP-WENO-X schemes on solving problems with discontinuities for long output times. We now discuss this in detail.

We calculate the problems of SLP and BiCWP (see Section 4.2) by using the sixth-order central schemes of WENO-NW6, WENO-CU6, and WENO-θ6 schemes. The computing conditions of $t = 200$ and $N = 3200$ are used here. In Figures 18 and 19, the results for SLP and BiCWP are shown. From these figures, we can see that the sixth-order central WENO schemes of WENO-NW6 and WENO-θ6 provide significantly lower resolutions than the fifth-order MOP-WENO-X schemes. The WENO-CU6 scheme appears to obtain the resolution equivalent to, or even better than those of the MOP-WENO-X schemes. However, it generates spurious oscillations, and the MOP-WENO-X schemes do not.

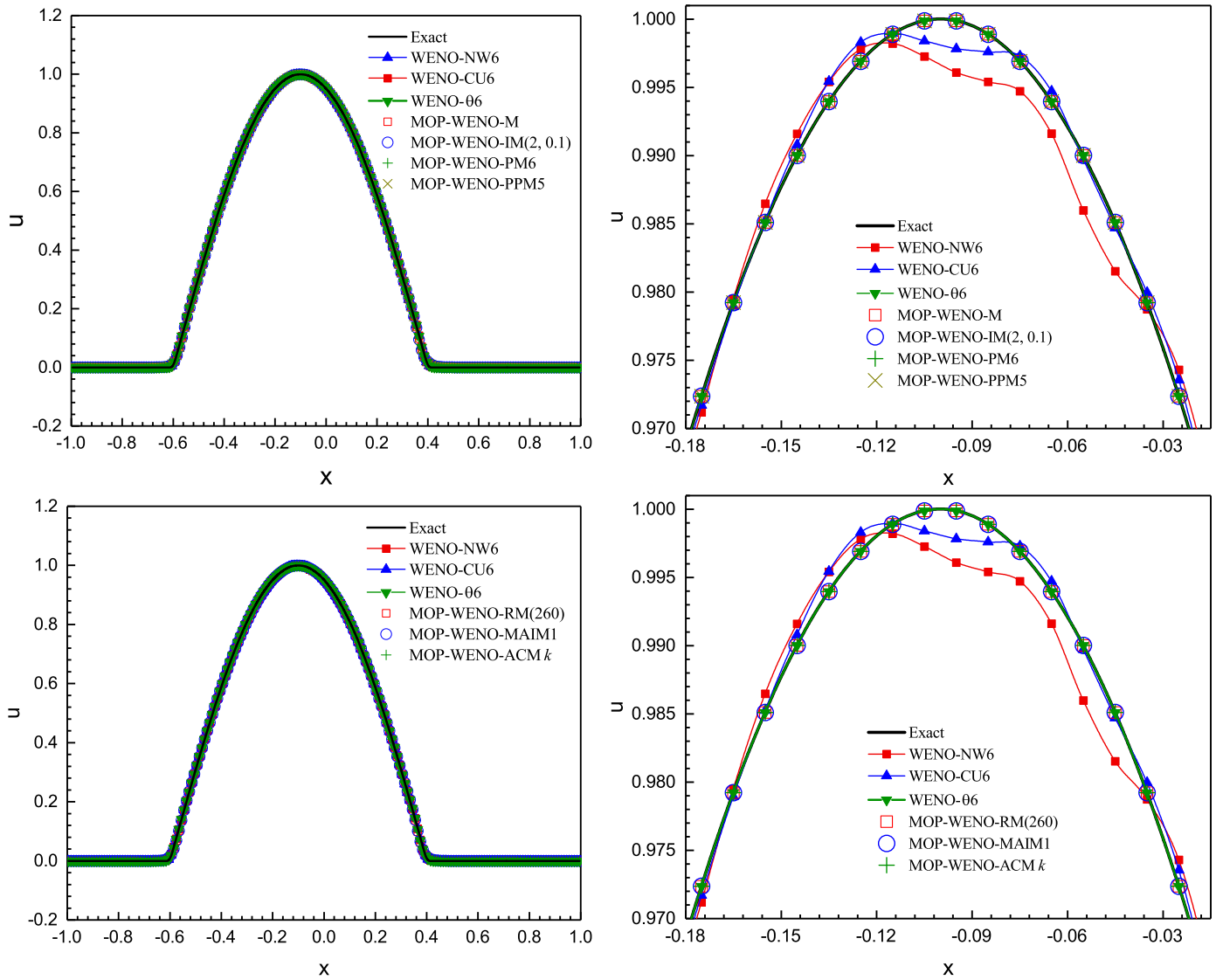

Figure 17. (**Left**): Numerical solutions of Equation (44) at time $t = 2.4$ obtained from different WENO schemes. (**Right**): Zoom near the critical region.

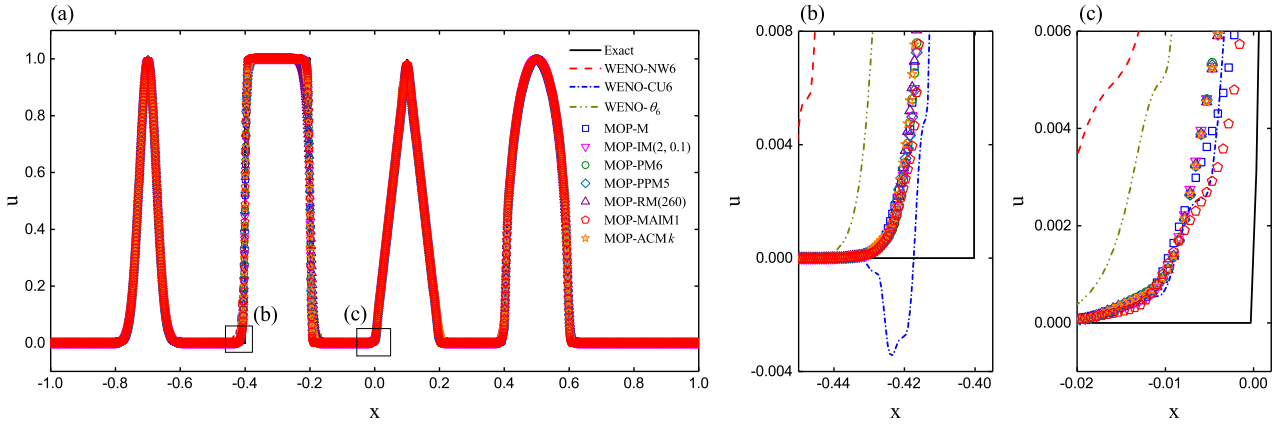

Figure 18. Performance of the WENO-NW6, WENO-CU6, WENO-θ6 and MOP-WENO-X schemes for the SLP at output time $t = 200$ with a uniform mesh size of $N = 3200$.

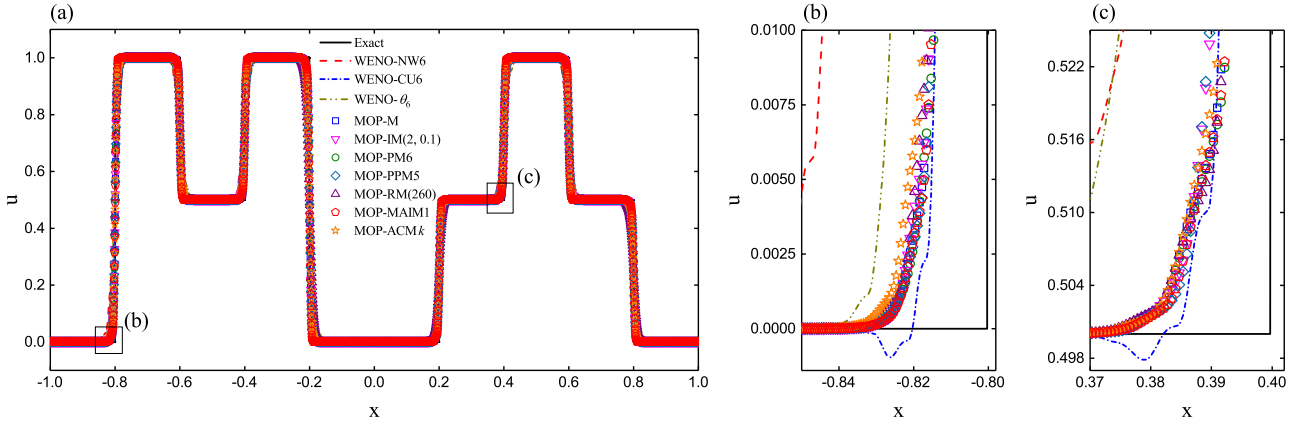

Figure 19. Performance of the WENO-NW6, WENO-CU6, WENO-θ6 and MOP-WENO-X schemes for the BiCWP at output time $t = 200$ with a uniform mesh size of $N = 3200$.

4.4. Euler System in Two Dimension

In this subsection, we focus on the numerical simulations of the shock-vortex interaction problem [41,42] and the 2D Riemann problem [43–45]. They are governed by the two-dimensional Euler system of gas dynamics, taking the following strong conservation form of mass, momentum and energy

$$\begin{aligned}
&\frac{\partial \rho}{\partial t} + \frac{\partial(\rho u)}{\partial x} + \frac{\partial(\rho v)}{\partial y} = 0,\\
&\frac{\partial(\rho u)}{\partial t} + \frac{\partial(\rho u^2 + p)}{\partial x} + \frac{\partial(\rho uv)}{\partial y} = 0,\\
&\frac{\partial(\rho v)}{\partial t} + \frac{\partial(\rho vu)}{\partial x} + \frac{\partial(\rho v^2 + p)}{\partial y} = 0,\\
&\frac{\partial E}{\partial t} + \frac{\partial(uE + up)}{\partial x} + \frac{\partial(vE + vp)}{\partial y} = 0,
\end{aligned} \tag{45}$$

where ρ, u, v, p, and E are the density components of velocity in the x and y coordinate directions, pressure, and total energy, respectively. The following equation of state for an ideal polytropic gas is used to close the two-dimensional Euler system Equation (45)

$$p = (\gamma - 1)\Big(E - \frac{1}{2}\rho(u^2 + v^2)\Big),$$

where γ is the ratio of specific heat, and we set $\gamma = 1.4$ in this paper. In the computations below, the CFL number is taken to be 0.5. All the considered WENO schemes are applied dimension-by-dimension to solve the two-dimensional Euler system and the local characteristic decomposition [8] is used. In [46], Zhang et al. investigated two commonly used classes of finite volume WENO schemes in two-dimensional Cartesian meshes, and we employ the one denoted as class A in this subsection.

Example 6. (Shock-vortex interaction) *We consider the shock-vortex interaction problem used in [41,42]. It consists of the interaction of a left moving shock wave with a right moving vortex. The computational domain is initialized by*

$$(\rho, u, v, p)(x, y, 0) = \begin{cases} \mathbf{U}_{\mathrm{L}}, & x < 0.5, \\ \mathbf{U}_{\mathrm{R}}, & x \geq 0.5, \end{cases}$$

where $\mathbf{U}_{\mathrm{L}} = (\rho_{\mathrm{L}}, u_{\mathrm{L}}, v_{\mathrm{L}}, p_{\mathrm{L}}) = (1, \sqrt{\gamma}, 0, 1)$, and $\mathbf{U}_{\mathrm{R}} = (\rho_{\mathrm{R}}, u_{\mathrm{R}}, v_{\mathrm{R}}, p_{\mathrm{R}})$ taking the form

$$p_{\mathrm{R}} = 1.3, \rho_{\mathrm{R}} = \rho_{\mathrm{L}}\left(\frac{\gamma - 1 + (\gamma + 1)p_{\mathrm{R}}}{\gamma + 1 + (\gamma - 1)p_{\mathrm{R}}}\right)$$
$$u_{\mathrm{R}} = u_{\mathrm{L}}\left(\frac{1 - p_{\mathrm{R}}}{\sqrt{\gamma - 1 + p_{\mathrm{R}}(\gamma + 1)}}\right), v_{\mathrm{R}} = 0.$$

The vortex $\delta\mathbf{U} = (\delta\rho, \delta u, \delta v, \delta p)$, defined by the following perturbations, is superimposed onto the left state $\mathbf{U}_{\mathrm{L}}$,

$$\delta\rho = \frac{\rho_{\mathrm{L}}^2}{(\gamma - 1)p_{\mathrm{L}}}\delta T, \delta u = \epsilon\frac{y - y_{\mathrm{c}}}{r_{\mathrm{c}}}\mathrm{e}^{\alpha(1-r^2)}, \delta vs. = -\epsilon\frac{x - x_{\mathrm{c}}}{r_{\mathrm{c}}}\mathrm{e}^{\alpha(1-r^2)}, \delta p = \frac{\gamma\rho_{\mathrm{L}}^2}{(\gamma - 1)\rho_{\mathrm{L}}}\delta T,$$

where $\epsilon = 0.3, r_{\mathrm{c}} = 0.05, \alpha = 0.204, x_{\mathrm{c}} = 0.25, y_{\mathrm{c}} = 0.5, r = \sqrt{((x - x_{\mathrm{c}})^2 + (y - y_{\mathrm{c}})^2)/r_{\mathrm{c}}^2}$, $\delta T = -(\gamma - 1)\epsilon^2\mathrm{e}^{2\alpha(1-r^2)}/(4\alpha\gamma)$. The transmissive boundary condition is used on all boundaries. A uniform mesh size of 800×800 is used and the output time is set to be $t = 0.35$.

We calculate this problem using all the considered mapped WENO-X schemes in Table 1 and their associated MOP-WENO-X schemes. For the sake of brevity though, we only present the solutions of the WENO-M, WENO-IM(2, 0.1), WENO-PPM5, WENO-MAIM1 schemes and their associated MOP-WENO-X schemes in Figures 20 and 21, where the first rows give the final structures of the shock and vortex in density profile of the existing mapped WENO-X schemes, the second rows give those of the associated MOP-WENO-X schemes, and the third rows give the cross-sectional slices of density plot along the plane $y = 0.65$ where $x \in [0.70, 0.76]$. We find that all the considered schemes perform well in capturing the main structure of the shock and vortex after the interaction. It can be seen that there are clear post-shock oscillations in the solutions of the WENO-M, WENO-IM(2, 0.1), and WENO-PPM5 schemes. However, in the solutions of the MOP-WENO-M, MOP-WENO-IM(2, 0.1), and MOP-WENO-PPM5 schemes, the post-shock oscillations are either gone or significantly reduced. The post-shock oscillations of the WENO-MAIM1 scheme are very slight and even hard to be noticed. Actually, it seems difficult to distinguish the solutions of the WENO-MAIM1 scheme from that of the MOP-WENO-MAIM1 scheme only according to the structure of the shock and vortex in the density profile. Nevertheless, when taking a closer look from the cross-sectional slices of the density profile along the plane $y = 0.65$ at the bottom right picture of Figure 21 where the reference solution is obtained using the WENO-JS scheme with a uniform mesh size of 1600×1600, we can see that the post-shock oscillation of the WENO-MAIM1 scheme is very remarkable while it is imperceptible for the MOP-WENO-MAIM1 scheme. Additionally, from the third rows of Figures 20 and 21, we find that the WENO-IM(2, 0.1) and WENO-PPM5 schemes generate the post-shock oscillations with much bigger amplitudes than that of the WENO-MAIM1 scheme. The WENO-M scheme also generates clear post-shock oscillations with the amplitudes slightly smaller than that of the WENO-IM(2, 0.1) and WENO-PPM5 schemes. Evidently, the solutions of the MOP-WENO-M, MOP-WENO-IM(2, 0.1) and

MOP-WENO-PPM5 schemes almost generate no post-shock oscillations or only generate some imperceptible numerical oscillations and their solutions are very close to the reference solution, and this should be an advantage of the mapped WENO schemes whose mapping functions are *OP*.

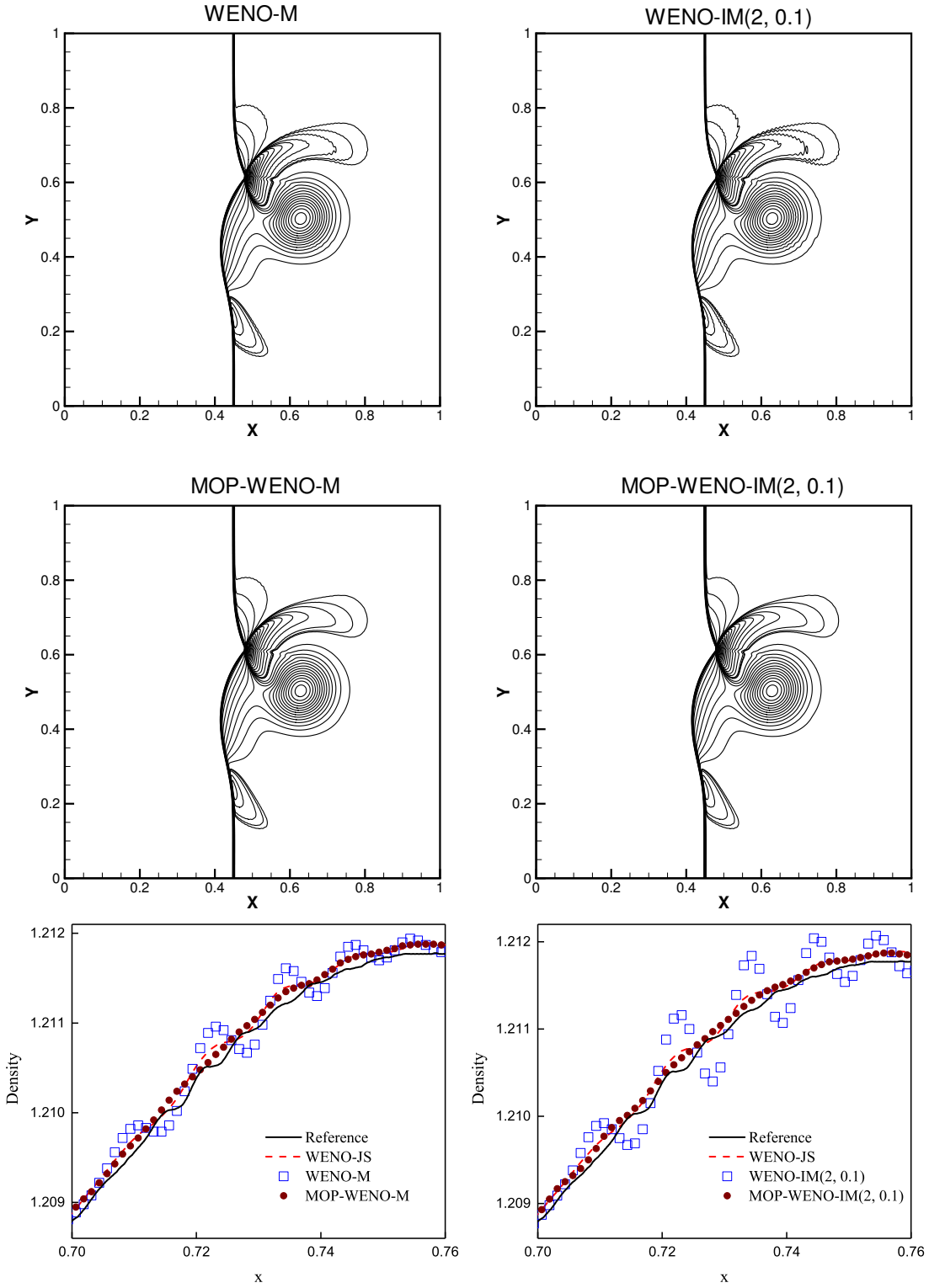

Figure 20. Density plots for the Shock-vortex interaction using 30 contour lines with range from 0.9 to 1.4 (the first two rows) and the cross-sectional slices of density plot along the plane $y = 0.65$ where $x \in [0.70, 0.76]$ (the third row), computed using the WENO-M and MOP-WENO-M (**left column**), WENO-IM(2, 0.1), and MOP-WENO-IM(2, 0.1) (**right column**) schemes.

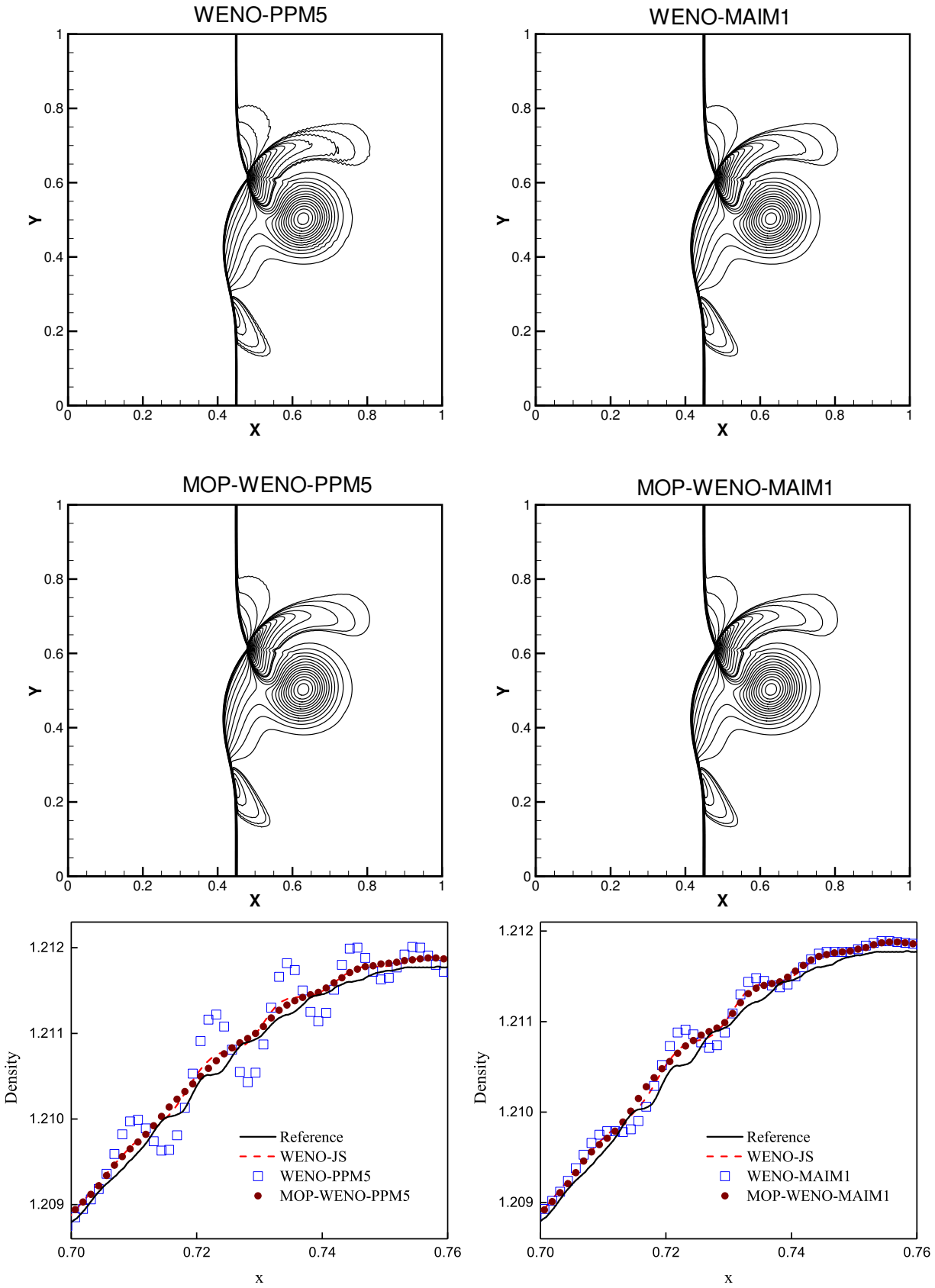

Figure 21. Density plots for the Shock-vortex interaction using 30 contour lines with range from 0.9 to 1.4 (the first two rows) and the cross-sectional slices of density plot along the plane $y = 0.65$ where $x \in [0.70, 0.76]$ (the third row), computed using the WENO-PPM5 and MOP-WENO-PPM5 (**left column**), WENO-MAIM1 and MOP-WENO-MAIM1 (**right column**) schemes.

Example 7. (2D Riemann problem) *It is very favorable to test the high-resolution numerical methods [30,45,47] using the series of 2D Riemann problems [43,44]. In [45], Lax et al. classified a total of 19 genuinely different Configurations for 2D Riemann problem and calculated all the numerical solutions. Configuration 4 is chosen here for the test, and the computational domain is initialized by*

$$(\rho,u,v,p)(x,y,0)=\begin{cases}(1.1,0.0,0.0,1.1), & 0.5\le x\le 1.0, 0.5\le y\le 1.0,\\ (0.5065,0.8939,0.0,0.35), & 0.0\le x\le 0.5, 0.5\le y\le 1.0,\\ (1.1,0.8939,0.8939,1.1), & 0.0\le x\le 0.5, 0.0\le y\le 0.5,\\ (0.5065,0.0,0.8939,0.35), & 0.5\le x\le 1.0, 0.0\le y\le 0.5.\end{cases}$$

The transmission boundary condition is used on all boundaries, and the numerical solutions are calculated on a uniform mesh size of 800×800. The computations proceed to $t=0.25$.

Similarly, although we calculate this problem using all the considered mapped WENO-X schemes in Table 1 and their associated MOP-WENO-X schemes, we only present the solutions of the WENO-M, WENO-PM6, WENO-RM260 and MIP-WENO-ACM*k* schemes and their associated MOP-WENO-X schemes here for the sake of brevity. We have shown the numerical results of density obtained by using these schemes in Figures 22 and 23, where the first rows give the structures of the 2D Riemann problem in density profile of the existing mapped WENO-X schemes, the second rows give those of the associated MOP-WENO-X schemes, and the third rows give the cross-sectional slices of density plot along the plane $y=0.5$ where $x\in[0.65,0.692]$. We can see that all schemes can capture the main structure of the solution. However, we can also observe that there are obvious post-shock oscillations (as marked by the pink boxes), which are unfavorable for the fidelity of the results, in the solutions of the WENO-M, WENO-PM6, WENO-RM(260) and MIP-WENO-ACM*k* schemes. These post-shock oscillations can be seen more clearly from the cross-sectional slices of density profile as presented in the third rows of Figures 22 and 23, where the reference solution is obtained by using the WENO-JS scheme with a uniform mesh size of 3000×3000. Noticeably, there are either almost no or imperceptible post-shock oscillations in the solutions of the MOP-WENO-M, MOP-WENO-PM6, MOP-WENO-RM(RM260) and MOP-WENO-ACM*k* schemes. Again, we believe that this should be an advantage of the mapped WENO schemes whose mapping functions are *OP*.

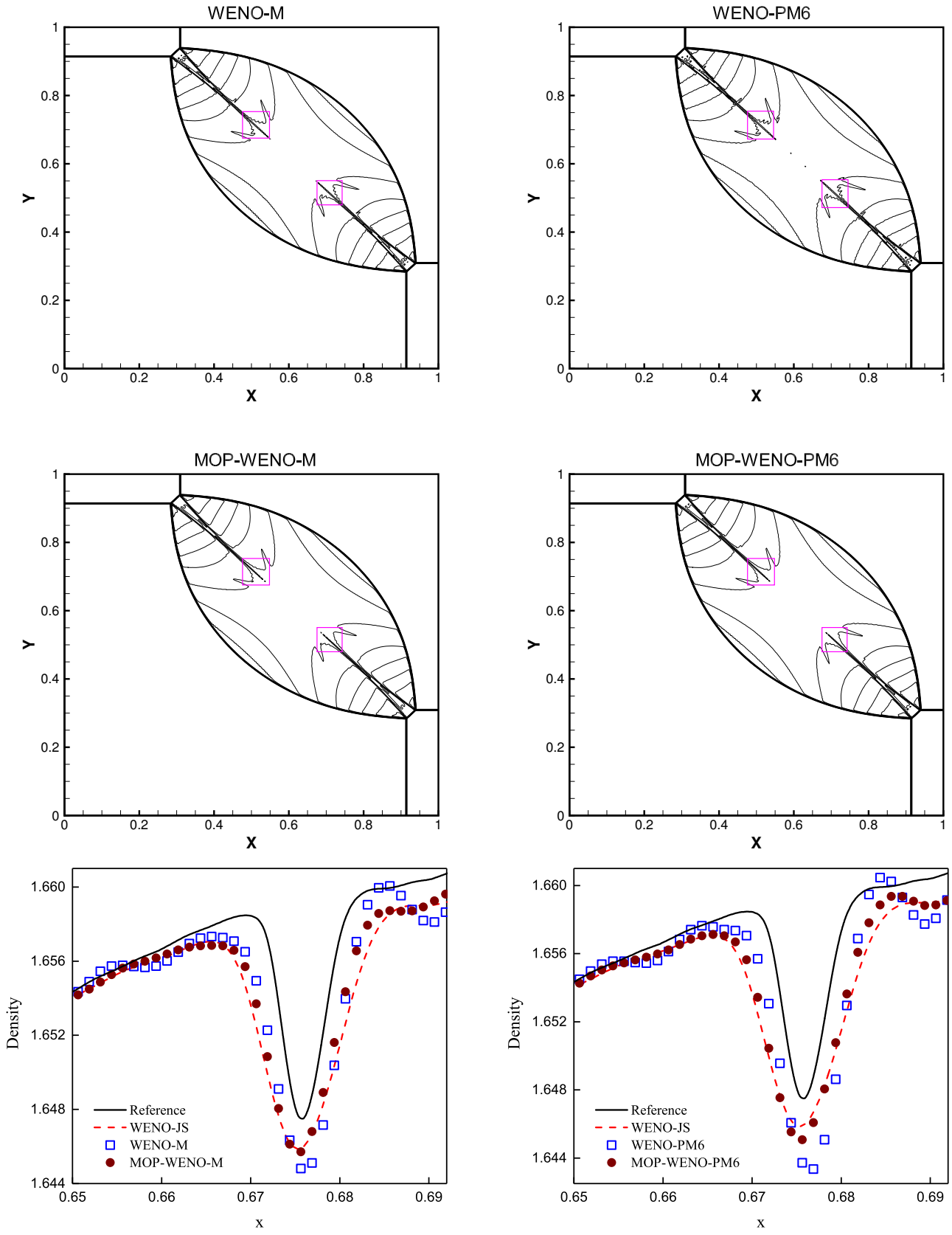

Figure 22. Density plots for the 2D Riemann problem using 30 contour lines with range from 0.5 to 1.9 (the first two rows) and the cross-sectional slices of density plot along the plane $y = 0.5$ where $x \in [0.65, 0.692]$ (the third row), computed using the WENO-M and MOP-WENO-M (**left column**), WENO-PM6 and MOP-WENO-PM6 (**right column**) schemes.

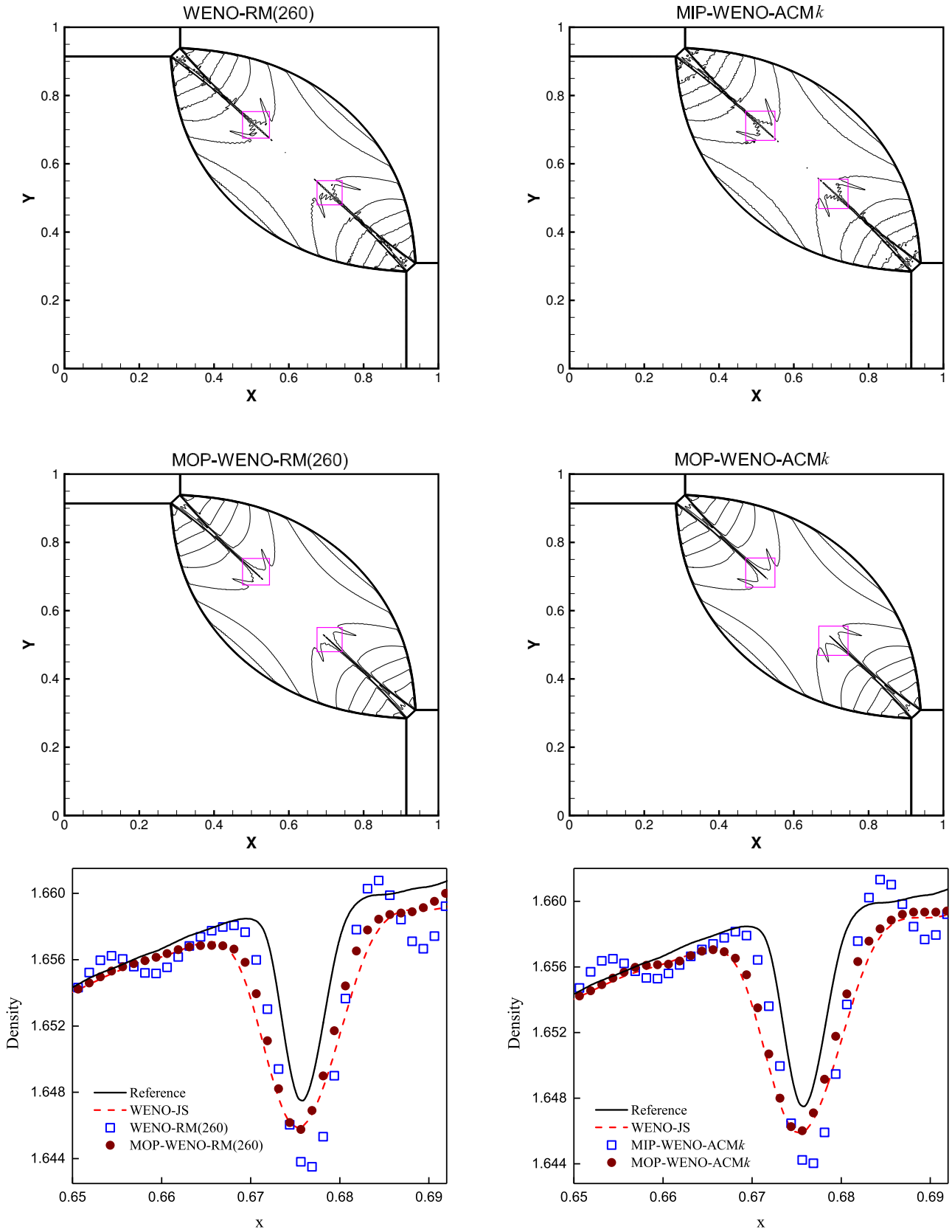

Figure 23. Density plots for the 2D Riemann problem using 30 contour lines with range from 0.5 to 1.9 (the first two rows) and the cross-sectional slices of density plot along the plane $y = 0.5$ where $x \in [0.65, 0.692]$ (the third row), computed using the WENO-RM(260) and MOP-WENO-RM(260) (**left column**), MIP-WENO-ACMk and MOP-WENO-ACMk (**right column**) schemes.

5. Conclusions

The concept of *OP-Mapped WENO* schemes standing for the family of the mapped WENO schemes with *order-preserving (OP)* mappings, as well as a general way to build one group of this kind of schemes, has been proposed in this paper. Specifically, we extended the *OP* mapping introduced in [9] to various existing mapped WENO schemes in references by providing a general formula of their mapping functions. A systematic analysis has been performed to prove that the improved mapped WENO scheme based on the existing mapped WENO-X scheme, denoted as MOP-WENO-X, generates numerical solutions with the same convergence rates of accuracy in smooth regions as the associated WENO-X scheme. Furthermore, numerical experiments were run to show that the MOP-WENO-X schemes have the same advantage as the mapped WENO scheme proposed in [9] in calculating the one-dimensional linear advection problems including discontinuities with long output times. The mapping functions of the MOP-WENO-X schemes are *OP* and hence able to attain high resolutions and avoid spurious oscillations meanwhile. Moreover, numerical results with the 2D Euler system problems were presented to show that the MOP-WENO-X schemes perform well in simulating the two-dimensional problems with strong shock waves to capture the main flow structures and remove or significantly reduce the post-shock oscillations.

Author Contributions: All authors have equally contributed to this paper. They have read and approved the final version of the manuscript. All authors have read and agreed to the published version of the manuscript.

Funding: This research received no external funding.

Conflicts of Interest: The authors declare no conflict of interest.

References

1. Harten, A.; Engquist, B.; Osher, S.; Chakravarthy, S.R. Uniformly high order accurate essentially non-oscillatory schemes III. *J. Comput. Phys.* **1987**, *71*, 231–303. [CrossRef]
2. Harten, A.; Osher, S. Uniformly high order accurate essentially non-oscillatory schemes I. *SIAM J. Numer. Anal.* **1987**, *24*, 279–309. [CrossRef]
3. Harten, A.; Osher, S.; Engquist, B.; Chakravarthy, S.R. Some results on uniformly high order accurate essentially non-oscillatory schemes. *Appl. Numer. Math.* **1986**, *2*, 347–377. [CrossRef]
4. Harten, A. ENO schemes with subcell resolution. *J. Comput. Phys.* **1989**, *83*, 148–184. [CrossRef]
5. Shu, C.W.; Osher, S. Efficient implementation of essentially non-oscillatory shock-capturing schemes. *J. Comput. Phys.* **1988**, *77*, 439–471. [CrossRef]
6. Shu, C.W.; Osher, S. Efficient implementation of essentially non-oscillatory shock-capturing schemes II. *J. Comput. Phys.* **1989**, *83*, 32–78. [CrossRef]
7. Liu, X.D.; Osher, S.; Chan, T. Weighted essentially non-oscillatory schemes. *J. Comput. Phys.* **1994**, *115*, 200–212. [CrossRef]
8. Jiang, G.S.; Shu, C.W. Efficient implementation of weighted ENO schemes. *J. Comput. Phys.* **1996**, *126*, 202–228. [CrossRef]
9. Li, R.; Zhong, W. A new mapped WENO scheme using order-preserving mapping. *Commun. Comput. Phys.* **2021**, under review.
10. Dumbser, M.; Zanotti, O.; Hidalgo, A.; Balsara, D.S. ADER-WENO finite volume schemes with space-time adaptive mesh refinement. *J. Comput. Phys.* **2013**, *248*, 257–286. [CrossRef]
11. Boscheri, W.; Dumbser, M. An Efficient Quadrature-Free Formulation for High Order Arbitrary-Lagrangian–Eulerian ADER-WENO Finite Volume Schemes on Unstructured Meshes. *J. Sci. Comput.* **2016**, *66*, 240–274. [CrossRef]
12. Boscheri, W.; Semplice, M.; Dumbser, M. Central WENO Subcell Finite Volume Limiters for ADER Discontinuous Galerkin Schemes on Fixed and Moving Unstructured Meshes. *Commun. Comput. Phys.* **2019**, *25*, 311–346. [CrossRef]
13. Boscheri, W.; Dumbser, M. High order accurate direct Arbitrary-Lagrangian–Eulerian ADER-WENO finite volume schemes on moving curvilinear unstructured meshes. *Comput. Fluids* **2016**, *136*, 48–66. [CrossRef]
14. Tsoutsanis, P.; Titarev, V.A.; Drikakis, D. WENO schemes on arbitrary mixed-element unstructured meshes in three space dimensions. *J. Comput. Phys.* **2011**, *230*, 1585–1601. [CrossRef]
15. Titarev, V.A.; Tsoutsanis, P.; Drikakis, D. WENO Schemes for Mixed-Element Unstructured Meshes. *Commun. Comput. Phys.* **2010**, *8*, 585–609. [CrossRef]
16. Titarev, V.A.; Toro, E.F. ADER: Arbitrary High Order Godunov Approach. *J. Sci. Comput.* **2002**, *17*, 609–618. [CrossRef]
17. Titarev, V.A.; Toro, E.F. Finite-volume WENO schemes for three-dimensional conservation laws. *J. Comput. Phys.* **2004**, *201*, 238–260. [CrossRef]

18. Titarev, V.A.; Toro, E.F. ADER schemes for three-dimensional non-linear hyperbolic systems. *J. Comput. Phys.* **2005**, *204*, 715–736. [CrossRef]
19. Titarev, V.A.; Toro, E.F. WENO schemes based on upwind and centred TVD fluxes. *Comput. Fluids* **2005**, *34*, 705–720. [CrossRef]
20. Semplice, M.; Coco, A.; Russo, G.; Titarev, V.A.; Toro, E.F. Adaptive Mesh Refinement for Hyperbolic Systems Based on Third-Order Compact WENO Reconstruction. *J. Sci. Comput.* **2016**, *66*, 692–724. [CrossRef]
21. Cravero, I.; Puppo, G.; Semplice, M.; Visconti, G. Cool WENO schemes. *Comput. Fluids* **2018**, *169*, 71–86. [CrossRef]
22. Puppo, G.; Semplice, M. Well-Balanced High Order 1D Schemes on Non-uniform Grids and Entropy Residuals. *J. Sci. Comput.* **2016**, *66*, 1052–1076. [CrossRef]
23. Levy, D.; Puppo, G.; Russo, G. Compact central WENO schemes for multidimensional conservation laws. *SIAM J. Sci. Comput.* **2000**, *22*, 656–672. [CrossRef]
24. Levy, D.; Puppo, G.; Russo, G. A fourth-order central WENO scheme for multidimensional hyperbolic systems of conservation laws. *SIAM J. Sci. Comput.* **2002**, *24*, 480–506. [CrossRef]
25. Henrick, A.K.; Aslam, T.D.; Powers, J.M. Mapped weighted essentially non-oscillatory schemes: Achieving optimal order near critical points. *J. Comput. Phys.* **2005**, *207*, 542–567. [CrossRef]
26. Borges, R.; Carmona, M.; Costa, B.; Don, W.S. An improved weighted essentially non-oscillatory scheme for hyperbolic conservation laws. *J. Comput. Phys.* **2008**, *227*, 3191–3211. [CrossRef]
27. Feng, H.; Huang, C.; Wang, R. An improved mapped weighted essentially non-oscillatory scheme. *Appl. Math. Comput.* **2014**, *232*, 453–468. [CrossRef]
28. Wang, R.; Feng, H.; Huang, C. A New Mapped Weighted Essentially Non-oscillatory Method Using Rational Function. *J. Sci. Comput.* **2016**, *67*, 540–580. [CrossRef]
29. Feng, H.; Hu, F.; Wang, R. A new mapped weighted essentially non-oscillatory scheme. *J. Sci. Comput.* **2012**, *51*, 449–473. [CrossRef]
30. Li, Q.; Liu, P.; Zhang, H. Piecewise Polynomial Mapping Method and Corresponding WENO Scheme with Improved Resolution. *Commun. Comput. Phys.* **2015**, *18*, 1417–1444. [CrossRef]
31. Li, R.; Zhong, W. A modified adaptive improved mapped WENO method. *Commun. Comput. Phys.* **2021**, accepted.
32. Li, R.; Zhong, W. An efficient mapped WENO scheme using approximate constant mapping. *Numer. Math. Theor. Meth. Appl.* **2021**, accepted.
33. Zhang, S.; Shu, C.W. A new smoothness indicator for the WENO schemes and its effect on the convergence to steady state solutions. *J. Sci. Comput.* **2007**, *31*, 273–305. [CrossRef]
34. Wang, R.; Feng, H. Observations on the fifth-order WENO method with non-uniform meshes. *Appl. Math. Comput.* **2008**, *196*, 433–447. [CrossRef]
35. Hu, G.; Li, R.; Tang, T. A robust WENO type finite volumn solver for steady Euler equations on unstructured grids. *Commun. Comput. Phys.* **2011**, *9*, 627–648. [CrossRef]
36. Yamaleev, N.K.; Carpenter, M.H. A systematic methodology for constructing high-order energy stable WENO schemes. *J. Comput. Phys.* **2009**, *228*, 4248–4272. [CrossRef]
37. Fu, L.; Hu, X.; Adams, N.A. A family of high-order targeted ENO schemes for compressible-fluid simulations. *J. Comput. Phys.* **2016**, *305*, 333–359. [CrossRef]
38. Jung, C.Y.; Nguyen, T.B. A new adaptive weighted essentially non-oscillatory WENO-θ scheme for hyperbolic conservation laws. *J. Comput. Appl. Math.* **2018**, *328*, 314–339. [CrossRef]
39. Gottlieb, S.; Shu, C.W. Total variation diminishing Runge–Kutta schemes. *Math. Comput.* **1998**, *67*, 73–85. [CrossRef]
40. Gottlieb, S.; Shu, C.W.; Tadmor, E. Strong stability-preserving high-order time discretization methods. *SIAM Rev.* **2001**, *43*, 89–112. [CrossRef]
41. Chatterjee, A. Shock wave deformation in shock-vortex interactions. *Shock Waves* **1999**, *9*, 95–105. [CrossRef]
42. Ren, Y.X.; Liu, M.; Zhang, H. A characteristic-wise hybrid compact-WENO scheme for solving hyperbolic conservation laws. *J. Comput. Phys.* **2003**, *192*, 365–386. [CrossRef]
43. Schulz-Rinne, C.W.; Collins, J.P.; Glaz, H.M. Numerical solution of the Riemann problem for two-dimensional gas dynamics. *SIAM J. Sci. Comput.* **1993**, *14*, 1394–1414. [CrossRef]
44. Schulz-Rinne, C.W. Classification of the Riemann problem for two-dimensional gas dynamics. *SIAM J. Math. Anal.* **1993**, *24*, 76–88. [CrossRef]
45. Lax, P.D.; Liu, X.D. Solution of two-dimensional Riemann problems of gas dynamics by positive schemes. *SIAM J. Sci. Comput.* **1998**, *19*, 319–340. [CrossRef]
46. Zhang, R.; Zhang, M.; Shu, C.W. On the order of accuracy and numerical performance of two classes of finite volume WENO schemes. *Commun. Comput. Phys.* **2011**, *9*, 807–827. [CrossRef]
47. Pirozzoli, S. Numerical methods for high-speed flows. *Annu. Rev. Fluid Mech.* **2011**, *43*, 163–194. [CrossRef]